nagra.

Technical Report 17-13

The development of a thermodynamic sorption data base for montmorillonite and the application to bentonite

November 2017

B. Baeyens, M.H. Bradbury

Paul Scherrer Institut, Villigen PSI

National Cooperative
for the Disposal of
Radioactive Waste

Hardstrasse 73
CH-5430 Wettingen
Switzerland
Tel. +41 56 437 11 11

www.nagra.ch

nagra.

Technical Report 17-13

The development of a thermodynamic sorption data base for montmorillonite and the application to bentonite

November 2017

B. Baeyens, M.H. Bradbury

Paul Scherrer Institut, Villigen PSI

National Cooperative
for the Disposal of
Radioactive Waste

Hardstrasse 73
CH-5430 Wettingen
Switzerland
Tel. +41 56 437 11 11

www.nagra.ch

ISSN 1015-2636

Preface

The Laboratory for Waste Management of the Nuclear Energy and Safety Research Department at the Paul Scherrer Institute is performing work to develop and test models as well as to acquire specific data relevant to performance assessments of Swiss radioactive waste repositories. These investigations are undertaken in close co-operation with, and with the financial support of, the National Cooperative for the Disposal of Radioactive Waste (Nagra). The present report is issued simultaneously as a PSI Bericht and a Nagra Technical Report.

Abstract

Over the past two decades measurements on the uptake of radionuclides on montmorillonite in the form of sorption edges and isotherms have been performed. The metals investigated include Co(II), Ni(II), Cd(II), Zn(II), Fe(II), Eu(III), Am(III), Sn(IV), Th(IV), Np(V), Pa(V) and U(VI), and all of these data are presented here. The two site protolysis non electrostatic surface complexation cation exchange (2SPNE SC/CE) sorption model has been applied to successfully model this extensive experimental sorption data set. Previously published results were not always modelled with the same set of thermodynamic data, particularly the hydrolysis constants. In this work the all of the sorption measurements have been consistently (re)modelled with the same selected hydrolysis constant data set and the modelled curves presented.

The conclusions from sorption competition studies are presented and discussed: briefly, chemically similar metals (valence state, hydrolysis behaviour) sorb on the same set of strong sites and exhibit sorption competition, chemically dissimilar metals sorb on different strong site sets and do not compete with one another. This information was used to construct linear free energy relationships (LFERs) between surface complexation constants and the appropriate corresponding aqueous hydrolysis constants separately for divalent transition metals, trivalent lanthanides/actinides and tetravalent actinides. LFERs provide a means for estimating surface site binding constants for metals where the data are either very poor or non-existent and thus allow sorption values to be calculated. How well such a procedure may (or may not) work was illustrated in an exercise where surface complexation constants for specific metals were taken from the appropriate LFERs and used to calculate sorption edges/isotherms which were then compared with the measured sorption values. A general methodology for using LFERs to calculate the sorption of metals for which no sorption data exist is suggested and applied to predict sorption edges/isotherms for Mn(II), Cu(II), Pu(III), U(IV), Np(IV) and Pu(IV).

In a final exercise to test the capabilities of the 2SPNE SC/CE sorption model, and the associated model parameters, to quantitatively describe the uptake of radionuclides in complex MX-80 bentonite/porewater systems, blind model predictions were made of sorption isotherms which were then compared with the measured values. The main assumption was that the sorption on MX-80 bentonite is controlled by the montmorillonite content.

The main conclusion drawn from this work is that the tables of surface complexation constants and cation exchange selectivity coefficients given and used in conjunction with the LFERs and the 2SPNE SC/CE sorption model, provide a powerful means of calculating the sorption of many radionuclides in complex porewater/bentonite systems. Together they constitute a Thermodynamic Sorption Data Base (TSDB) for montmorillonite/bentonite systems.

Zusammenfassung

Im Verlauf der letzten beiden Jahrzehnte wurden Untersuchungen zur Aufnahme von Radionukliden in Montmorillonit in Form von Messungen von Sorptionskanten und -isothermen durchgeführt. Die untersuchten Metalle umfassen Co(II), Ni(II), Cd(II), Zn(II), Fe(II), Eu(III), Am(III), Sn(IV), Th(IV), Np(V), Pa(V) und U(VI) und alle entsprechenden Messdaten werden in diesem Bericht präsentiert. Der extensive experimentelle Datensatz wurde erfolgreich mit dem "two site protolysis non electrostatic surface complexation cation exchange" (2SPNE SC/CE) Sorptionsmodell modelliert. Früher publizierte Resultate wurden nicht immer mit demselben Satz von Hydrolysekonstanten ausgewertet. In diesem Bericht werden deshalb sämtliche Sorptionsmessungen noch einmal mit einem konsistenten Satz von Hydrolysekonstanten modelliert und die so erhaltenen Sorptionskurven präsentiert.

Lineare Freie-Energie-Beziehungen ("linear free energy relationships", LFERs) zwischen Oberflächenkomplexierungskonstanten und entsprechenden wässrigen Hydrolysekonstanten wurden separat für zweiwertige Übergangsmetalle, dreiwertige Lanthaniden/Actiniden und vierwertige Actiniden abgeleitet. Die LFER-Methode ermöglicht es, Oberflächenkomplexierungskonstanten abzuschätzen, falls experimentelle Daten von schlechter Qualität sind oder gänzlich fehlen, um so Sorptionswerte zu berechnen. Wie gut oder schlecht solch eine Schätzmethode funktioniert, wird an einem Beispiel erläutert, wo Oberflächenkomplexierungskonstanten für spezifische Metalle mittels LFERs abgeschätzt wurden, um damit Sorptionskanten und -isothermen zu berechnen, die dann mit experimentellen Sorptionswerten verglichen wurden. Zudem wird eine generelle Methodik vorgeschlagen, um LFER zur Berechnung der Metallsorption in Fällen zu verwenden, wo keine Sorptionsdaten vorhanden sind. Sie wird auf die Voraussage von Sorptionskanten und -isothermen für Mn(II), Cu(II), Pu(III), U(IV), Np(IV) und Pu(IV) angewandt.

Schliesslich wird die Fähigkeit des 2SPNE SC/CE-Sorptionsmodells und der damit verbundenen Modellparameter geprüft, die Aufnahme von Radionukliden in komplexen MX-80-Bentonit/Porenwassersystemen quantitativ zu beschreiben. Dazu wurden Blindvoraussagen gemacht und mit gemessenen Sorptionsdaten verglichen. Die Hauptannahme dabei war, dass die Sorption an MX-80-Bentonit durch den Gehalt an Montmorillonit kontrolliert wird.

Die Hauptschlussfolgerung der vorliegenden Arbeit lautet, dass die vorgestellten Tabellen mit Oberflächenkomplexierungskonstanten und Selektivitätskoeffizienten für Kationenaustausch in Verbindung mit der LFER-Methode und dem 2SPNE SC/CE-Sorptionsmodell ein leistungsfähiges Mittel sind, um die Sorption vieler Radionuklide in komplexen Porenwasser/Bentonit-Systemen zu berechnen, und sie stellen eine eigentliche thermodynamische Sorptionsdatenbank für Montmorillonit/Bentonitsysteme dar.

Résumé

Au cours des deux dernières décennies, la rétention du Co(II), Ni(II), Cd(II), Zn(II), Fe(II), Eu(III), Am(III), Sn(IV), Th(IV), Np(V), Pa(V) et U(VI) sur la montmorillonite a été mesurée en fonction du pH et de la concentration (isotherme) en nucléides. Cet important ensemble de données expérimentales a été modélisé avec succès en utilisant le modèle de sorption « two site protolysis non electrostatic surface complexation cation exchange » (2SPNE SC/CE). Les modélisations effectuées par le passé ne reposaient pas toutes sur les mêmes données thermodynamiques, en particulier les constantes d'hydrolyse. Pour ce rapport, l'ensemble des mesures de sorption a été (re)modélisé en utilisant les mêmes constantes d'hydrolyse; les courbes de sorption ainsi obtenues sont présentées ici.

Par ailleurs, les conclusions des études de sorption compétitive sont présentées et discutées brièvement. En résumé, les métaux chimiquement proches (valence, hydrolyse) adsorbent sur les mêmes sites de forte affinité, et sont de ce fait compétitifs. Les éléments dissimilaires adsorbent sur des sites de forte affinité différents, et ne sont donc pas en concurrence. Cette information a été utilisée pour construire des relations linéaires d'énergies libres (« linear free energy relationships », LFER) entre les constantes de complexation de surface et les constantes d'hydrolyse correspondantes pour différents groupes d'éléments, en l'occurrence les métaux de transition divalents, les lanthanides/actinides trivalents, ainsi que pour les actinides tétravalents. Ces relations permettent d'estimer des constantes de complexation de surface dans le cas de métaux pour lesquels les données expérimentales sont absentes ou de qualité insuffisante, et de calculer ainsi des valeurs de sorption. Cette approche d'estimation a été testée en calculant des valeurs de sorption (en fonction du pH et de la concentration) pour certains éléments en utilisant les constantes de complexation de surface obtenues avec la LFER et en les comparant aux données expérimentales. Une méthodologie générale permettant de calculer la sorption de métaux pour lesquels aucune donnée n'existe est proposée. Cette méthodologie est en outre utilisée pour prédire la sorption (en fonction du pH et concentration) pour le Mn(II), Cu(II), Pu(III), U(IV), Np(IV) et Pu(IV) sur la montmorillonite.

Finalement, on a testé la capacité du modèle de sorption « 2SPNE SC/CE », avec les paramètres qui lui sont associés, à prédire la sorption de radionucléides dans les systèmes complexes bentonite/eaux interstitielles. Pour cela, des isothermes de sorption ont été calculées en aveugle et comparées avec les données expérimentales obtenues sur la bentonite. Ces calculs présupposaient que la sorption sur la bentonite MX-80 était contrôlée par la teneur en montmorillonite.

La principale conclusion de cette étude est que les constantes de complexation de surface et les sélectivités d'échange cationique pour la montmorillonite, utilisées en combinaison avec la LFER et le model de sorption « 2SPNE SC/CE », constituent un outil performant pour prédire la sorption de nombreux radionucléides dans des systèmes complexes bentonite/eaux interstitielles. L'ensemble constitue une base de données de sorption thermodynamique pour les systèmes montmorillonite/bentonite.

Table of Contents

List of Tables

List of Figures

1 Introduction

The uptake of metal contaminants by clay minerals in argillaceous rocks and high clay mineral content materials such as bentonite is an important process governing their rate of migration through such systems. Sorption depends on many factors such as the metal itself and its concentration, the water chemistry including redox, the quantity and properties of the sorbent, the presence and concentration of metals competing for the available sorption sites etc. In these varied and complex systems experimental measurements can only offer a restricted overview in specific cases. A verified predictive sorption model is the only practical means of providing the sorption values in the wide-ranging and changing conditions met in nature.

In order to obtain a (quasi) mechanistic understanding of radionuclide uptake on clay minerals and argillaceous rocks, sorption experiments have been carried out on purified clay minerals under well-defined conditions in simple background electrolytes as a function of pH at trace concentrations (sorption edges) or as a function of concentration at constant pH and ionic strength (sorption isotherms) (Baeyens & Bradbury 1995a and b, 1997, Bradbury & Baeyens 1999, 2002a). As a result of such studies, a sorption model, the two site protolysis non electrostatic surface complexation cation exchange (2SPNE SC/CE) model was developed. This sorption model was incorporated in the speciation code MINEQL and the resulting combination, the MINSORB code, has been successfully applied to quantitatively describe the sorption of metals with valences from II to VI as a function of pH and concentration on 2:1 clay minerals over a wide range of conditions (Bradbury & Baeyens 1999, 2002a, 2005a, 2009a and b). Sorption is described in terms of cation exchange and surface complexation. Generally, one or the other mechanism dominates the uptake, depending on the chemical conditions, but both mechanisms are always operating together and are calculated simultaneously.

For some metals experimental sorption data are not available, and since surface complexation constants cannot be calculated from theoretical considerations, there was a strong motivation to try to develop tools whereby surface stability constants could be estimated. It is common practice in solution thermodynamics to seek relationships between the free energies of formation of aqueous complexes and the thermodynamic properties of the metal ions or ligands, so called linear free energy relationships (LFERs; Larsson 1934, Hammett 1940, Chapman & Shorter 1972). Using this as an example LFERs were found for metal sorbates between the logarithms of the surface site binding constants on the strong and weak sites and the logarithm of the corresponding aqueous hydrolysis constants (Bradbury & Baeyens 2005a). LFERs and their application are discussed in Chapters 5 and 6 especially in the light of the results from sorption competition investigations, Chapter 4.

Using the surface complexation constants and the cation exchange selectivity coefficients derived from the experimental sorption data measured on clay minerals, this essentially simple sorption model was then applied to model aqueous metal species uptake in more complex MX-80 bentonite/porewater and argillaceous rock/groundwater systems (again successfully); the so called "bottom-up" sorption modelling approach (Bradbury & Baeyens 2011a).

Further investigations and modelling studies allowed the broad rules governing the sorption competition between different metals simultaneously present in solution to be elucidated and modelling approaches were proposed enabling the effects to be quantified (Bradbury & Baeyens 2005c, Bradbury et al. 2017. Spectroscopic studies were an important part of this work and provided additional information and support for the sorption model itself and the conclusions drawn (Dähn et al. 2002, 2003, 2011, Marques Fernandes et al. 2012, 2016). The combination of wet chemistry experiments, sorption modelling and spectroscopic investigations provided a coherent

and consistent picture. Although the original simple model and model assumptions have been modified (see section 4.3), the sorption model has remained essentially the same and is still very easy to apply, even in the cases of complex geochemical systems, and can be readily included in reactive transport codes (Pfingsten et al. 2011).

The experience gained over the past decade or more has led to the conclusion that the model, together with the associated parameters, can be used with confidence and provide a good quantitative description of sorption in natural systems, including sorption competition, where 2:1 clay minerals (montmorillonite, illite, illite-smectite mixed layers) are the dominant sorbing phases. This report concentrates on montmorillonite and MX-80 bentonite (> 70 % montmorillonite).

The time is now deemed appropriate to review the sorption data and bring together all of the knowledge and information gathered over the years and present them all together in one report. In particular, different hydrolysis constants from different sources have been used in the past in the modelling, sometimes for the same metal sorption data. The aim here is to define a set of the "best available" aqueous metal hydrolysis stability constants and to use these in a consistent manner to model all of the in-house and reliable literature sorption data measured on montmorillonite. This inevitably involved the re-modelling of already published data leading to (slightly) different surface complexation constants for some metals.

The end goal of this report is to present a thermodynamic sorption data base (TSDB) for montmorillonite which can be used to calculate sorption values in natural bentonite systems under any realistic conditions. It is important to realise that the sorption model, the assumptions in the model, the aqueous thermodynamic data used and the surface complexation constants and cation exchange selectivity coefficients in the TSDB are all linked and make up a complete package. Thus, in order to be able to use the data in the TSDB properly to calculate sorption values, it is essential to understand what lies behind such a data base, and this is described in the following chapters.

In the concept of the Swiss deep geological disposal for radioactive waste bentonite is foreseen as backfill material (Nagra 2002). The retention of radionuclides on montmorillonite, which is the main constituent of bentonite, contributes significantly to the safety functions of a geological repository. Sorption databases on bentonite are indispensable for the safety analysis.

2 The two site protolysis non electrostatic surface complexation and cation exchange (2SPNE SC/CE) sorption model

The 2SPNE SC/CE sorption model describes the sorption of dissolved metal species on 2:1 clay minerals by cation exchange and surface complexation. In this work the uptake by both mechanisms is calculated simultaneously using the MINSORB code (Bradbury & Baeyens 1997). The model has been described on a number of occasions (Bradbury & Baeyens 1997, 1999, 2002a, 2005a, 2006a) and will only be outlined here for completeness.

2.1 Surface complexation

In the 2SPNE SC/CE sorption model used to describe the pH dependent component of sorption on 2:1 clay minerals (Bradbury & Baeyens 1997), the amphoteric surface hydroxyl groups (sites) situated at clay platelet edges (see for example Sposito 1984, Davis & Kent 1990) are characterised in terms of different site types (strong sites, $\equiv S^{S}OH$, and weak sites, $\equiv S^{W1}OH$ and $\equiv S^{W2}OH$) together with their associated protonation and deprotonation constants, K^{+}_{app} and K^{-}_{app} respectively. The $\equiv S^{W1}OH$ and $\equiv S^{W2}OH$ sites have the same capacities but different protolysis constants and determine the titration behaviour of montmorillonite.

Protolysis equations and their corresponding constants are given by:

$$\equiv SOH + H^{+} \Leftrightarrow \equiv SOH_2^{+} \qquad K_{app} = \frac{[\equiv SOH_2^{+}]}{[\equiv SOH]\cdot\{H^{+}\}} \tag{2.1}$$

$$\equiv SOH \Leftrightarrow \equiv SO^{-} + H^{+} \qquad K_{app} = \frac{[\equiv SO^{-}]\cdot\{H^{+}\}}{[\equiv SOH]} \tag{2.2}$$

where [ ] terms are concentrations and { } terms are activities.

Only the $\equiv S^{S}OH$ and $\equiv S^{W1}OH$ type sites are required to model sorption edge and isotherm data (Bradbury & Baeyens 1997). The $\equiv S^{S}OH$ sites have a much smaller capacity, approximately 2.5 % of that of the weak sites. The former form much stronger surface complexes with metals and dominate the sorption at trace concentrations. A summary of site types, capacities and protolysis constants for montmorillonite are given in Appendix A.

A general equation for surface complexation may be written as:

$$\equiv SOH + Me^{z} + y\,H_2O \Leftrightarrow \equiv SOMe(OH)_y^{z-(y+1)} + (y+1)\,H^{+} \tag{2.3}$$

for which the surface complexation constant, K_y is given by:

$$K_y = \frac{[\equiv SOMe(OH)_y^{z-(y+1)}]}{[\equiv SOH]} \cdot \frac{f_{\equiv SOMe(OH)_y^{z-(y+1)}}}{f_{\equiv SOH}} \cdot \frac{\{H\}^{(y+1)}}{\{Me^{z}\}} \tag{2.4}$$

K_y is the surface complexation constant,

"f" terms are surface activity coefficients (generally assumed to be unity).

It is assumed that only cations and neutral and positively charged hydroxy species are sorbing on the edge sites. All other aqueous species are taken to be non-sorbing (Bradbury & Baeyens 2011b). While this assumption has been shown to be sufficient to model a wide range of experimental data, ternary carbonate surface complexes have been used to model the sorption of trivalent metals on clay minerals in the alkali pH range at relatively high carbonate concentrations (Marques Fernandes et al. 2008a, 2012). Such ternary compounds have been confirmed by EXAFS investigations (Marques Fernandes et al. 2012, 2016). These data are included in the TSDB below but are not generally critical at the pH values and porewater/groundwater compositions normally encountered in the geochemical systems important for radioactive waste disposal. At the present time, no evidence has been found for the existence of ternary carbonate surface complexes for bi- and tetravalent metals.

2.2 Cation exchange

The surfaces of 2:1 type clay minerals carry a permanent negative charge arising from isomorphic substitution of lattice cations by cations of a lower valence. Charge neutrality is maintained by the presence of an excess of cations in solution in close proximity to the surface. These cations, held around the outside of the Si-Al-Si clay mineral structural units, "belong" to the surface and cannot be separated away from it, but are exchangeable and can undergo exchange reactions with cations in the aqueous phase. The cation exchange capacity (CEC) of a solid is defined as the total quantity of cations sorbed exchangeable per unit mass, *e.g.* equivalents kg^{-1}.

If cation B, valence z_B, in the aqueous phase exchanges with cation A, valence z_A, bound to the clay mineral surface, the exchange reaction can be written as:

$$z_B\text{A-clay} + z_A\text{B} \Leftrightarrow z_A\text{B-clay} + z_B\text{A} \tag{2.5}$$

Cation exchange reactions are reversible, fast and stoichiometric. In the case of heterovalent exchange, the latter characteristic arises from the electro-neutrality condition. A mass action relation is normally used to describe the reaction in terms of a so-called selectivity coefficient. Following the Gaines & Thomas (1953) convention (there are others) the selectivity coefficient, ${}^{B}_{A}K_c$, for equation (2.5) is written as:

$${}^{B}_{A}K_c = \frac{N_B^{z_A}}{N_A^{z_B}} \cdot \frac{\{A\}^{z_B}}{\{B\}^{z_A}} \tag{2.6}$$

where {} terms are solution activities. N_A and N_B are equivalent fractional occupancies defined as the equivalents of A (or B) sorbed per unit mass divided by the cation exchange capacity, in equivalents per unit mass.

The exchange behaviour of each of the cations in solution is usually described with respect to a master cation, usually Na^+ ("A" in Eqs. 2.5 and 2.6), since Na usually has the highest aqueous concentration and highest occupancy on the planar sites of the clay. These equations can be used to calculate the loadings on the chosen clay mineral component from which a sorption value for any of the aqueous cations present can be deduced. If there is more than one major clay mineral component, then a separate set of selectivity coefficients is required for each of the clay minerals considered.

Monovalent, bivalent, trivalent etc. cations all compete with one another for the planar sorption sites on montmorillonite according to the value of their respective selectivity coefficients. Cation exchange is the dominant sorption mechanism for nuclides such as K, Ca, Sr, and Cs and Rb on montmorillonite.

2.3 Competition

The results from sorption competition experiments on montmorillonite (Bradbury & Baeyens 2005c) showed clearly that all metals are not mutually competitive with respect to sorption, but rather competition is selective. This in turn implied that the (strong) sorption sites at the edges of the clay mineral must be different for different groups of metals. Generally, chemically similar metals (valence state, hydrolysis behaviour) sorb on the same set of strong sites while chemically dissimilar metals sorb on different strong site sets (Bradbury et al. 2017).

The modification made to the 2SPNE SC/CE sorption model as a consequence of these findings was that multiple sets of strong sites, $\equiv S^{S}OH$, were proposed to exist as subsets of the $\equiv S^{W1}OH$ weak site population, with average site capacities of 2 mmol kg^{-1}, i.e. metals in the same valence state have their own set of strong sites. Extensive spectroscopic measurements have supported this interpretation (Dähn et al. 2002, 2003, 2011 and Marques Fernandes et al. 2012, 2016). The value of the $\equiv S^{W1}OH$ site capacity of 40 mmol kg^{-1} was retained.

2.4 Summary of framework and assumptions in the 2SPNE SC/CE sorption model

The main assumptions associated with the 2SPNE SC/CE sorption model are as follows:

1. The uptake of metals on 2:1 clay minerals is controlled by cation exchange and surface complexation reactions which take place simultaneously.
2. Sorption is assumed to be fast and reversible.
3. In montmorillonite cation exchange takes place on the planar sites and the site capacity is given by the CEC in equivalents kg^{-1}.
4. Surface complexation reactions take place on amphoteric surface hydroxyl edge sites.
5. The protolysis behaviour of 2:1 clay minerals is governed by two site types called "weak-1 ($\equiv S^{W1}OH$)" and "weak-2 ($\equiv S^{W2}OH$)" sites, each having a site capacity of 40 mmol kg^{-1} and characterised by their own protonation and de-protonation constants.
6. Sorption by surface complexation occurs on so called "strong sites ($\equiv S^{S}OH$)" and "weak-1 ($\equiv S^{W1}OH$)" sites. Both have the same protolysis constants.
7. Sorption at trace concentrations occurs predominantly on the $\equiv S^{S}OH$ sites which have an average site capacity of 2 mmol kg^{-1}.
8. Surface activity coefficients for both cation exchange and surface complexation are taken to be unity.
9. Only cations and neutral and positively charged hydroxy species are sorbing. All other aqueous species are taken to be non-sorbing (however, see Appendix E).
10. The selectivity coefficients (K_c values) given in Appendix F are valid in the ionic strength range from ~ 0.01 M to ~ 0.3 M (outside this range the K_c values are not assured).
11. The protolysis constants (Appendix A) and surface complexation constants (Appendices C and D) are only valid for ionic strengths < 0.5 M.

All metals are not mutually competitive with respect to sorption, but rather competition is selective (see section 2.3).

3 Measured sorption edges and isotherms and modelled curves

3.1 Preamble

Commercially available montmorillonite contains significant levels of background impurities which can influence the sorption properties of the clay suspensions and may lead to difficulties in the interpretation of data. A conditioning procedure was therefore applied to all of the montmorillonites used in the various sorption studies (mainly SWy-1 and SWy-2 montmorillonite but also STx-1) in order to remove these background metal impurities, soluble salts and sparingly soluble minerals. Part of the conditioning process was designed to convert the purified clay into the homo-ionic Na-form which was then thoroughly physico-chemically characterised. Most of the sorption experiments were carried out in a background electrolyte of $NaClO_4$ which was also purified (Baeyens & Bradbury 1995b). The majority of the data sets are "in house" data (published and unpublished) carried out in controlled N_2 atmosphere glove boxes where the partial pressure of CO_2 was $< 10^{-5.5}$ bar at temperatures between 22 °C and 26 °C. There are some additional data sets taken from the open literature which have been carried under atmospheric conditions at room temperature. The total nuclide concentration (Me_{TOT}) and the sorbent concentration (*S*) has been included in the figure caption of the sorption edges.

It was essential to the modelling that experimental data were carried out under well-defined conditions, *e.g.* pH, background electrolyte, background impurities, total metal concentration, solid to liquid ratio. Without this information it was not feasible to perform the modelling.

The sorption edge/isotherm measurements were modelled in terms of cation exchange and surface complexation mechanisms via a stepwise iterative fitting/modelling procedure using the computer code MINSORB (Bradbury & Baeyens 1997). This code allowed the uptake of radionuclides by both mechanisms to be calculated simultaneously. Aqueous activity coefficients were calculated using the Davies relation (Davies 1962). In all of the calculations the site types and site capacities and protonation/de-protonation constants for the amphoteric surface hydroxyl groups (≡SOH) were fixed (Appendix A). The metal hydrolysis constants used are summarised in Appendix B.

3.2 Sorption edges: Figures and modelled curves

This section contains all of the sorption edges measured "in house" together with some data taken from the literature. In the vast majority of cases sorption is expressed as a distribution ratio, R_d, defined as:

$$R_d = \frac{C_{init.} - C_{eq.}}{C_{eq.}} \cdot \frac{V}{m} \qquad (3.1)$$

where:

$C_{init.}$ = initial aqueous concentration of active and inactive metal [M]
$C_{eq.}$ = equilibrium aqueous concentration of active and inactive metal [M]
V = volume of liquid phase [L]
m = mass of solid phase [kg]

The experimental methodology has been described on numerous occasions and the details can be found in Baeyens & Bradbury (1997), Bradbury & Baeyens (2002a), for example.

The errors on the "in house" log R_d values are 0.3 log units, and up to 0.5 log units for sorption values greater than 10^5 L kg^{-1}.

A compilation of sorption edges for the elements Co(II), Ni(II), Cd(II), Zn(II), Fe(II), Eu(III), Am(III), Sn(IV), Th(IV), Np(V), Pa(V) and U(VI) together with the modelled curves are presented in Figs. 3.1 to 3.12. The experimental data points are given as filled circles and the modelled curves as continuous black lines. A summary of the surface complexation reactions and constants is given in Appendix C and the selectivity coefficients in Appendix F.

3.2.1 Cobalt

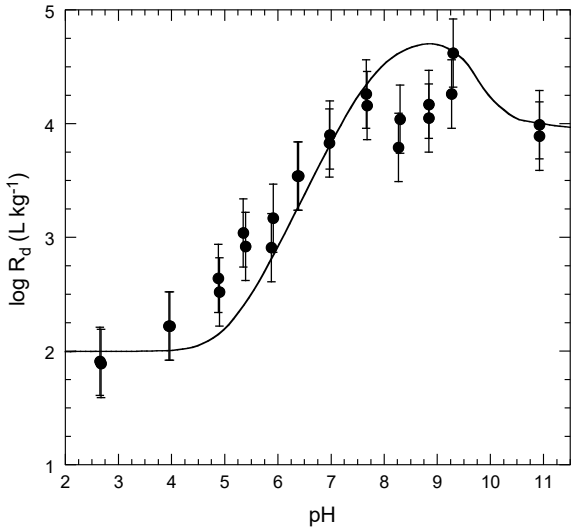

Fig. 3.1: Sorption edge for Co(II) on Na-SWy-2 in 0.1 M $NaClO_4$, $Co_{TOT} < 2.2 \times 10^{-7}$ M, S = 1.6 g L^{-1}.

Experimental data (●) and modelled curve (—) (*this study*).

3.2.2 Nickel

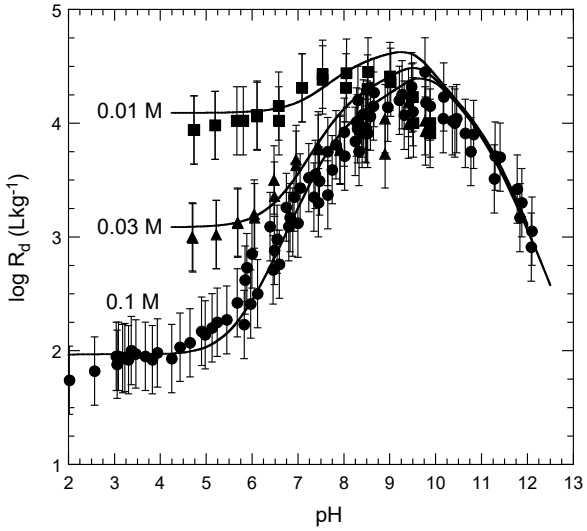

Fig. 3.2: Sorption edges for Ni(II) on Na-SWy-1. $Ni_{TOT} < 3 \times 10^{-7}$ M, $S = 1.1$ g L^{-1}.

Experimental data (■) 0.01 M $NaClO_4$, (▲) 0.03 M $NaClO_4$, (●) 0.1 M $NaClO_4$ and modelled curves (—) (Bradbury & Baeyens 1997).

3.2.3 Cadmium

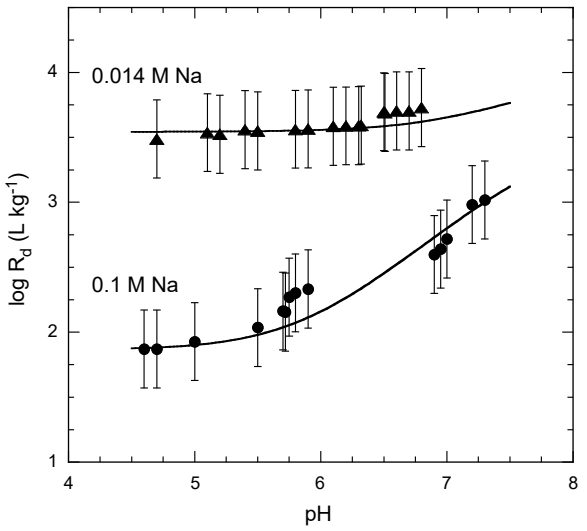

Fig. 3.3: Sorption edges for Cd(II) on Na-SWy-1. $Cd_{TOT} \sim 10^{-6}$ M, $S = 1$ g L^{-1}.

Experimental data (▲) 0.014 M $NaClO_4$ and (●) 0.1 M $NaClO_4$ (Zachara et al. 1993) and modelled curves (—) (Bradbury & Baeyens 2005a).

3.2.4 Zinc

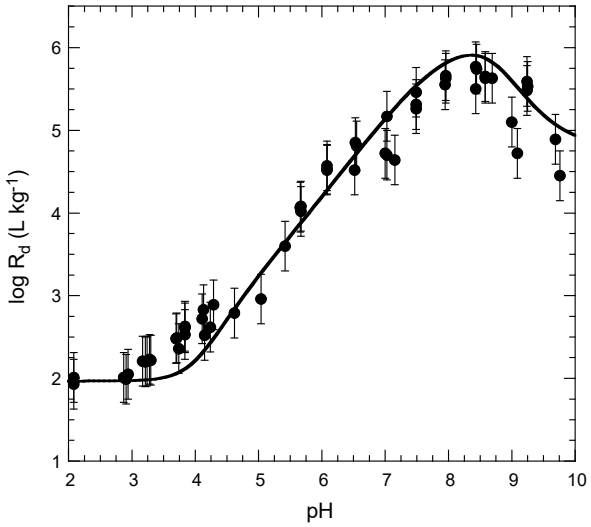

Fig. 3.4: Sorption edge for Zn(II) on Na-SWy-1 in 0.1 M $NaClO_4$. $Zn_{TOT} \sim 10^{-6}$ M, S = 1.2 g L^{-1}.

Experimental data (●) (Baeyens & Bradbury 1997) and modelled curve (—) (Bradbury & Baeyens 1997).

3.2.5 Iron

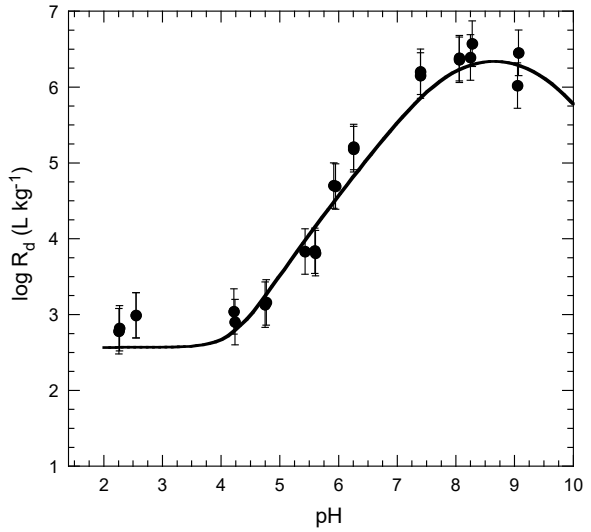

Fig. 3.5: Sorption edge for Fe(II) on Na-STx-1 in 0.1 M $NaClO_4$.

$Fe_{TOT} < 3 \times 10^{-8}$ M, $S = \sim 1$ g L^{-1}. Experimental data (●) (Soltermann et al. 2014) and modelled curve (—) (*this study*).

3.2.6 Europium

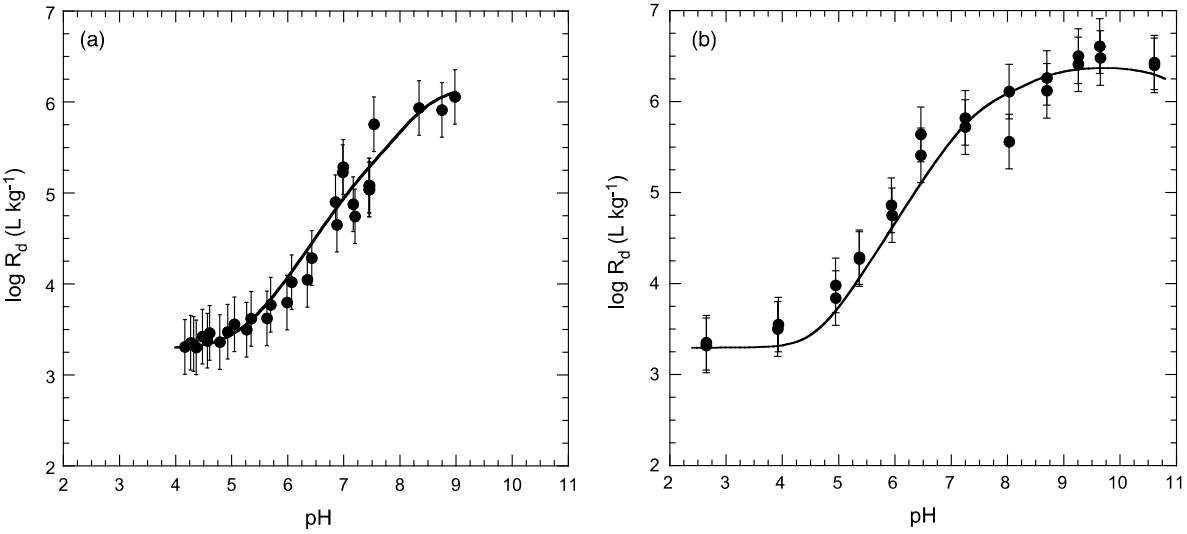

Fig. 3.6: Sorption edge for Eu(III) on Na-SWy-1 in 0.1 M $NaClO_4$.

Experimental data (●): (a) Bradbury & Baeyens (2002a), $Eu_{TOT} = 1.3 \times 10^{-7}$ M, $S = 1.5$ g L^{-1} and (b) Bradbury & Baeyens (2006b), $Eu_{TOT} = 3.6 \times 10^{-9}$ M, $S = 0.62$ g L^{-1} and modelled curves (—) *this study*. Excluding aqueous Eu silicate complexes (see Appendix G).

3.2.7 Americium

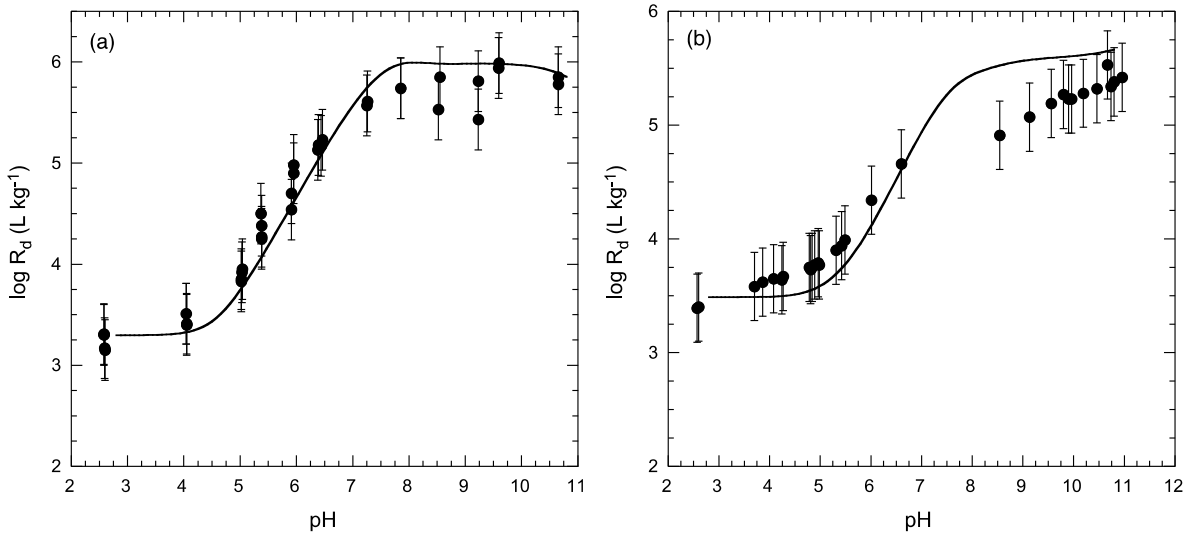

Fig. 3.7: Sorption edges for Am(III) in 0.1 M $NaClO_4$ on Na-SWy-1 (a) and Na-smectite (b).

Experimental data (●): (a) $Am_{TOT} = 1.5 \times 10^{-10}$ M, $S = 0.62$ g L^{-1}(Bradbury & Baeyens 2006b) and (b) $Am_{TOT} = 3 \times 10^{-8}$ M; $S = 4$ g L^{-1} (Gorgeon 1994) and modelled curves (—) *this study*. Excluding aqueous Am silicate complexes (see Appendix G).

3.2.8 Tin

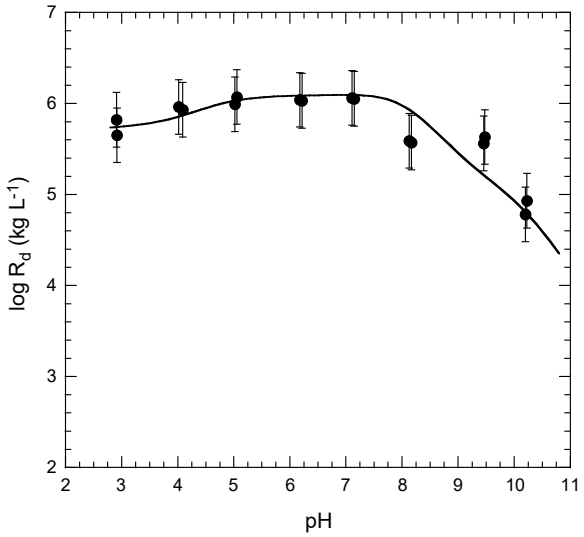

Fig. 3.8: Sorption edge for Sn(IV) on Na-SWy-1 in 0.1 M $NaClO_4$.

$Sn_{TOT} < 5 \times 10^{-8}$ M, $S = 0.54$ g L^{-1}. Experimental data (●)and modelled curve (—) (Bradbury & Baeyens 2005a).

3.2.9 Thorium

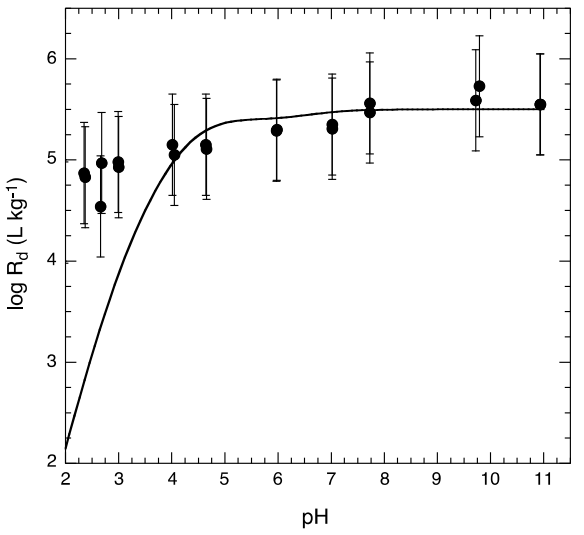

Fig. 3.9: Sorption edge for Th(IV) on Na-SWy-1 in 0.1 M $NaClO_4$.

$Th_{TOT} < 10^{-9}$ M, $S = 0.42$ g L^{-1}. Experimental data (●) and modelled curve (—) (Bradbury & Baeyens 2005a).

3.2.10 Protactinium

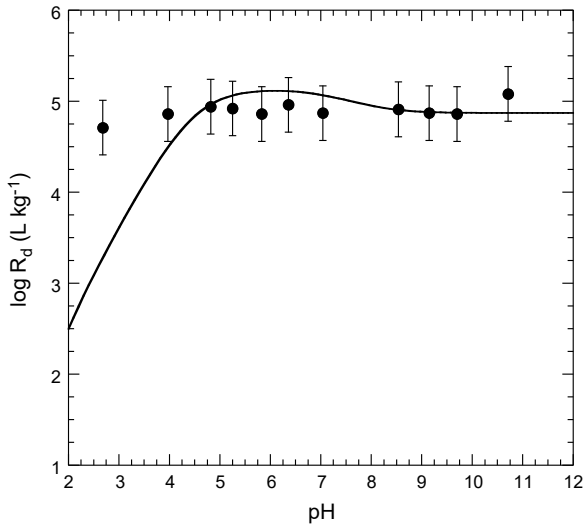

Fig. 3.10: Sorption edge for Pa(V) on Na-SWy-1 in 0.1 M $NaClO_4$.

$Pa_{TOT} < 10^{-13}$ M, S = 0.65 g L^{-1}. Experimental data (●) and modelled curve (—) (Bradbury & Baeyens 2006b).

3.2.11 Neptunium

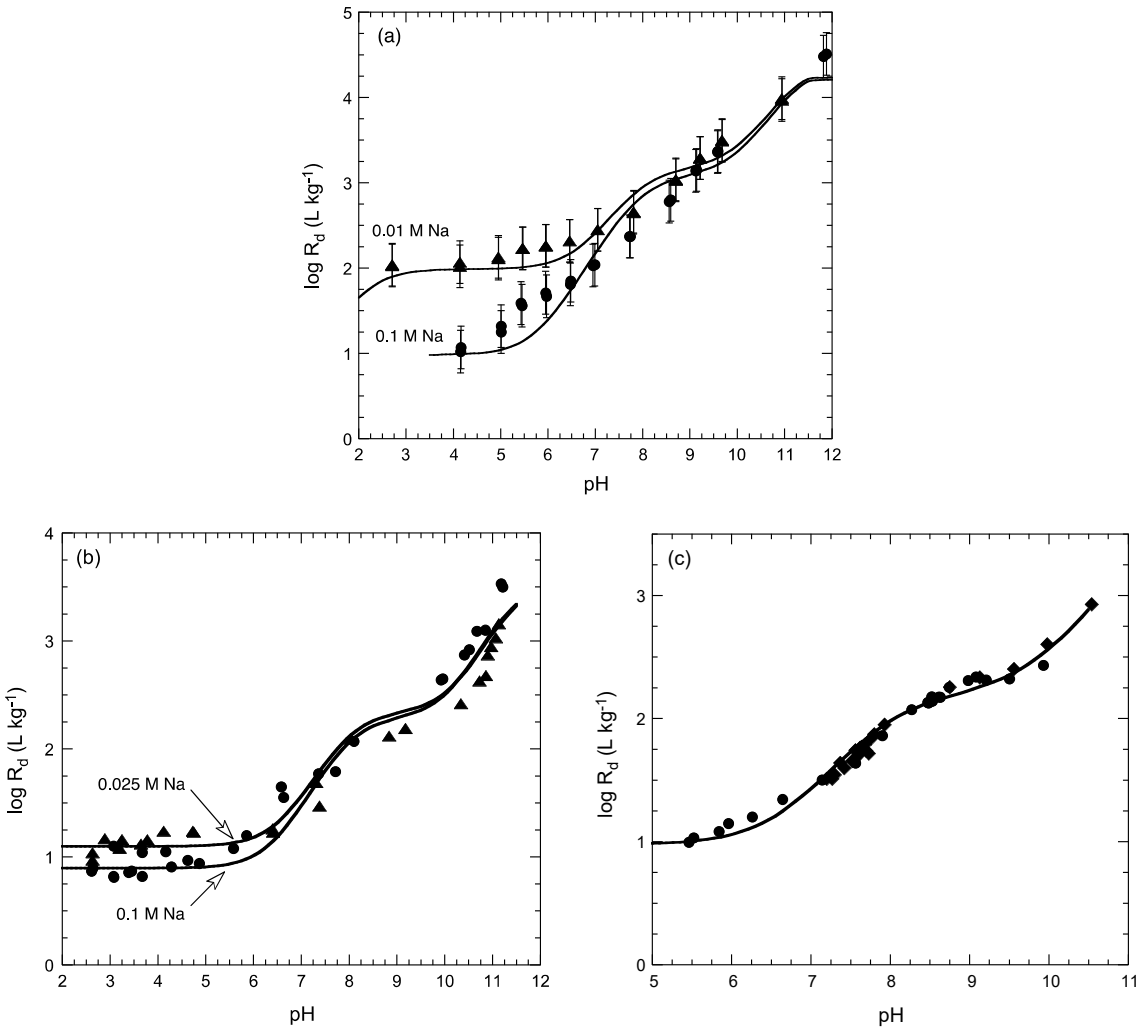

Fig. 3.11: Sorption edges for Np(V) on Na-montmorillonite.

(a) Experimental data on SWy-1 in (▲) 0.01 M $NaClO_4$, $Np_{TOT} < 10^{-13}$ M, $S = 0.61 – 3.2$ g L^{-1} and (●) 0.1 M $NaClO_4$; $Np_{TOT} < 10^{-13}$ M, $S = 1.2$ g L^{-1} and modelled curves (—) (Bradbury & Baeyens 2006b). (b) Experimental data on Na-smectite in (▲) 0.025 M $NaClO_4$ and (●) 0.1 M $NaClO_4$, $Np_{TOT} < 1.1 \times 10^{-6}$ M, $S = 8.7$ g L^{-1} (Gorgeon 1994) and modelled curves (—) (Bradbury & Baeyens 2005a). (c) Experimental data on SAz-1 in (●,▲,◆) 0.1 M $NaNO_3$, $Np_{TOT} < 9.5 \times 10^{-7}$ M, $S = 4.2$ g L^{-1} (Turner et al. 1998) and modelled curve (—) (Bradbury & Baeyens 2005a).

3.2.12 Uranium

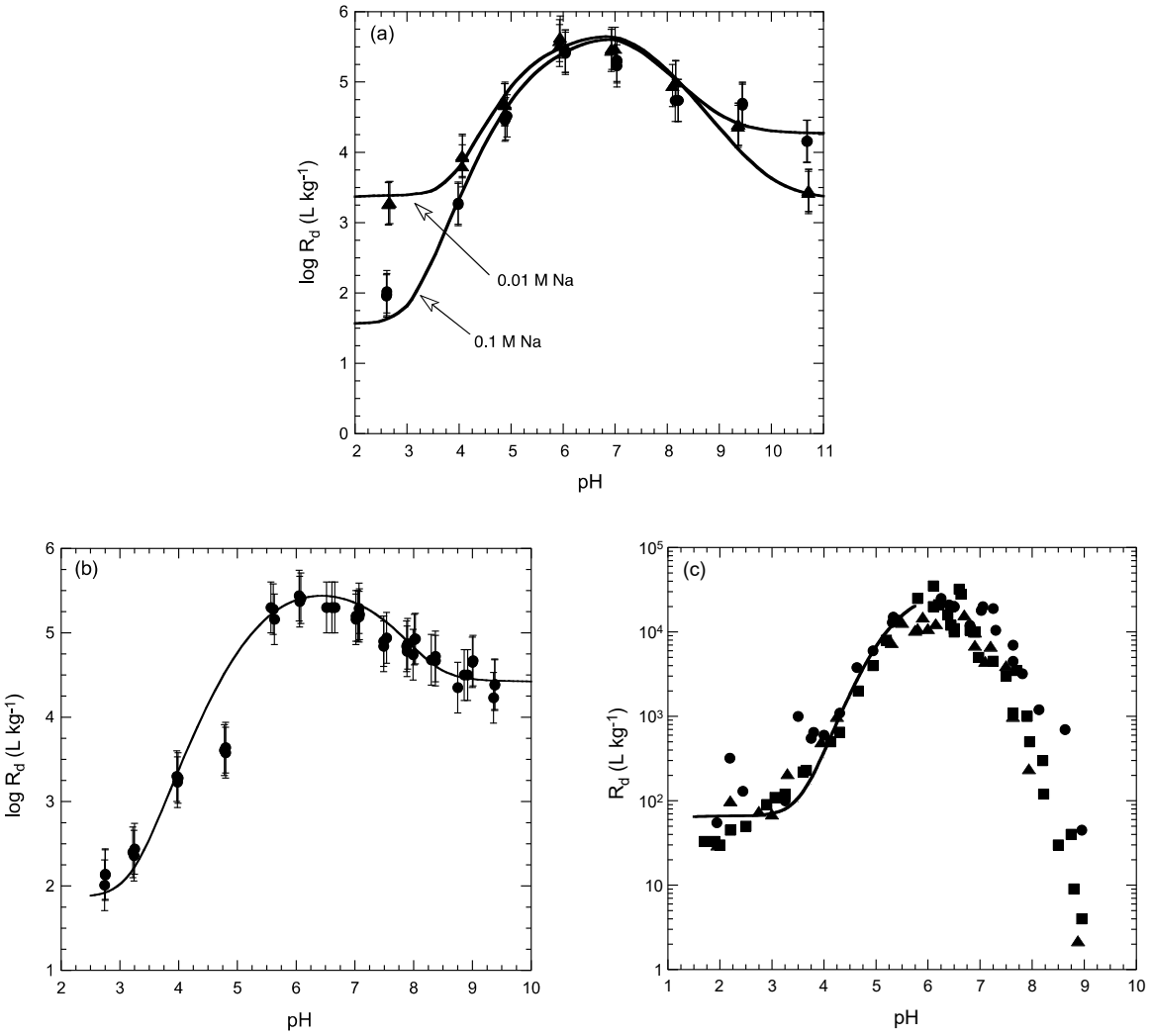

Fig. 3.12: Sorption edges for U(VI) on Na-montmorillonite.

(a) Experimental data on SWy-1 in (▲) 0.01 M $NaClO_4$ and (●) 0.1 M $NaClO_4$, $U_{TOT} < 1.4 \times 10^{-7}$ M, S = 1.2 g L^{-1} and modelled curves (—) (Bradbury & Baeyens 2005a). (b) Experimental data on SWy-1 in (●) 0.1 M $NaClO_4$, $U_{TOT} = 9 \times 10^{-8}$ M, S = 0.9 g L^{-1} and modelled curve (—) (Marques Fernandes et al. 2012). (c) Experimental data on SAz-1 (●, ■, ▲) 0.1 M $NaClO_4$, $U_{TOT} < 2 \times 10^{-7}$ M, S = 3.2 g L^{-1} (Pabalan & Turner 1997) and modelled curve (—) (Bradbury & Baeyens 2005a).

3.3 Sorption isotherms: Figures and modelled curves

A compilation of sorption isotherms for the elements Co(II), Ni(II), Zn(II), Fe(II), Eu(III), Np(V), and U(VI) measured in the pH range 5 to 9 together with the modelled curves are presented in the Figs. 3.13 to 3.18. The experimental data points are given as black circles and the modelled curves as continuous black lines. A summary of the surface complexation reactions and constants on the weak sites are given in Appendix D.

The sorption isotherms in this report are presented as sorbed radionuclide concentrations (C_{sorb}) vs. the equilibrium aqueous concentrations of active and inactive metal (C_{eq}) in a plot of log C_{sorb} vs. log C_{eq} (for more details see Baeyens & Bradbury 1995b).

3.3.1 Cobalt

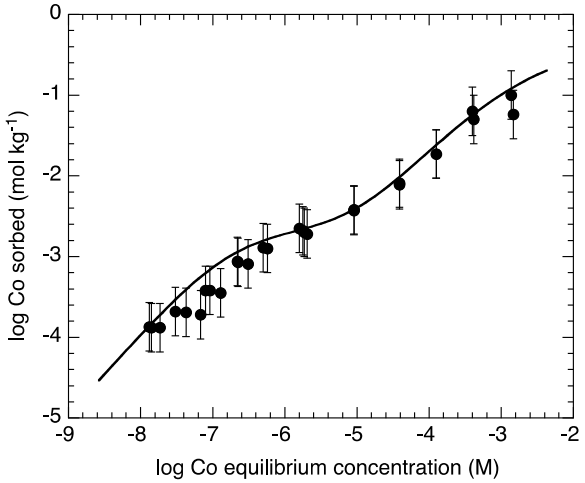

Fig. 3.13: Sorption isotherm for Co(II) on Na-SWy-2 at pH 7.3 in 0.1 M $NaClO_4$.
Experimental data (●) and modelled curve (—) (*this study*).

3.3.2 Nickel

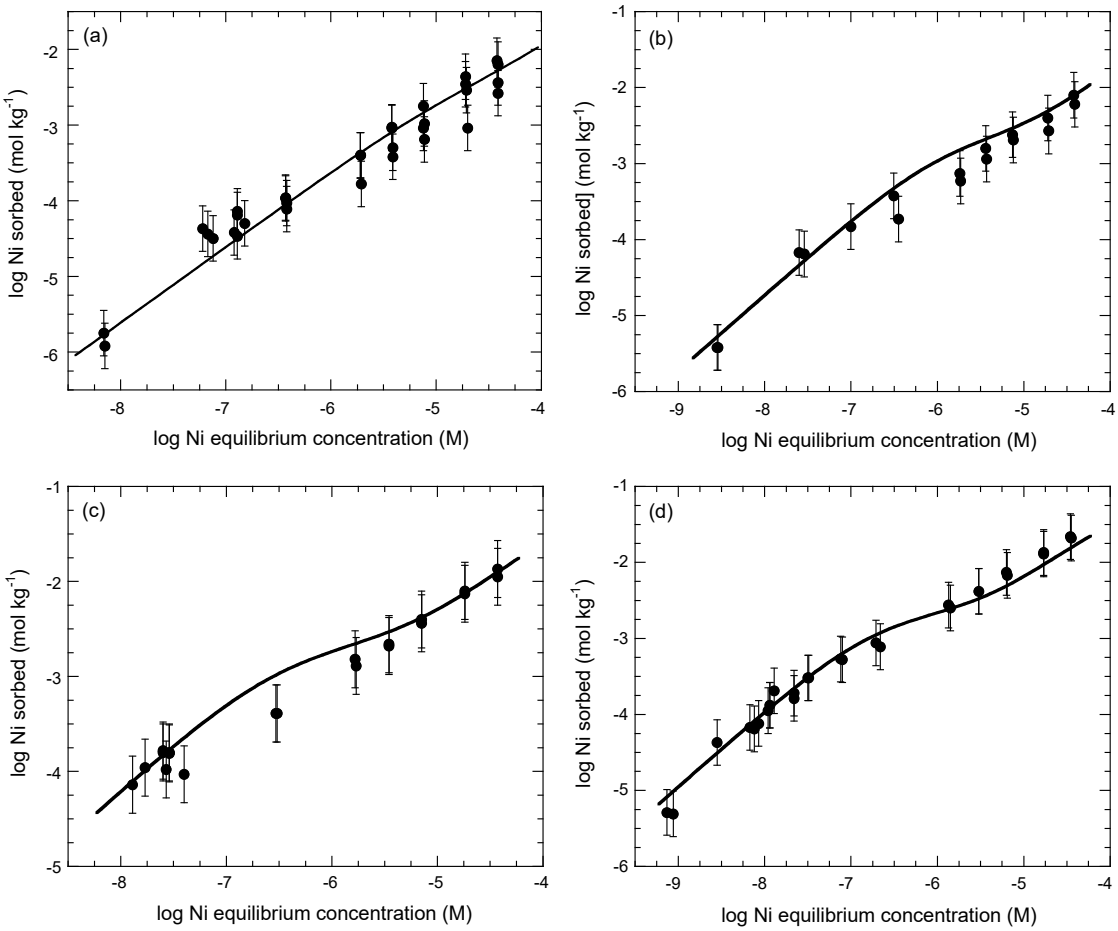

Fig. 3.14: Sorption isotherms for Ni(II) on SWy-1 in 0.1 M $NaClO_4$ at (a) pH = 5.9, (b) pH = 7.0, (c) pH = 7.7 and (d) pH = 8.2.

Experimental data (●) (Baeyens & Bradbury 1995b) and modelled curves (—) (Bradbury & Baeyens 1995).

3.3.3 Zinc

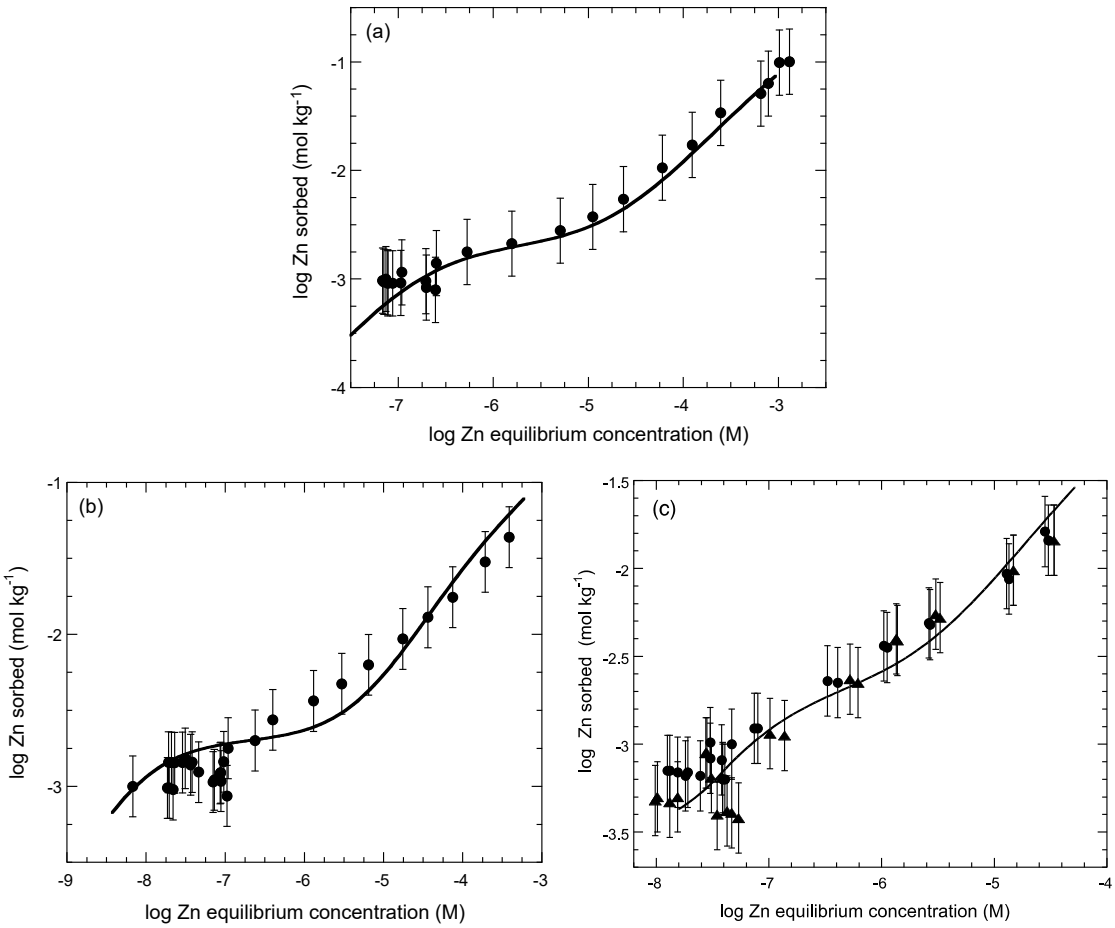

Fig. 3.15: Sorption isotherms for Zn(II) on Na-SWy-1 in 0.1 M $NaClO_4$ at (a) pH = 5.6 and (b) pH = 7.0 and on Na-Milos and Na-STx-1 at (c) pH = 7.

(a), (b) Experimental data on Na-SWy-1 (●) in in 0.1 M $NaClO_4$ (Baeyens & Bradbury 1995) and (c) on Na-Milos (●) and Na-STx-1 (▲) (Dähn et al. 2011); modelled curves (—) (*this study*).

3.3.4 Iron

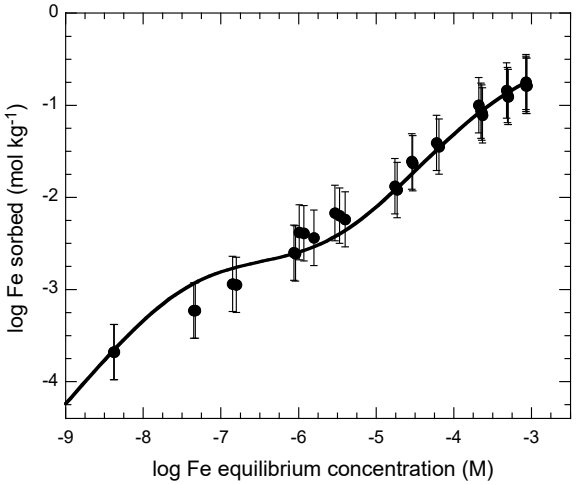

Fig. 3.16: Sorption isotherm for Fe(II) on Na-STx-1 in 0.1 M $NaClO_4$ at pH = 6.2.

Experimental data (●) (Soltermann et al. 2014) and modelled curve (—) (this study).

3.3.5 Europium

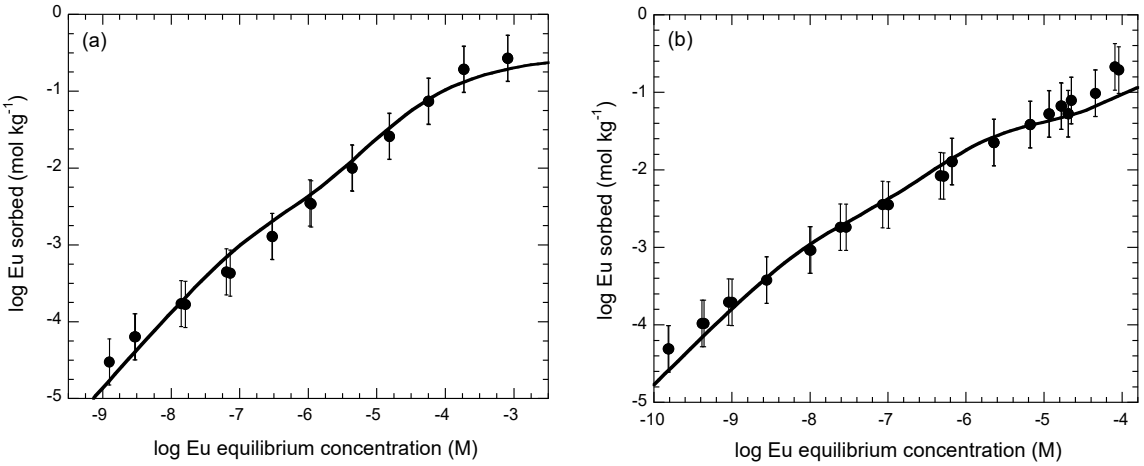

Fig. 3.17: Sorption isotherms for Eu(III) on Na-SWy-1 in 0.1 M $NaClO_4$ at pH = 6.0 (a) and pH = 7.2 (b).

Experimental data (●) (Bradbury & Baeyens 2002a) and modelled curves (—) (*this study*). Excluding aqueous Eu silicate complexes (see Appendix G).

3.3.6 Uranium

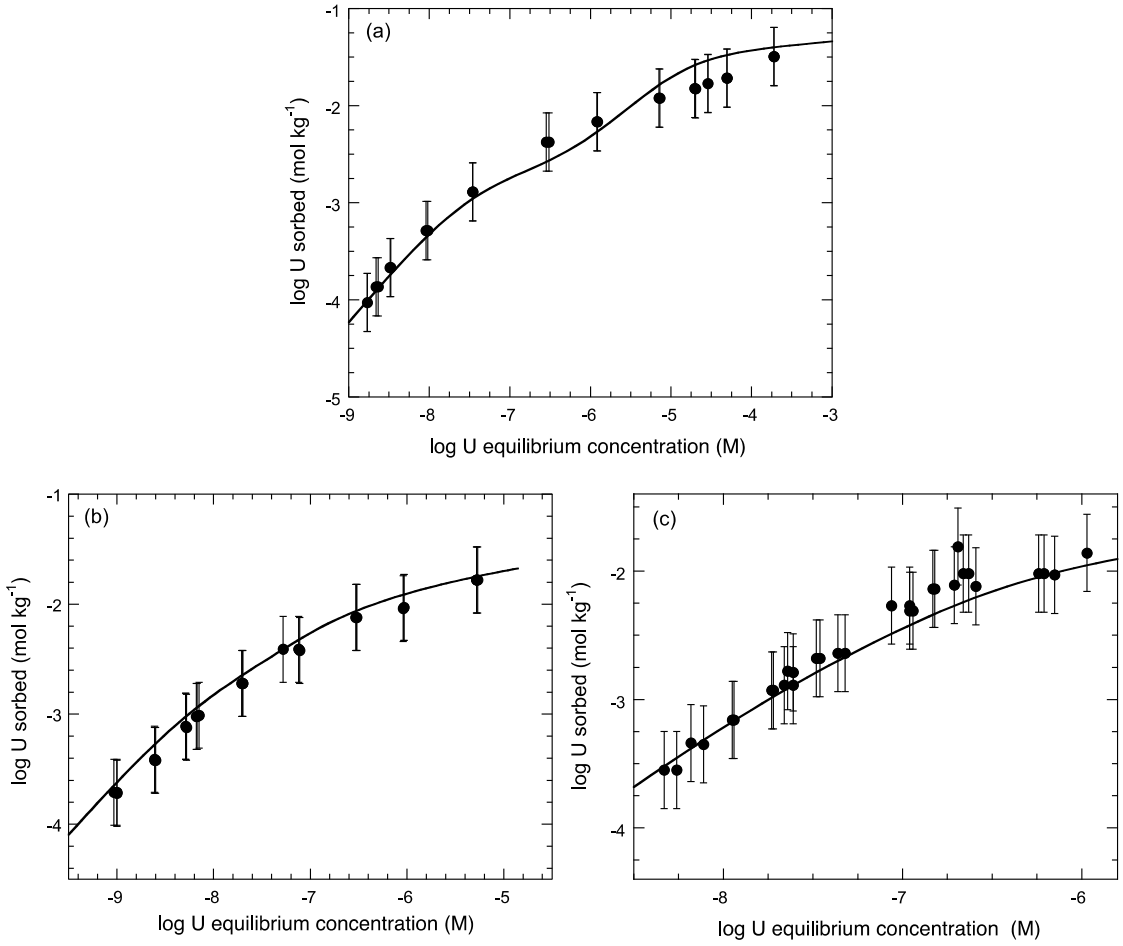

Fig. 3.18: Sorption isotherms for U(VI) on Na-SWy-1 0.1 M $NaClO_4$ at (a) pH 5.0, (b) pH 6.8 and (c) pH 8.0.

Experimental data (●) in (a) and (b) (Bradbury & Baeyens 2005a) and (c) (Marques Fernandes et al. 2012) and modelled curves (*this study*).

4 Linear free energy relationships for montmorillonite

4.1 General considerations for Linear Free Energy Relationships (LFER)

In solution thermodynamics it is common practice to seek relationships between the free energies of formation of aqueous complexes and the thermodynamic properties of the metal ions or ligands, such systematic dependencies are commonly termed linear free energy relationships, LFERs (Larsson 1934, Hammett 1940, Chapman & Shorter 1972). Surface complexation constants are difficult to derive from theoretical considerations. Therefore, the motivation behind seeking LFERs for surface site binding constants was to obtain estimates for these constants for metals where the data are either very poor or non-existent which would then allow sorption values to be calculated.

The 2SPNE SC/CE sorption model has been used to quantitatively describe sorption edge and isotherm data sets measured on montmorillonite for radionuclides with valences between II and VI (see Chapter 3).

For a metal Me with valency z_{Me}, it may be stated in general terms that an aqueous species of the form:

$$Me(OH)_{(x-1)}^{z_{Me}-(x-1)} \tag{4.1}$$

sorbs to form a surface complex of the form:

$$\equiv S^{S}OMe(OH)_{y}^{z_{Me}-(y+1)} \tag{4.2}$$

which in turn correlates with the hydrolysed species:

$$Me(OH)_{x}^{z_{Me}-x} \tag{4.3}$$

where $x = y + 1$ and all three equations are valid when $x \geq 1$.

Generally, a good systematic linear correlation between the logarithms of the surface site binding constants on the strong and weak sites and the logarithm of the corresponding aqueous hydrolysis constants ${}^{OH}K_x$ was found (Fig. 4.1).

4.2 Further considerations to the LFERs approach

Although the LFER correlation such as that shown in Fig. 4.1a for the strong sites on montmorillonite look very good, i.e. extend over more than 30 orders of magnitude and has a correlation coefficients, R, near to unity implying that the probability that the values are linearly correlated lies very close to 100 % (Taylor 1982), closer inspection shows that there are some difficulties associated with the LFERs in their current form.

There may be significant errors associated with the hydrolysis constants given in Appendix B. Broadly speaking the first hydrolysis constant values tend to be the most reliable because they can often be determined at high metal concentrations by potentiometric methods. An optimistic estimate for the uncertainty in log ${}^{OH}K_1$ values might be ± 0.1 but could be as high as ± 0.5. For the 1:2, 1:3 etc. hydrolysed species the constants are often obtained by fits to solubility measure-

ments in which, for example, it is not always clear what the solid phase is, and solubility products and hydrolysis constants have to be fitted simultaneously. For these hydrolysis constants the values may be poorly defined.

At higher sorption values (> ~ 10^4 L kg^{-1}), generally occurring at higher pH values (> 8.5), there is scatter in the sorption values which may be ± 0.5 log units or more. Therefore, the error in the surface complexation constants modelled in this region are of this order.

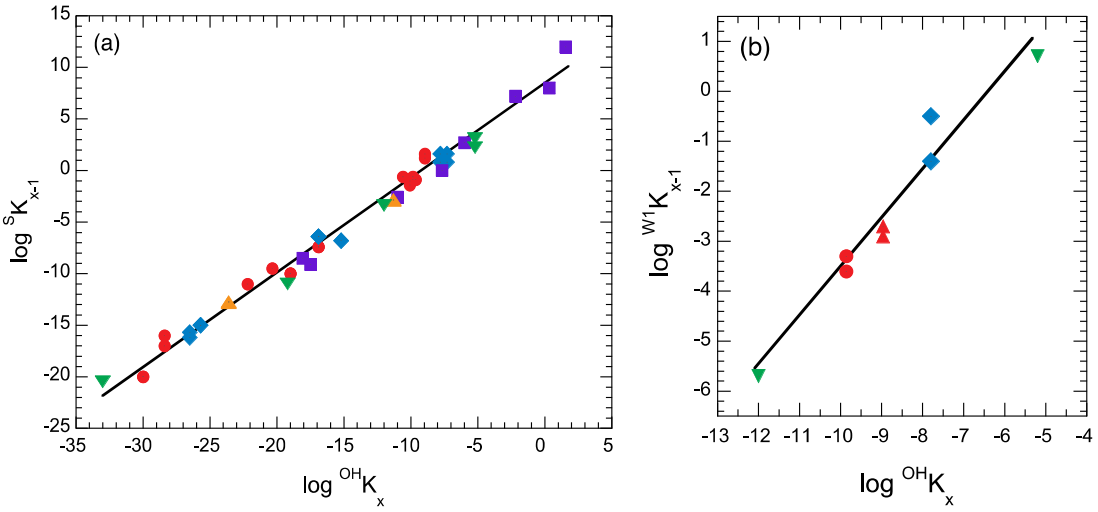

Fig. 4.1: Correlation of surface complexation constants of species sorbing on the strong sites of montmorillonite (a) and the weak sites of montmorillonite (b) with the corresponding hydrolysis constants (Bradbury & Baeyens 2005b).

Strong sites of montmorillonite: (●) Mn(II), Co(II), Cd(II), Ni(II), Zn(II), (◆) Eu(III), Am(III), (■) (Sn(IV), Th(IV), (▲) Np(V), (▼) U(VI) and weak sites of montmorillonite: (●) Ni(II), (▲) Zn(II), (◆) Eu(III) and (▼) U(VI).

The LFERs for ≡S^{S}OH sites presented for montmorillonite (Fig. 4.1a) include surface complexation constants for all of the metals investigated, irrespective of their valence. In view of the discussion in section 2.3 and in Bradbury et al. (2017) on competition in which it was concluded that metals in the same valence state have their own set of strong sites, it would now seem to be inconsistent to plot all metals together. Rather, only metals with the same valence should be included in LFER plots.

Generally, the whole of the sorption edge data has been considered, normally in the pH range ~ 3 to over 10, and all of the modelled surface complexation constants have been included in the LFER plots. At low pH values (~ < 5) and high pH values (> 9) 2:1 clay minerals are unstable and tend to dissolve. Further, in real bentonite systems the pH range of interest is ~ 7 to ~ 8.

The above considerations lead to the following proposals for modified LFER plots.

Separate LFER plots should be made for divalent transition metals, trivalent actinides and tetravalent metals. This condition arises from the results from sorption competition experiments. Only those surface complexation constants making major contributions to the sorption in the range $5 \leq pH \geq 9$ should be considered in the LFER plots. This restriction takes into account the 2:1 clay mineral stability issue, reflects the pH range important in real systems, and in many cases

(but not all) tends to result in the use of the first (and most reliable) hydrolysis constant values in the LFERs. The hydrolysis constants and corresponding surface complexation constants selected according to the above considerations are shown in bold type in Appendices B and C/E respectively and are used in the modified LFERs for montmorillonite (Figs. 4.7, 4.10, 4.12 and 4.18).

A number of comments need to be made concerning the LFERs for montmorillonite given here.

Firstly, the relationships between surface complexation constants and aqueous hydrolysis constants given in the following sections for montmorillonite are dependent on the sorption model itself, the model parameters used and the values of the stability constants for the hydrolysed species. Therefore, sorption model, surface parameters, hydrolysis constants and surface stability constants constitute an inseparable unit.

Secondly, in the case of tri- and tetravalent elements the number of elements for which there are data is limited, as is the number of data points in the LFERs. For trivalent metals, only data for Eu and Am are available, and both elements have essentially the same hydrolysis constants. For tetravalent metals, only data for Sn and Th are available. The chemistries of Sn and tetravalent actinides are so different that it was not considered justifiable to plot them together. Only the data for Th were plotted on a LFER. Unfortunately, the lack of data does not allow anything better at the present time. The above factors should be clearly held in mind if the LFERs for trivalent and tetravalent elements are used.

Thirdly, there is no information available on sorption competition on the weak sites. Because the site capacity of the weak sites is so large, no competitive sorption is assumed to take place on them. Also, it is currently not known whether there are different sorption site types for the different valence state of sorbing metals (*c.f.* strong sites). The assumption is made here that metals of different valence can be included on the same LFER plot.

In section 4.3 the data sources and modelled curves are as referenced in Chapter 3.

4.3 Derivation of revised LFERs from speciation and modelling

4.3.1 Divalent transition metals: Co, Ni, Zn, Fe, Cd

In the following, plots of the aqueous speciation and surface speciation of each metal are shown. The aqueous sorbing species and the corresponding sorbed complexes are colour coded. Uptake by cation exchange is represented by broken black lines and surface complexation by continuous lines in the sorption edges.

From Figs. 4.2a to 4.6a it can be seen that the most prominent aqueous species in the pH range 5 to 9 are Co^{2+}, Ni^{2+}, Zn^{2+}, Fe^{2+} and Cd^{2+} respectively, which are also the dominant sorbing species (Figs. 4.2b to 4.6b, forming $\equiv^{S}SOCo^{+}$, $\equiv^{S}SONi^{+}$, $\equiv^{S}SOZn^{+}$, $\equiv^{S}SOFe^{+}$ and $\equiv^{S}SOCd^{+}$, respectively (the sorbing aqueous species has the same colour as the sorbed complex). According to section 4.1, the correlating hydrolysed species are $CoOH^{+}$, $NiOH^{+}$, $ZnOH^{+}$, $FeOH^{+}$ and $CdOH^{+}$, respectively.

Thus, a modified LFER for divalent transition metals for the pH range 5 to 9 can be constructed from the surface complexation constants and hydrolysis constants given in bold in Appendices B and C (Tab. C3; Fig. 4.7).

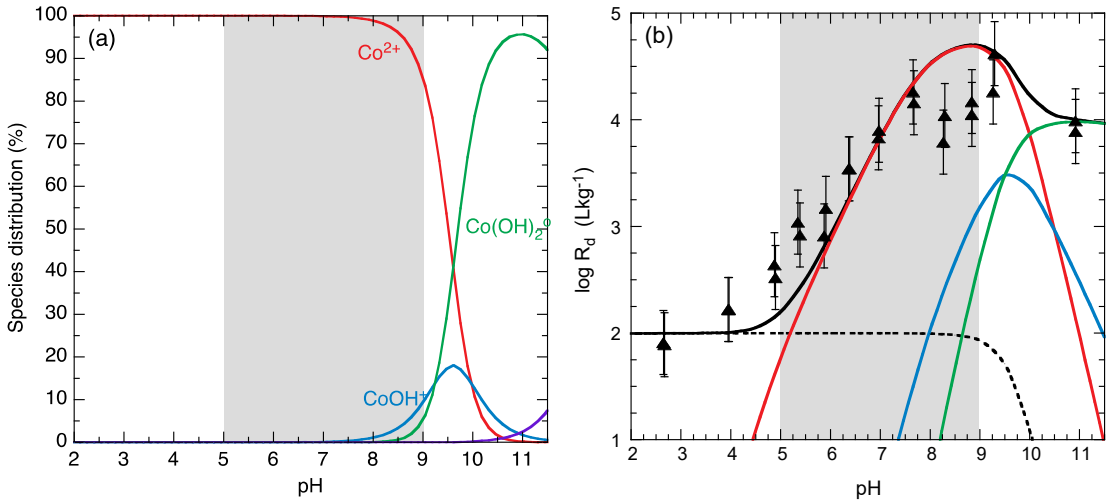

Fig. 4.2: (a) The aqueous speciation (Co_{TOT} = 10^{-8} M) and (b) sorption edge for Co(II) on Na-SWy-2 in 0.1 M $NaClO_4$.

Corresponding to Fig. 3.1.

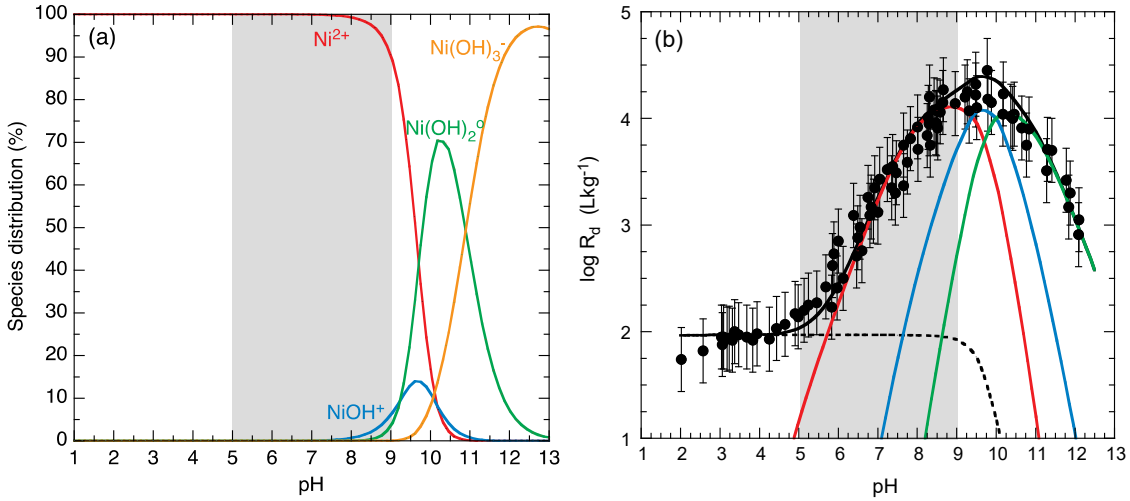

Fig. 4.3: (a) The aqueous speciation (Ni_{TOT} = 10^{-8} M) and (b) sorption edge for Ni(II) on Na-SWy-1 in 0.1 M $NaClO_4$.

Corresponding to Fig. 3.2.

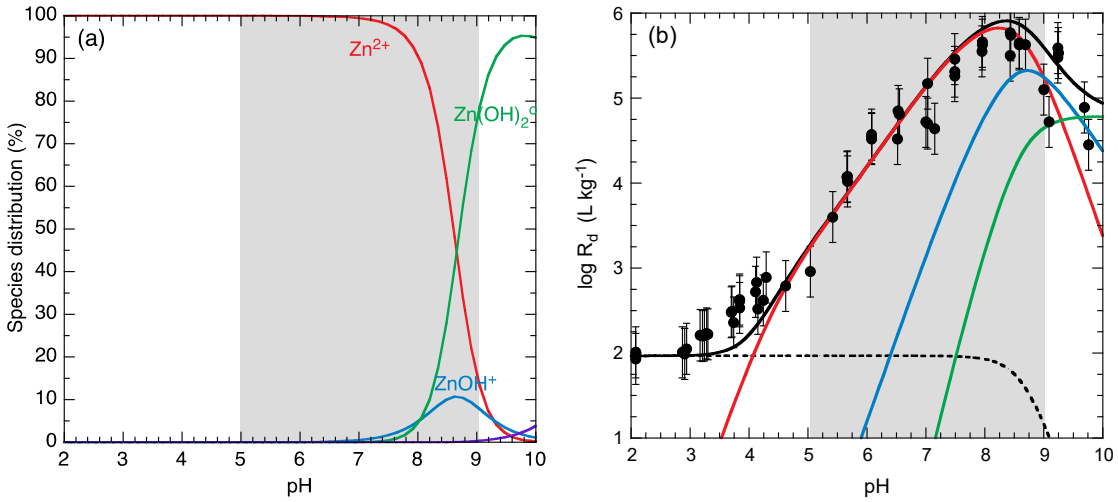

Fig. 4.4: (a) Aqueous speciation (Zn_{TOT} = 10^{-8} M) and (b) sorption edge for Zn(II) on Na-SWy-1 in 0.1 M $NaClO_4$.

Corresponding to Fig. 3.4.

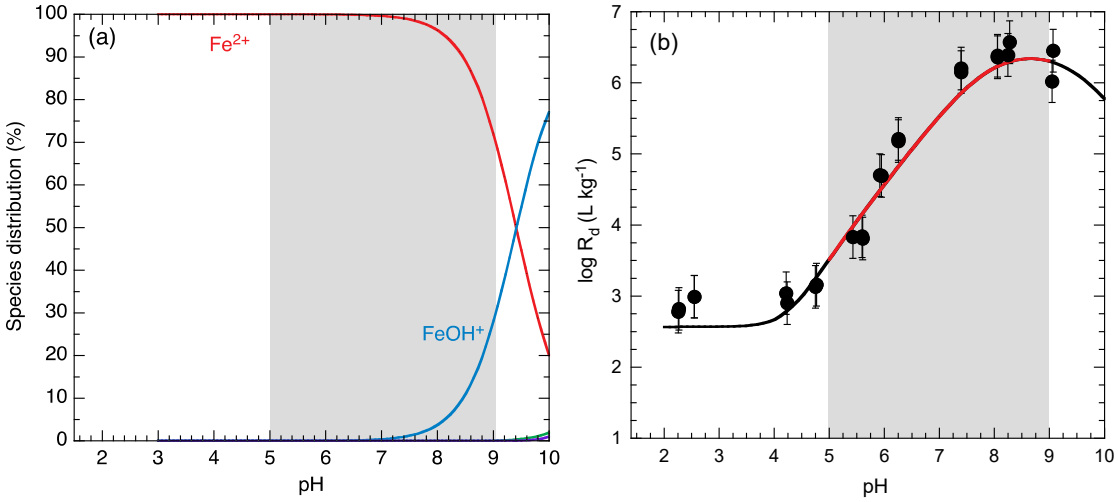

Fig. 4.5: (a) The aqueous speciation (Fe_{TOT} = 10^{-8} M) and (b) sorption edge for Fe(II) on Na-STx-1 in 0.1 M $NaClO_4$.

Corresponding to Fig. 3.5.

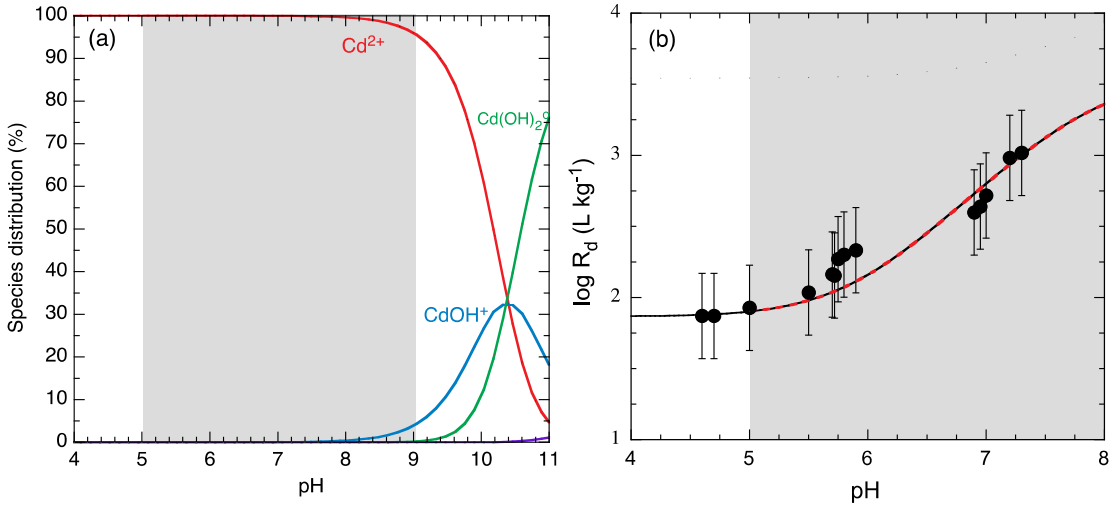

Fig. 4.6: (a) The aqueous speciation ($Cd_{TOT} = 10^{-8}$ M) and (b) sorption edge for Cd(II) on Na-SWy-1 in 0.1 M NaClO4.

Corresponding to Fig. 3.3.

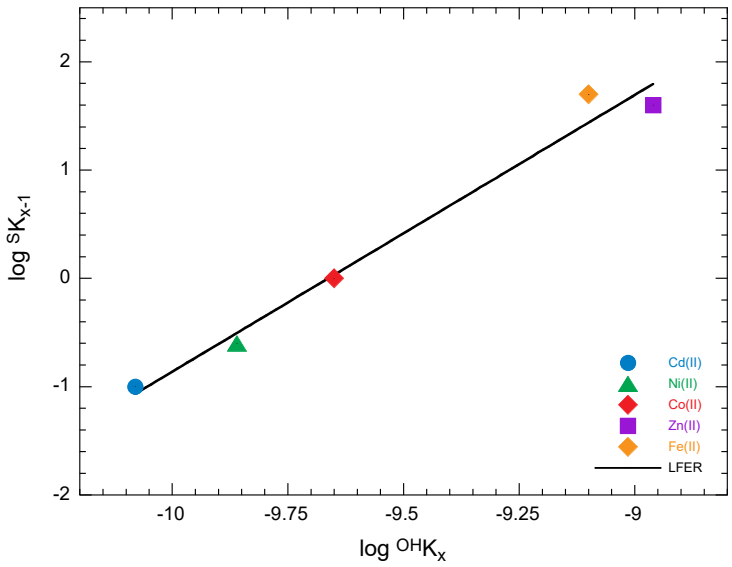

Fig. 4.7: LFER of divalent transition metals on strong sites using the hydrolysis constants from Appendix B and the surface complexation constants from Appendix C (Tab. C1).

Values in bold type: $\log {}^{S}K_{x-1} = (24.70 \pm 2.0) + (2.56 \pm 0.21) \log {}^{OH}K_x$ (R = 0.990).

4.3.2 Trivalent lanthanides and actinides metals: Eu, Am

Speciation and surface species plots for Eu and Am are illustrated below. It should be noted that the hydrolysis constants for Eu and Am are taken to be the same, Appendix B. Again, the aqueous sorbing species and the corresponding sorbed complexes are colour coded.

From Figs. 4.8a and 4.9a it can be seen that the most prominent aqueous species in the pH range 5 to 9 are Eu^{3+}, $EuOH^{2+}$ and $Eu(OH)_2^+$ and Am^{3+}, $AmOH^{2+}$ and $Am(OH)_2^+$ respectively, which are also the dominant sorbing species (Figs. 4.8b and 4.9b). From this a modified LFER can be made taking the hydrolysis and surface complexation constants given in bold in Appendix B and Appendix C (Tab. C3) respectively and Fig. 4.10.

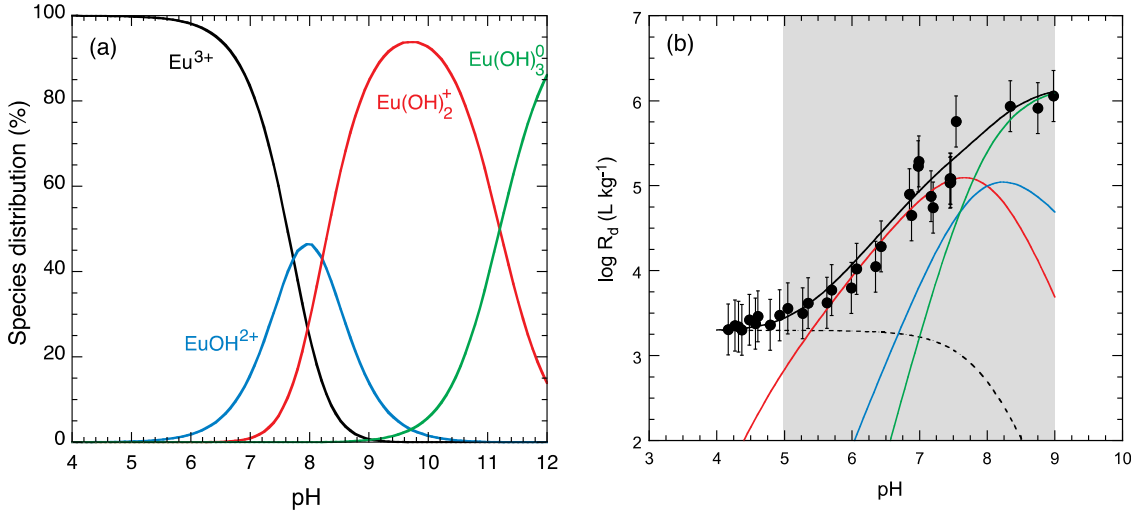

Fig. 4.8: (a) The aqueous speciation ($Eu_{TOT} = 10^{-8}$ M) and (b) sorption edge for Eu(III) on Na-SWy-1 in 0.1 M $NaClO_4$.

Corresponding to Fig. 3.6a.

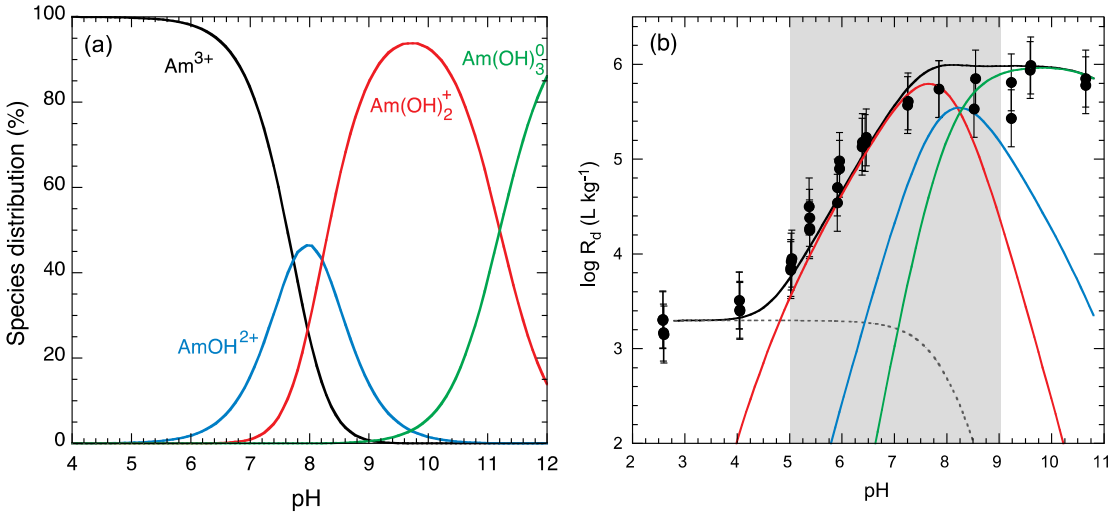

Fig. 4.9: (a) The aqueous speciation ($Am_{TOT} = 10^{-8}$ M) and (b) sorption edge for Am(III) on Na-SWy-1 in 0.1 M $NaClO_4$.

Corresponding to Fig. 3.7b.

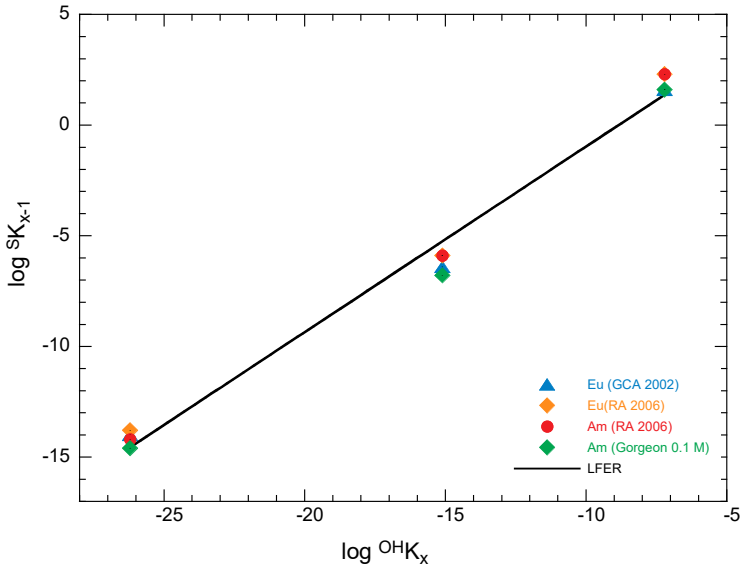

Fig. 4.10: LFER of trivalent elements on strong sites using the hydrolysis constants from Appendix B and the surface complexation constants from Tab. C3 (values in bold).

$\log {}^{S}K_{x-1} = (7.41 \pm 0.57) + (0.84 \pm 0.03) \log {}^{OH}K_x$ (R = 0.993).

4.3.3 Tetravalent actinides metals: Th(IV)

Speciation and surface complex plots for tetravalent Th are illustrated in Fig. 4.11. From these plots it can be seen that the most prominent aqueous hydrolysed species in the pH range 5 to 9 are $Th(OH)^{3+}$, $Th(OH)_2^{2+}$, $Th(OH)_3^{+}$ and $Th(OH)_4^{0}$ which are also the dominant sorbing species (Fig. 4.11b). From this a modified LFER can be made taking the hydrolysis surface and complexation constants given in bold in Appendix B and C (Tab. C4) respectively and Fig. 4.12. However, for the sorbed complex $\equiv SOTh(OH)_4^-$, there is no corresponding aqueous hydrolysis species and can therefore not be included in the LFER plot.

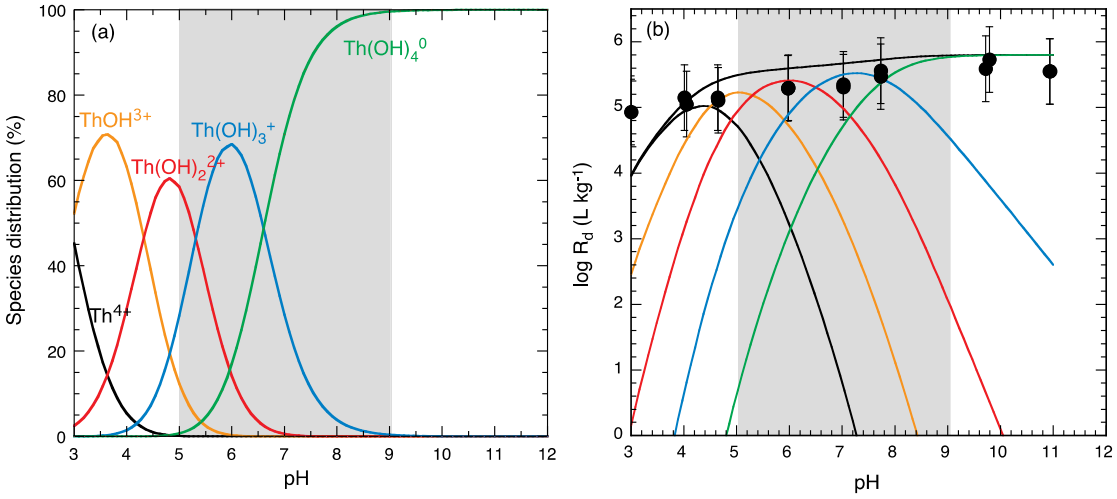

Fig. 4.11: (a) The aqueous speciation ($Th_{TOT} = 10^{-8}$ M) and (b) sorption edge for Th(IV) on Na-SWy-1 in 0.1 M $NaClO_4$.

Corresponding to Fig. 3.9.

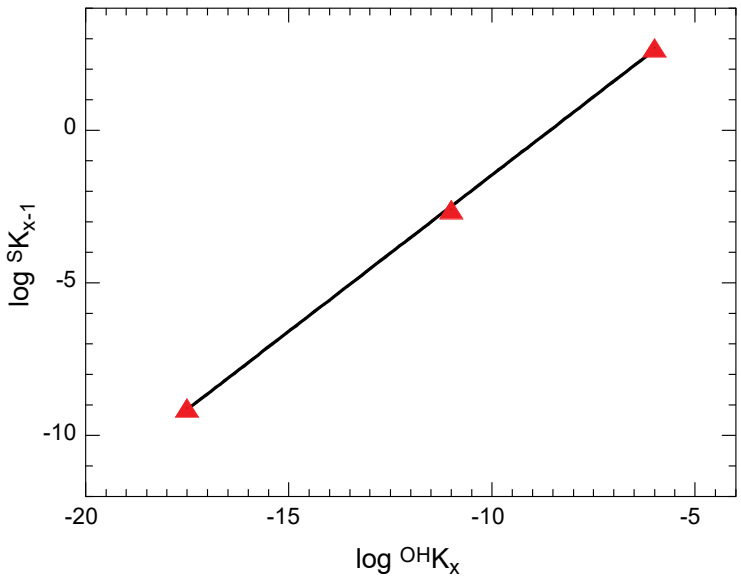

Fig. 4.12: LFER of tetravalent elements on strong sites using the hydrolysis constants from Appendix B and the surface complexation constants from Appendix C, Tab. C4 (values in bold type).

$\log {}^{S}K_{x-1} = (8.79 \pm 0.21) + (1.02 \pm 0.02) \log {}^{OH}K_x$ (R = 0.999).

4.3.4 Summary of the equations for the modified LFERs

The LFERs for strong sites on montmorillonite can be described by the following equations:

Divalent transition metals

$$\log {}^{S}K_{x-1} = (24.70 \pm 2.0) + (2.56 \pm 0.21) \log {}^{OH}K_x \quad (R = 0.990) \tag{4.4}$$

Trivalent lanthenides and actinides

$$\log {}^{S}K_{x-1} = (7.41 \pm 0.57) + (0.84 \pm 0.03) \log {}^{OH}K_x \quad (R = 0.993) \tag{4.5}$$

Tetravalent actinides

$$\log {}^{S}K_{x-1} = (8.79 \pm 0.21) + (1.02 \pm 0.02) \log {}^{OH}K_x \quad (R = 0.999) \tag{4.6}$$

where "x" is an integer in all the above equations.

4.3.5 Metals for which sorption edge data are available, but are not included in the LFERs: Sn(IV), Np(V), Pa(V) and U(VI)

4.3.5.1 Sn(IV)

The results of the speciation and modelling calculations are shown in Fig. 4.13. The hydrolysis behaviour of Sn is very uncertain, especially in the acidic region. It was not possible to model the Sn sorption edge using the hydrolysis constants given in Hummel et al. (2002) alone. In some previous work Bradbury & Baeyens (2005a) used the first four conditional hydrolysis constants (log Q values) given in Baes & Mesmer (1976), converted to thermodynamic constants, and the Hummel et al. (2002) hydrolysis constants re-written with Sn^{4+} as the master species instead of $Sn(OH)_4^0$ (Appendix B) to calculate the Sn speciation (Fig. 4.13a), and model the Sn sorption edge. Although the modelling appeared to be successful (Fig. 4.13b), it has to be pointed out that there is considerable uncertainty concerning the log Q values given in Baes & Mesmer (1976), but there are, at present, no better hydrolysis data available in the open literature (Thoenen 2015, pers. comm.). In the pH range 5 to 9 the major aqueous species are $Sn(OH)_4^0$ and $Sn(OH)_5^-$, but the main sorbing species, according to the modelling, are $Sn(OH)_3^+$ and $Sn(OH)_4^0$, dominated by the uptake of the former. This behaviour is different from that observed in all previously described cases.

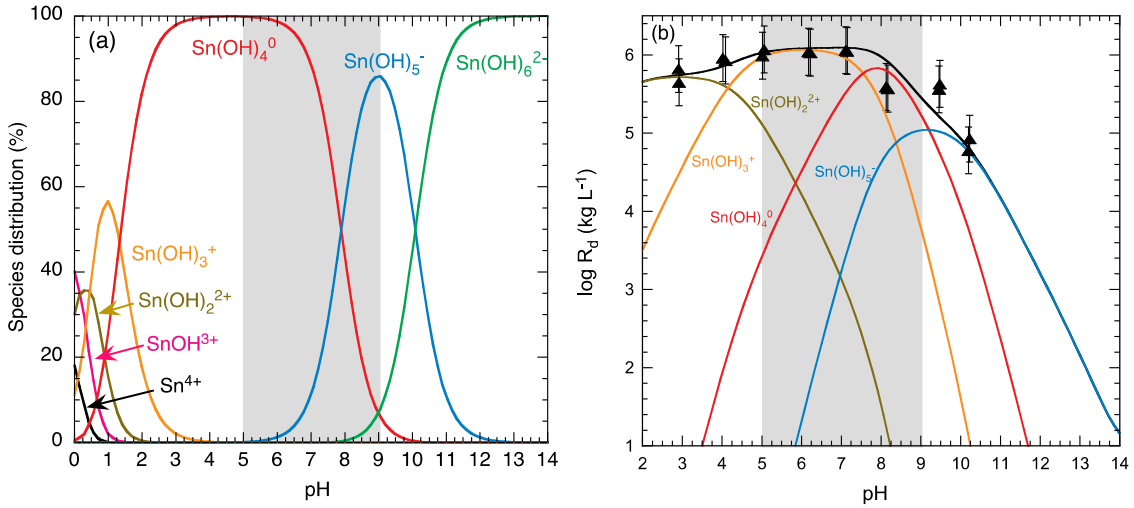

Fig. 4.13: (a) The aqueous speciation ($Sn_{TOT} = 10^{-8}$ M) and (b) sorption edge for Sn(IV) on Na-SWy-1 in 0.1 M $NaClO_4$.

Corresponding to Fig. 3.8.

4.3.5.2 Np(V), Pa(V)

The results of the speciation and modelling calculations for Np(V) and Pa(V) are shown in Figs. 4.14 and 4.15, respectively.

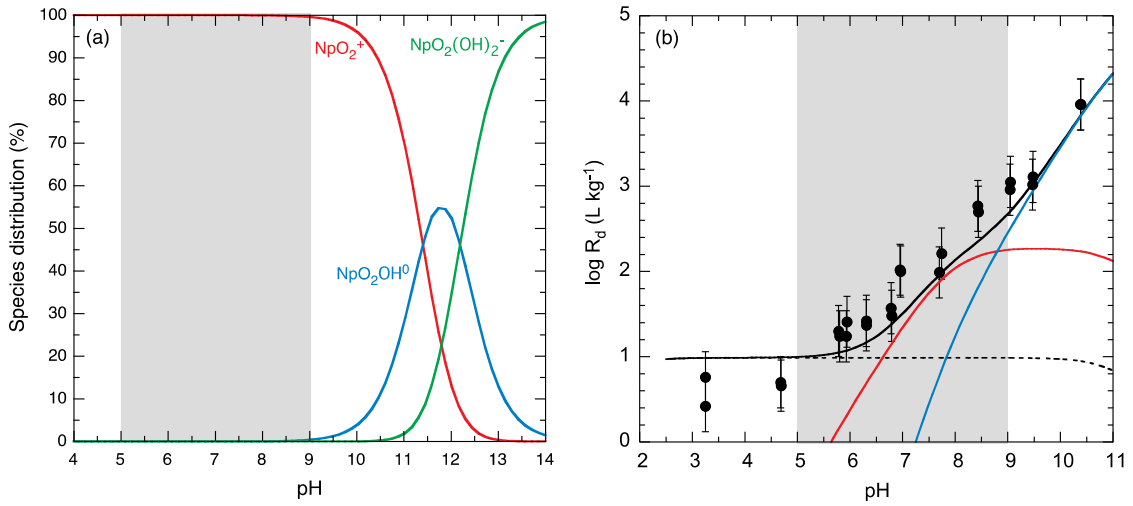

Fig. 4.14: (a) The aqueous speciation (Np_{TOT} = 10^{-8} M) and (b) sorption edge for Np(V) on Na-SWy-1 in 0.1 M $NaClO_4$.

Corresponding to Fig. 3.11a.

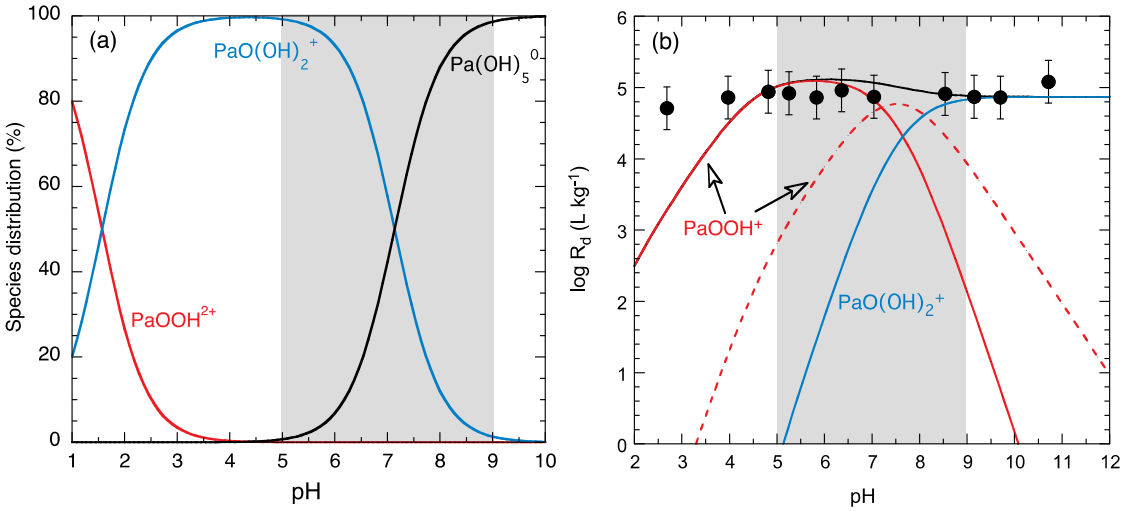

Fig. 4.15: (a) The aqueous speciation (Pa_{TOT} = 10^{-8} M) and (b) sorption edge for Pa(V) on Na-SWy-1 in 0.1 M $NaClO_4$.

Corresponding to Fig. 3.10.

The significant differences in the speciation behaviour of Np(V) and Pa(V) do not allow a LFER with these pentavalent elements to be made.

4.3.5.3 U(VI)

The results of the speciation and modelling calculations for U(VI) are shown in Fig. 4.16.

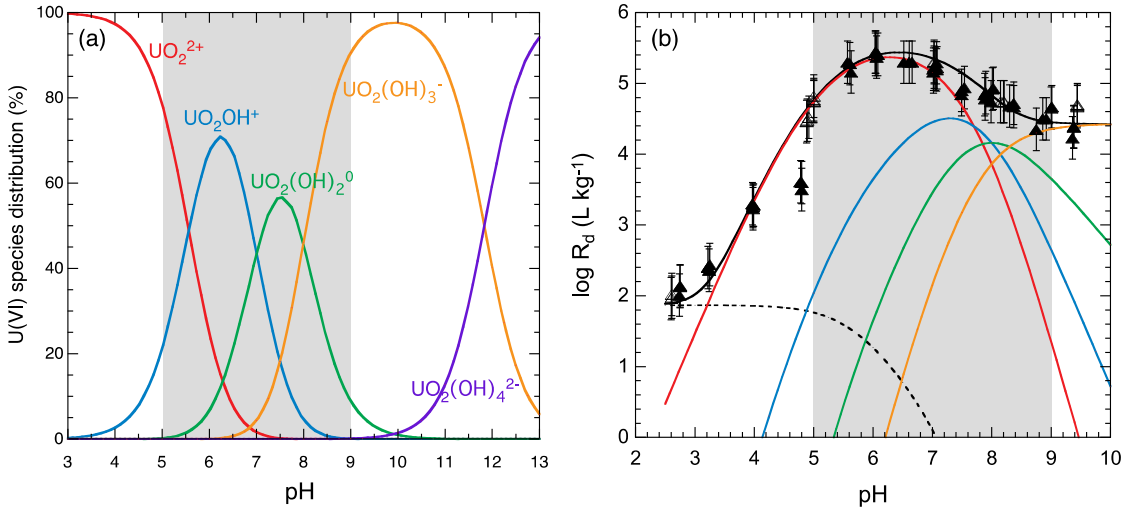

Fig. 4.16: The aqueous speciation (U_{TOT} = 10^{-8} M) and sorption edge for U(VI) on Na-SWy-1 in 0.1 M $NaClO_4$.

Corresponding to Fig. 3.12a (0.1 M $NaClO_4$) and Fig. 3.12b.

A LFER for the hexavalent uranyl can be made for the monomeric U species. However, there are no other hexavalent elements for which sorption data needs to be derived, hence there is no need for a LFER.

4.4 LFERs for weak sites

For the elements Ni(II), Co(II), Zn(II), Fe(II), Eu(III) and U(VI) isotherms in the pH range from 5 to 8 have been measured and surface complexation constants for weak sites derived. The LFER for the weak sites (Fig. 4.17) was constructed for the above metals from the hydrolysis constants given in Appendix B (bold type) and the surface complexation constants given in Appendix C (Tab. C6). As mentioned previously in section 4.2, it is assumed that there is no sorption competition on the weak sites and all metals can be included in the LFER plot in Fig. 4.19.

For the tetravalent elements Sn and Th, and the pentavalent Pa, no isotherms are available due to solubility limits.

Np(V) isotherms have been measured, but no weak sites were needed to fit the data. In the pH and Np equilibrium concentration range considered, sorption on strong sites and planar sites was sufficient to describe the isotherms measurements.

The LFER for weak sites can be described by the following equation:

$$\log {}^{W1}K_{x-1} = (5.67 \pm 0.63) + (0.91 \pm 0.07) \log {}^{OH}K_x \qquad (R = 0.98) \qquad (4.7)$$

where "x" is an integer equal to or greater than unity.

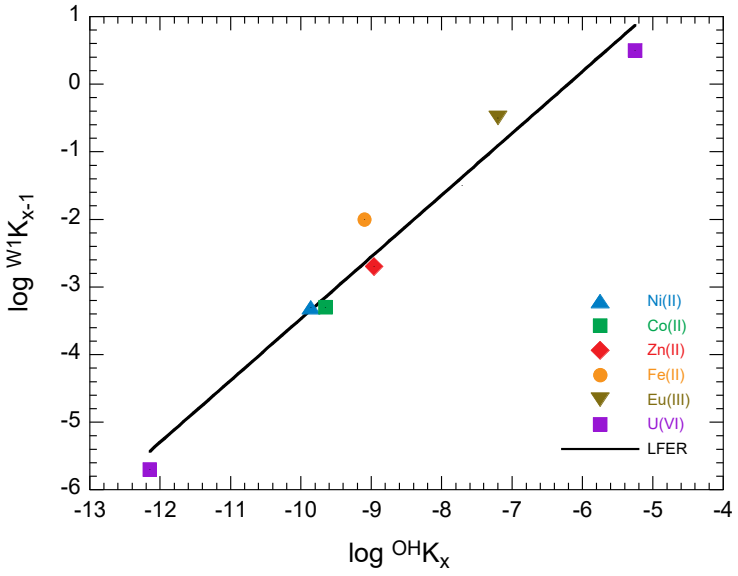

Fig. 4.17: LFER of elements on weak sites using the hydrolysis constants from Appendix B and the surface complexation constants from Appendix D (Tab. D1; values in bold type).

$\log {}^{W1}K_{x-1} = (5.67 \pm 0.63) + (0.91 \pm 0.07) \log {}^{OH}K_x$ (R = 0.98).

5 Comparison of the sorption predicted from LFERs with measured values

The inevitable result arising from the restrictions given above in section 4.2 is that the number of data points in each of the LFERs is considerably reduced, which may give rise to questions regarding their general applicability. Also, the LFERs average out the surface complexation constants derived from the experimental measurements in which the errors at higher sorption values may be as high as ± 0.5 log units. (Note: a general uncertainty value for all of the sorption measurements has been taken to be ± 0.3 log units.) Consequently, the sorption values calculated for a particular radionuclide from the appropriate LFER equation might not necessarily be expected to exactly reproduce the measured sorption data because of this averaging process occurring over many data sets.

Balanced against this is that the LFERs provide a chemically consistent, plausible and internally consistent relation between metal hydrolysis constants and surface complexation constants resulting from the application of a sorption model in which all of the basic parameters are fixed (Appendix A) for a particular clay mineral, irrespective of the metal under consideration. It may be argued that averaging over the data from many separate measurements performed at different times on samples of clay minerals sometimes obtained from different sources and subjected to different treatments may provide a more realistic representation of "sorption in general" than just relying on individual measurements.

The exercise illustrated in the following is intended to try to put the use of data from LFERs into some kind of perspective. The idea is to take the surface complexation constants for specific metals from the appropriate LFERs and compare the sorption edges/isotherms calculated with these values with the measured ones.

In the following, the measured sorption edge/isotherm data for Co(II), Ni(II), Zn(II), Fe(II), Eu(III), U(VI) and sorption edges for Cd(II), Am(III), and Th(IV) (filled circles) and modelled curves (black continuous lines) are compared with curves calculated with surface complexation constants taken from the appropriate LFERs (red continuous lines). The calculations were only performed in the pH range 5 to 9. All comparisons are grouped element by element.

The surface complexation constants derived from the LFERs (Eqs. 4.4 to 4.7) and used in the calculations are summarised in Tab. 5.1. The K_c values used are taken from Appendix D. In the case of U(VI), surface complexation constants derived from LFERs are only available for the weak sites. The predicted sorption edge and/or isotherm curves are shown in Figs. 5.1 to 5.8 element by element.

These comparisons give an idea of the quality of the sorption values which would be predicted just using surface complexation constants taken from LFERs. From all the graphs shown, it can be seen that all predictions based on the LFERs are within ± 0.5 log units of the experimental data. The only exceptions to this are Figs. 5.7b and 5.8. For Th there is no correlating hydrolysis constant for the $=S^sOTh(OH)_4^-$ surface complex.

The results of this exercise give an idea of the quality of the predictions of sorption values that might be predicted from LFER data for metals for which no measurements are available and for which the appropriate LFER exists (see Chapter 7).

Tab. 5.1: Surface complexation constants for the elements Ni(II), Zn(II), Fe(II), Cd(II), Eu(III), Am(III) and Th(IV) taken from LFER for strong and weak sites and the corresponding hydrolysis constants.

Element	**Hydrolysis constants**	**Surface complexation constants**	
	log ^{OH}K	log ^{S}K	log ^{W1}K
Ni(II)	-9.86	-0.54	-3.30
Zn(II)	-8.96	1.76	-2.48
Fe(II)	-9.1	1.40	-2.61
Cd(II) *	-10.08	-1.10	-
Eu(III)/	-7.2	1.36	-0.88
Am(III)	-15.1	-5.27	
	-26.2	-14.60	
Th(IV) *	-6.0	2.67	
	-11.0	-2.43	
	-17.5	-9.06	

* There are no measured isotherms for Cd and Th.

5.1 Cobalt

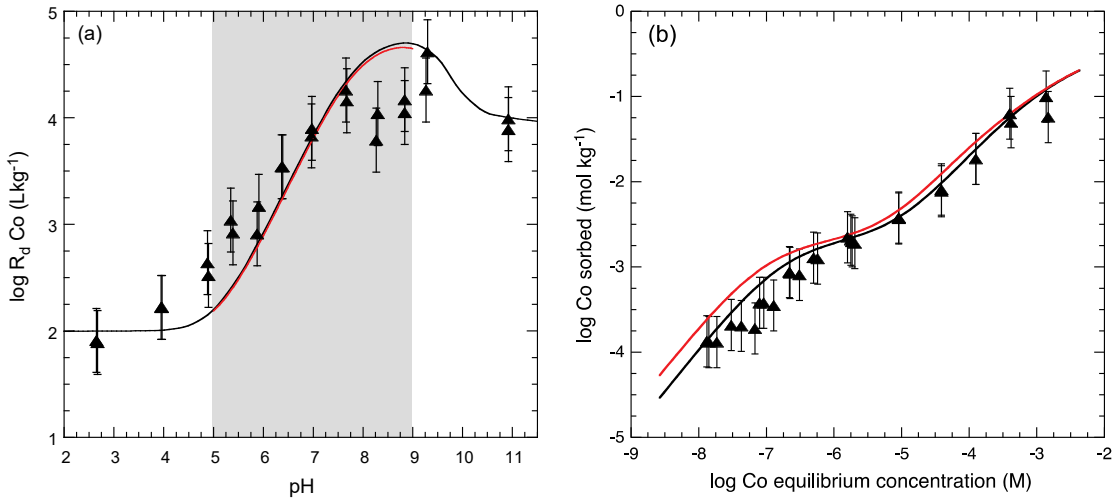

Fig. 5.1: Comparison of LFER calculations with model predictions for Co(II): (a) Measured sorption edge and (b) isotherm at pH 7.25.

Experimental data (▲) and modelled curves (—). Predicted curves in the pH range 5 to 9 (—) using the surface complexation constants given in Tab. 5.1.

5.2 Cadmium

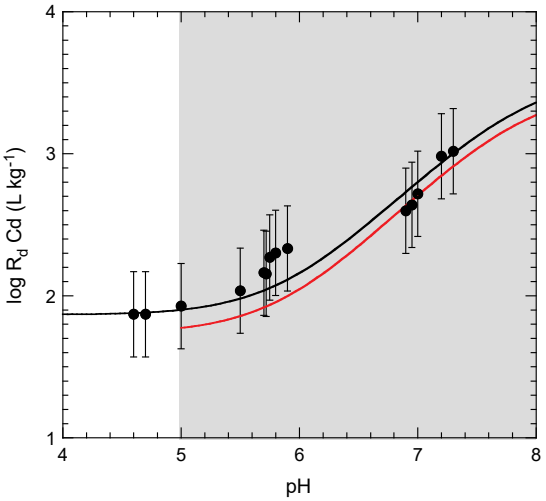

Fig. 5.2: Comparison of LFER calculations with model predictions for Cd(II).

Measured sorption edge (●) and modelled curve (—). Predicted curve in the pH range 5 to 9 (—) using the surface complexation constants given in Tab. 5.1.

5.3 Ferrous iron

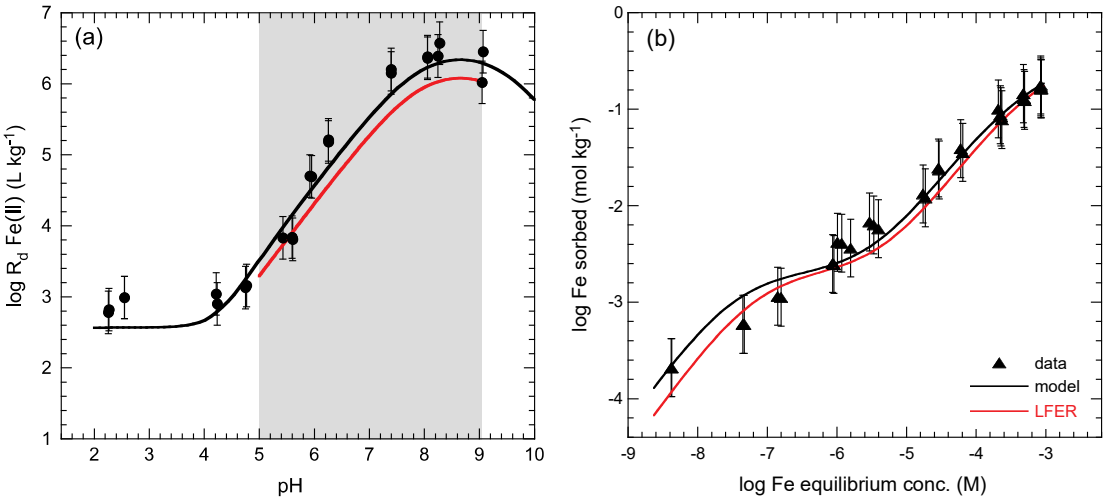

Fig. 5.3: Comparison of LFER calculations with model predictions for Fe(II): (a) Measured sorption edge and (b) isotherm at pH 6.2 on Na-STx-1.

Experimental data (●, ▲) and modelled curves (—). Predicted curves in the pH range 5 to 9 (—) using the surface complexation constants given in Tab. 5.1.

5.4 Nickel

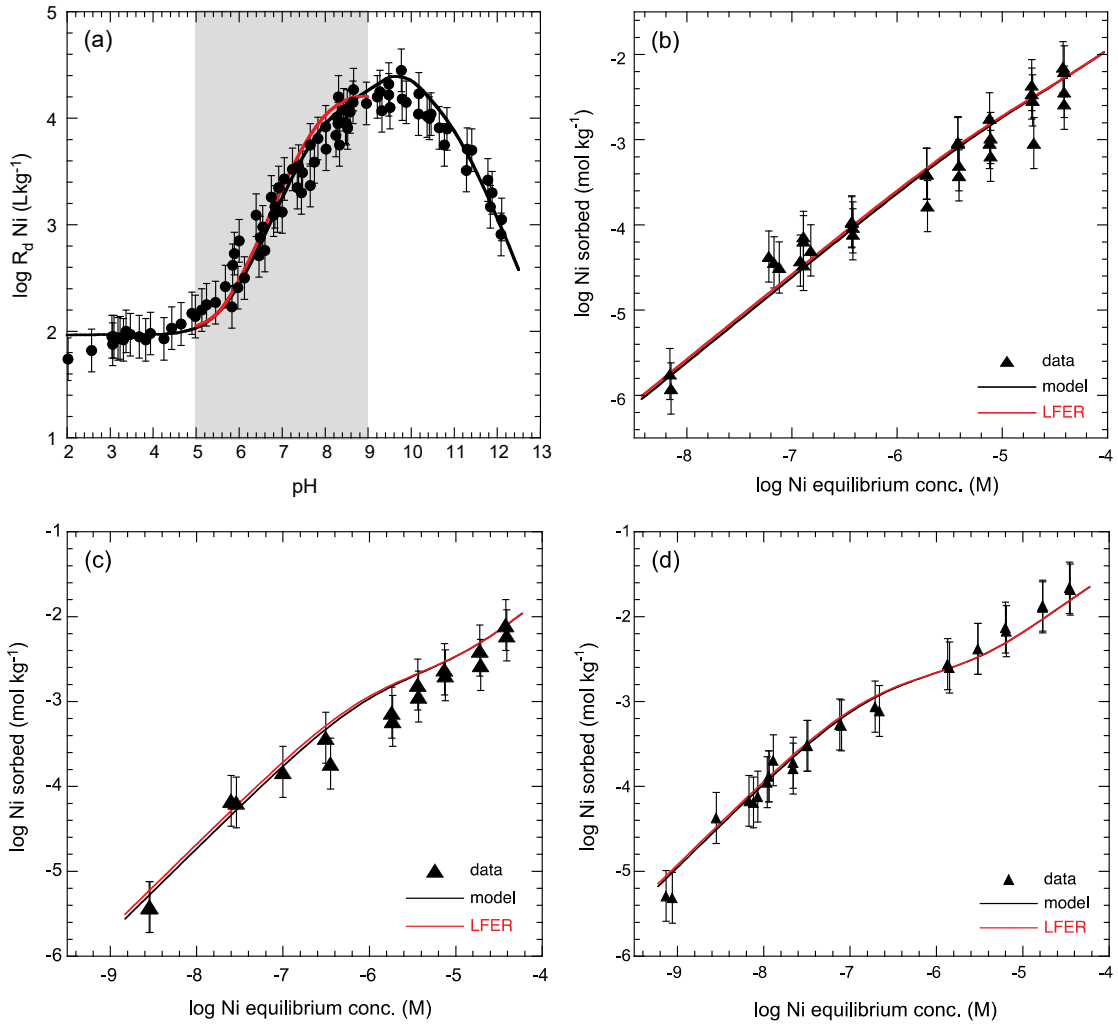

Fig. 5.4: Comparison of LFER calculations with model predictions for Ni(II): (a) Measured sorption edge and (b) isotherms at pH = 5.9, (c) at pH = 7.0 and (d) at pH = 8.2.

Experimental data (●, ▲) and modelled curves (—). Predicted curves in the pH range 5 to 9 (—) using the surface complexation constants given in Tab. 5.1.

5.5 Zinc

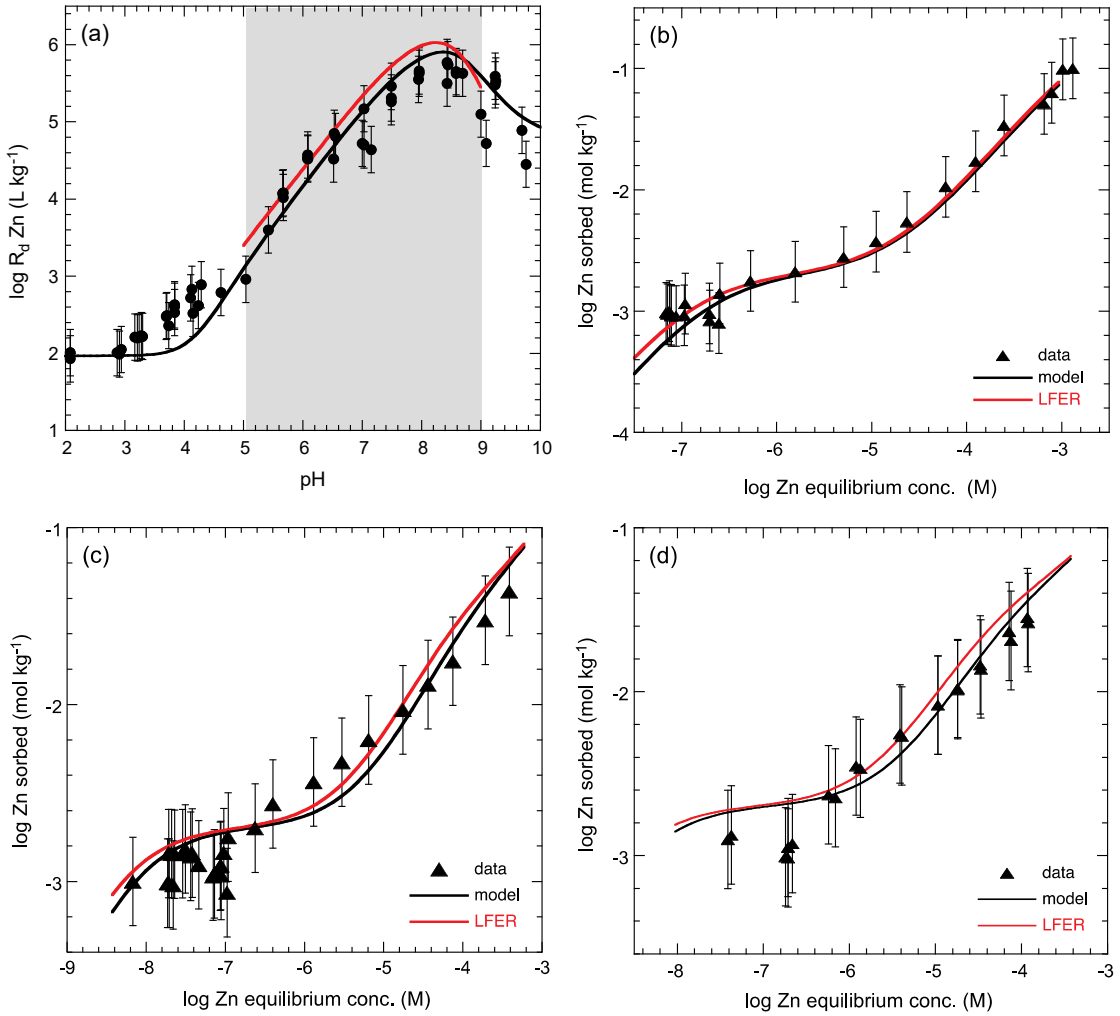

Fig. 5.5: Comparison of LFER calculations with model predictions for Zn(II): (a) Measured sorption edge and (b) isotherms at pH = 5.6, (c) at pH = 7.0 and (d) at pH = 7.3.

Experimental data (●, ▲) and modelled curves (—). Predicted curves in the pH range 5 to 9 (—) using the surface complexation constants given in Tab. 5.1.

5.6 Europium

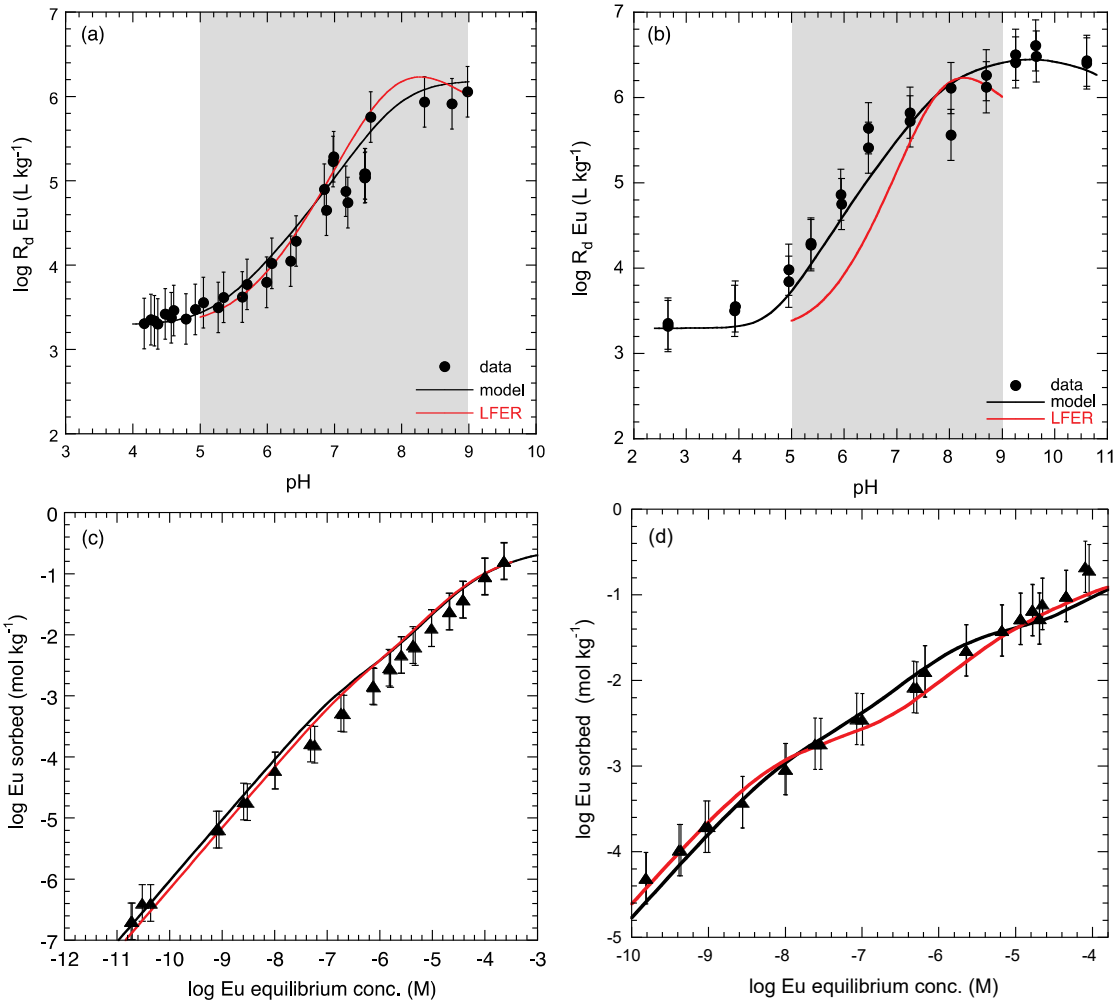

Fig. 5.6: Comparison of LFER calculations with model predictions for Eu(III): (a) and (b) Measured sorption edge and (c) isotherms at pH = 5.9 and (d) at pH = 7.2.

Measured sorption edge (●) and isotherm (▲) data and modelled curves (—). Predicted curves in the pH range 5 to 9 (—) using the surface complexation constants given in Tab. 5.1.

5.7 Americium

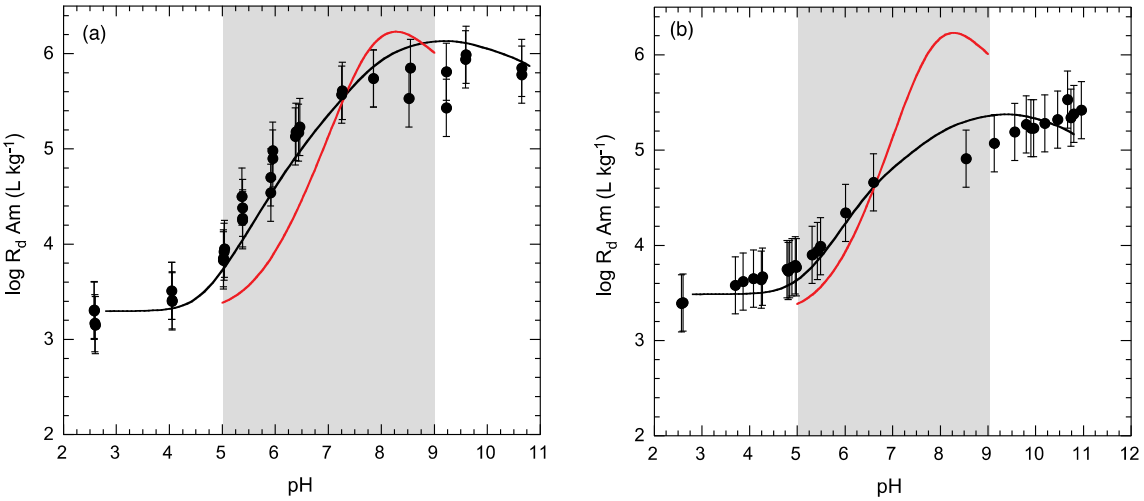

Fig. 5.7: Comparison of LFER calculations with model predictions for Am(III).

Measured sorption edges (●) from (a) Bradbury & Baeyens (2006) and (b) Gorgeon (1994) and modelled curves (—). Predicted curves in the pH range 5 to 9 (—) using the surface complexation constants given in Tab. 5.1.

5.8 Thorium

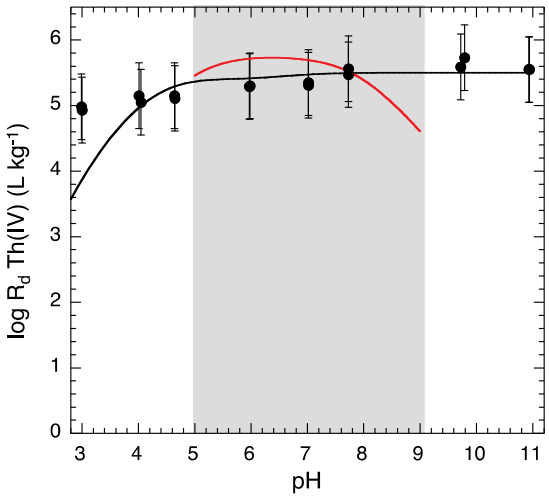

Fig. 5.8: Comparison of LFER calculations with model prediction for Th(IV).

Measured sorption edge (●) and modelled curve (—). Predicted curve in the pH range 5 to 9 (—) using the surface complexation constants given in Tab. 5.1.

6 Examples of modelling predictions of sorption edges and isotherms for metals for which no sorption data are available

6.1 General application of the thermodynamic sorption data base (TSDB)

The surface complexation reactions and constants derived from experimental measurements using the aqueous metal hydrolysis constants in Appendix B (bold type) are given in Appendix C (strong sites, bold type) and Appendix D (weak sites). The reactions and constants in bold type are those which essentially describe the sorption in the pH range 5 – 9 and are considered to be the values of choice for modelling. The reasons behind the preference for the data given in bold type were explained in section 4.2 (stability of the clay, the reliability of the hydrolysis constants and the pH range in natural systems).

Surface complexation constants should only be taken from LFERs in those cases where no other reliable data are available

The suggested general methodology for using LFERs to calculate the sorption of metals for which no sorption data exist is to first select the best available aqueous hydrolysis data and calculate the speciation in a simple 1:1 background electrolyte at 0.1 M. The dominant aqueous hydroxyl species occurring in the pH window from 5 to 9 are considered to be the sorbing species. The surface complexation constants and their corresponding hydrolysis constants (for the appropriate LFER) can then be deduced using Eqs. 4.1 to 4.3 given in section 4.1.

6.2 Modelling predictions of sorption edges/isotherms for Mn(II), Cu(II), Pu(III), U(IV), Np(IV) and Pu(IV) from LFERs

The surface complexation constants derived from the LFERs (Eqs. 4.4 to 4.7) and used in the predictive calculations of edges/isotherms on montmorillonite in the pH range 5 to 9 are summarised in Tab. 6.1. For each element the dominant aqueous species in the pH range 5 to 9 are given together with the corresponding surface complex and the correlating hydrolysed species. The K_c values used are taken from Appendix F.

In the cases of the tetravalent actinides U, Np and Pu, only sorption edges are predicted because of solubility constraints.

In Fig. 6.1 the positions of the elements listed in Tab. 6.1 are illustrated on the LFER plots obtained for the di-, tri- and tetravalent elements in Chapter 4. In the case of Mn and Cu the estimated hydrolysis and surface complexation constants fall outside the range of the transition elements for which experimental data was available. For Pu(III) and the tetravalent the surface complexations constants are lying on the LFERs.

The predicted sorption edge/isotherm curves are shown in Figs. 6.2 to 6.7, metal by metal.

Tab. 6.1: Surface complexation constants for the elements Mn(II), Cu(II), Pu(III), U(IV), Np(IV) and Pu(IV) taken from appropriate LFERs for strong and weak sites and the corresponding hydrolysis constants.

Element	**Aqueous species:** 5 < pH > 9	**Surface complex**	**Correlating aqueous species**	**log ^{OH}K**	**log ^{S}K**	**log ^{W1}K**	**LFER**
Mn(II)	Mn^{2+}	$\equiv SOMn^{+}$	$MnOH^{+}$	-10.59	-2.41	-3.98	Eqs. 4.4 & 4.7
Cu(II)	Cu^{2+}	$\equiv SOCu^{+}$	$CuOH^{+}$	-7.95	4.2	-1.6	Eqs. 4.4 & 4.7
	$CuOH^{+}$	$\equiv SOCuOH^{0}$	$Cu(OH)_2^{0}$	-16.2	-		No LFER
	$Cu(OH)_2^{0}$	$\equiv SOCu(OH)_2^{-}$	$Cu(OH)_3^{-}$	-26.6	-		No LFER
Pu(III)	Pu^{3+}	$\equiv S^{S}OPu^{2+}$	$PuOH^{2+}$	-6.9	1.61	-0.61	Eqs. 4.5 & 4.7
	$PuOH^{2+}$	$\equiv S^{S}OPuOH^{+}$	$Pu(OH)_2^{+}$	-14.8	-5.27		Eq. 4.5
	$Pu(OH)_2^{+}$	$\equiv S^{S}OPu(OH)_2^{0}$	$Pu(OH)_3^{0}$	-25.9	-14.6		Eq. 4.5
U(IV) *	$U(OH)_3^{+}$	$\equiv SOU(OH)_3^{0}$	$U(OH)_4^{0}$	-10	-1.41	-	Eq. 4.6
	$U(OH)_4^{0}$	$\equiv SOU(OH)_4^{-}$	$U(OH)_5^{-}$	no ^{OH}K	no ^{S}K		-
Np(IV) *	$Np(OH)_3^{+}$	$\equiv SONp(OH)_3^{0}$	$Np(OH)_4^{0}$	-8.3	0.32	-	Eq. 4.6
	$Np(OH)_4^{0}$	$\equiv SONp(OH)_4^{-}$	$Np(OH)_5^{-}$	no ^{OH}K	no ^{S}K		-
Pu(IV) *	$Pu(OH)_3^{+}$	$\equiv SOPu(OH)_3^{0}$	$Pu(OH)_4^{0}$	-9.3	-0.70	-	Eq. 4.6
	$Pu(OH)_4^{0}$	$\equiv SOPu(OH)_4^{-}$	$Pu(OH)_5^{-}$	no ^{OH}K	no ^{S}K		-

* Because of solubility limits in the pH range 5 to 9, isotherms for these metals are inappropriate.

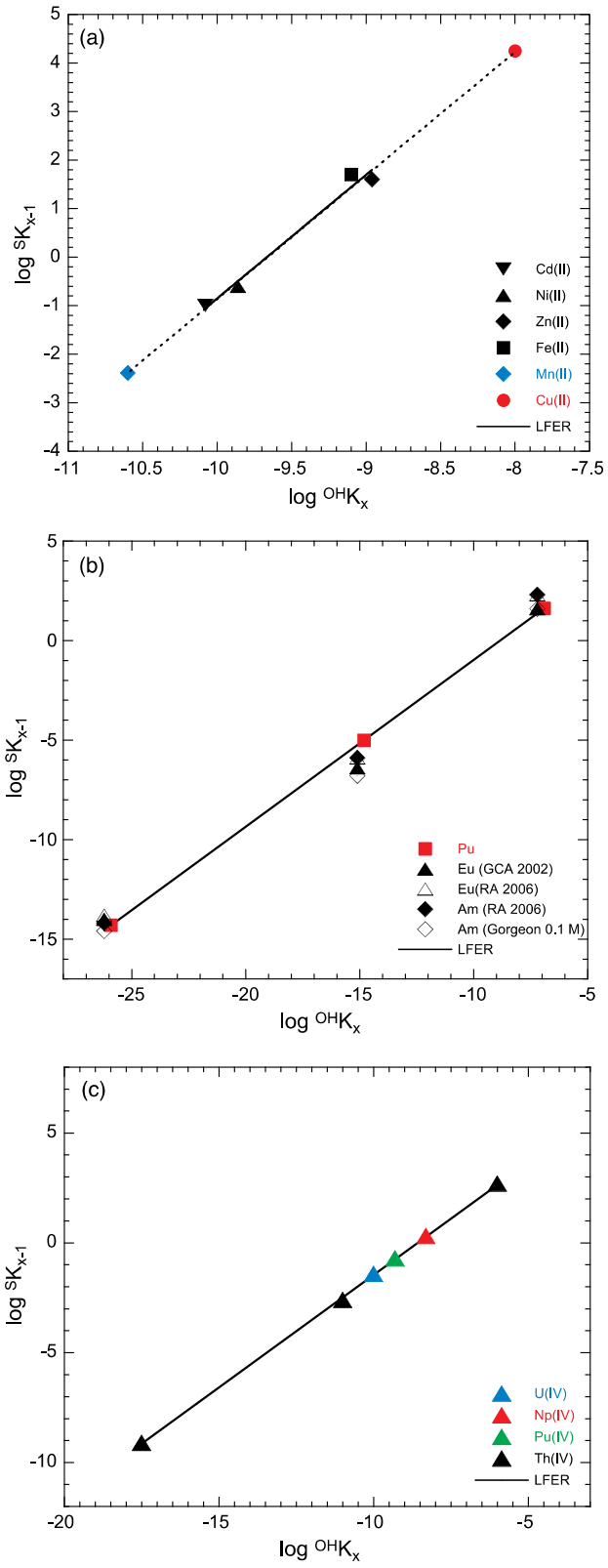

Fig. 6.1: Estimates of the surface complexation constants for (a) Mn(II) and Cu(II), (b) Pu(III) and (c) U(IV), Np(IV) and Pu(IV) using the corresponding LFER.

6.2.1 Mn(II)

Although sorption edge data for Mn(II), derived from water chemistry measurements, have been presented and modelled (Bradbury & Baeyens 1997), the results have not been included in Fig. 4.7. There are some doubts about their accuracy/reliability because of the manner in which they were obtained, and the hydrolysis/surface complex constants relationship is inconsistent with the other transition metals. However, Mn(II) is often present in the porewater of natural systems and may, depending on the system, be of some importance as a metal which competes for the available sorption sites with other transition metals. In view of this, it is recommended that for modelling purposes the surface stability constants for Mn are taken from the LFERs in Figs. 6.1 and given in Tab. 6.1. In the pH range from 5 to 9 the main sorbing species is taken to be Mn^{2+}, and the predicted sorption edge in this pH range, and the isotherm at pH = 7, are given in Fig. 6.2.

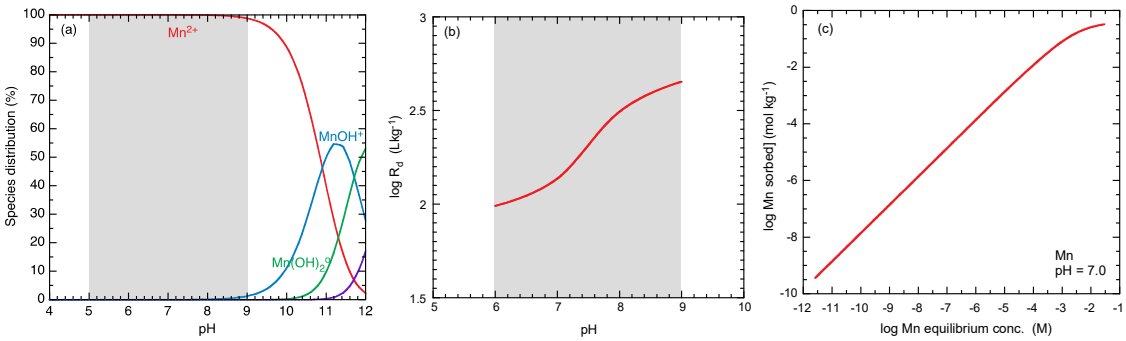

Fig. 6.2: (a) The aqueous speciation of Mn(II) ($Mn_{TOT} = 10^{-8}$ M), (b) the sorption edge in the pH range 5 to 9 and (c) the sorption isotherm at pH = 7 on montmorillonite in 0.1 M $NaClO_4$ calculated using the surface complexation constants given in Tab. 6.1.

6.2.2 Cu(II)

According to the thermodynamic data given in Appendix B, Cu is, with the exception of Pd(II), the most strongly hydrolysed of all the transition metals considered in this report. In addition to Cu^{2+}, $CuOH^+$ and $Cu(OH)_2^0$ are also present as major, potentially sorbing, species in the pH range 5 to 9. However, there is no appropriate LFER from which surface complexation constants for these hydrolysed species can be obtained. Thus, on the basis of the information available, any predictions of the sorption of Cu are restricted to the uptake of Cu^{2+}. Because of the very strong hydrolysis behaviour of Cu, the predicted surface complexation constant is very high and lies well outside the range of the other transition metals (see Fig. 6.1). This in turn leads to exceedingly high predicted sorption values (Fig. 6.3b) and implies that the strong sites reach saturation already at Cu equilibrium concentrations of 10^{-10} M at pH = 7 (see Fig. 6.3c). Such predictions for the sorption behaviour of Cu, which are significantly at variance with the other transition metals, may well imply that they should be treated with some misgivings.

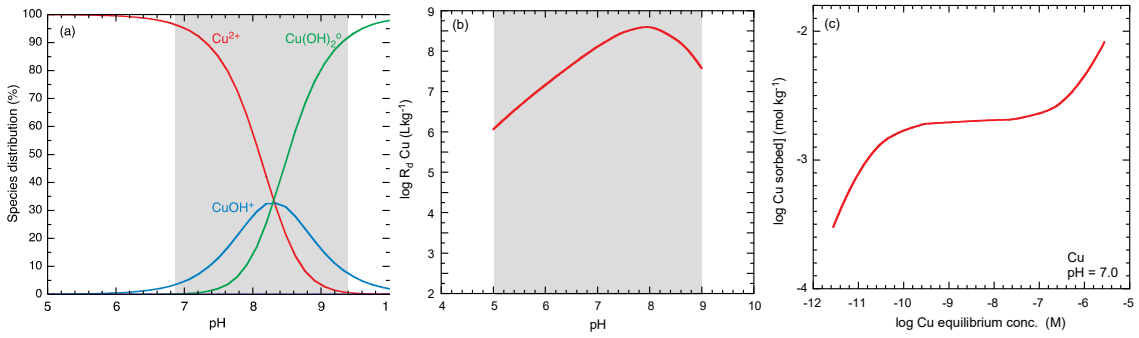

Fig. 6.3: (a) The aqueous speciation of Cu(II) (Cu_{TOT} = 10^{-8} M), (b) the sorption edge in the pH range 5 to 9 and (c) the sorption isotherm at pH = 7 on montmorillonite in 0.1 M $NaClO_4$ calculated using the surface complexation constants given in Tab. 6.1.

6.2.3 Pu(III)

According to Fig. 6.4a, the main sorbing species for Pu in the pH range 5 to 9 are taken to be Pu^{3+}, $PuOH^{2+}$ and $Pu(OH)_2^{+}$. The predicted sorption edge and isotherm at pH = 7 are given in Fig. 6.4b and c. The contribution of the predominant sorbing species to the overall sorption is included in the edge. (The sorbing aqueous species has the same colour as the sorbed complex.)

For lanthanides and the trivalent actinides (Ac, Cm) the same approach can be used to predict sorption edges and isotherms in the pH range 5 to 9.

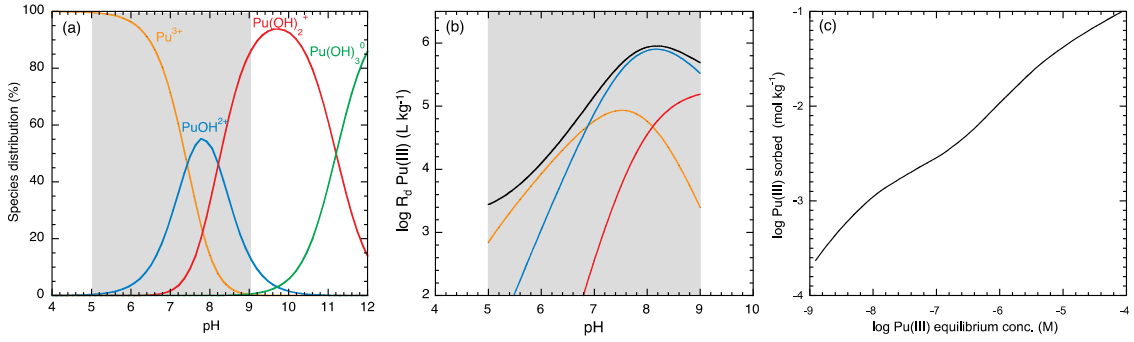

Fig. 6.4 : (a) The aqueous speciation of Pu(III) (Pu_{TOT} = 10^{-8} M), (b) the sorption edge in the pH range 5 to 9 and (c) the sorption isotherm at pH = 7 on montmorillonite in 0.1 M $NaClO_4$ calculated using the surface complexation constants given in Tab. 6.1.

6.2.4 Tetravalent actinides: U(IV), Np(IV) and Pu(IV)

For U(IV) the dominant sorbing species in the pH range 5 to 9 are $U(OH)_3^+$ and the neutral $U(OH)_4^0$ species, and likewise for Np(IV), $Np(OH)_3^+$ and $Np(OH)_4^0$, and for Pu(IV), $Pu(OH)_3^+$ and $Pu(OH)_4^0$. The predicted sorption edges are given in Figs. 6.5b, 6.6b and 6.7b for U(IV), Np(IV) and Pu(IV) respectively.

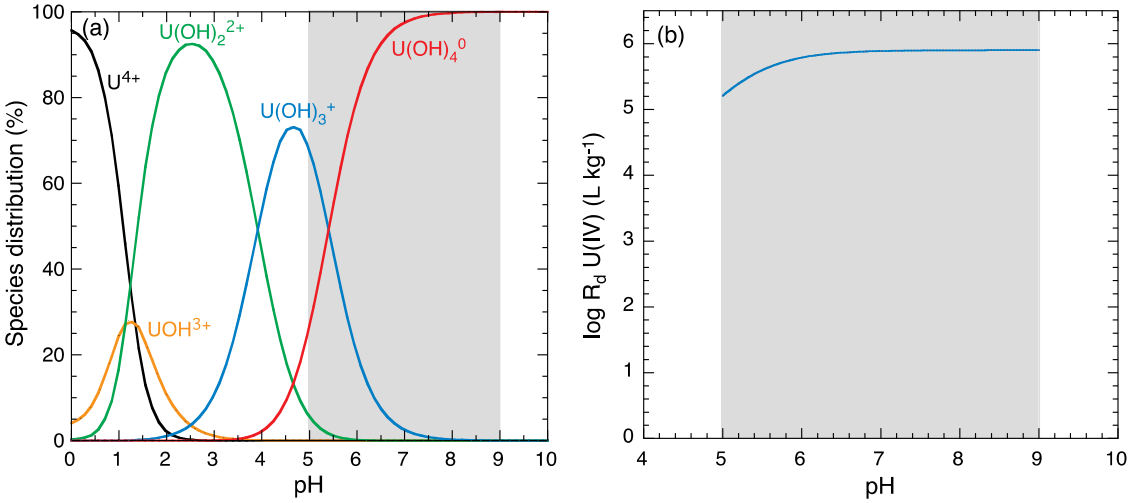

Fig. 6.5: (a) The aqueous speciation of U(IV) ($U_{TOT} = 10^{-8}$ M), (b) the sorption edge of U(VI) in the pH range 5 to 9 on montmorillonite in 0.1 M $NaClO_4$ calculated using the surface complexation constants given in Tab. 6.1.

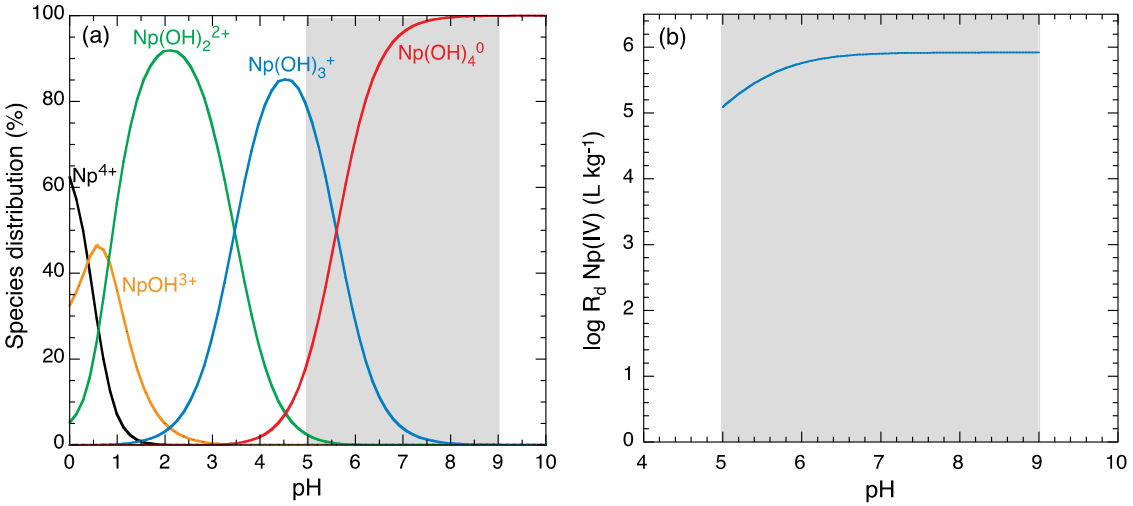

Fig. 6.6: (a) The aqueous speciation of Np(IV) ($Np_{TOT} = 10^{-8}$ M) and (b) the sorption edge in the pH range 5 to 9 on montmorillonite in 0.1 M $NaClO_4$ calculated using the surface complexation constants given in Tab. 6.1.

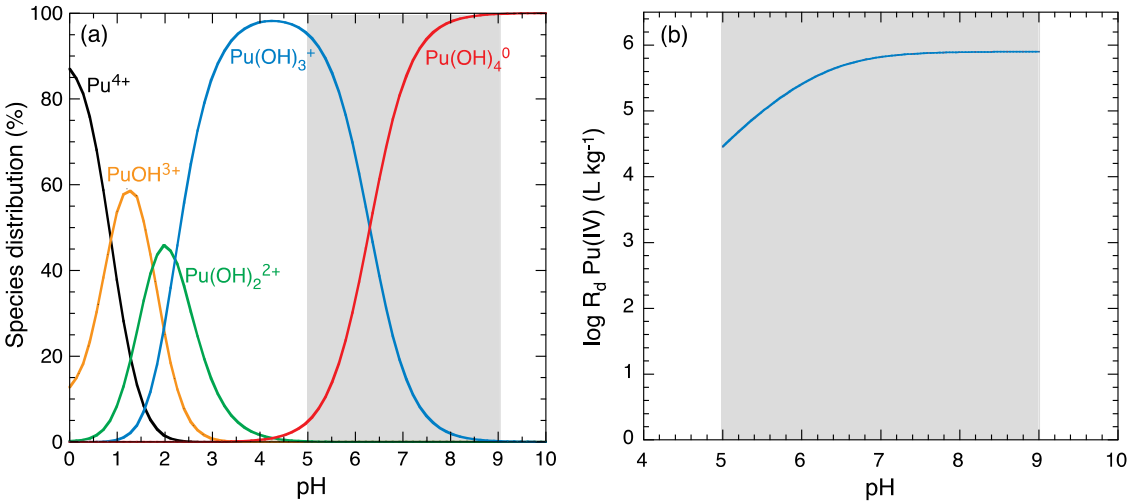

Fig. 6.7: (a) The aqueous speciation of Pu(IV) ($Pu_{TOT} = 10^{-8}$ M) and (b) the sorption edge in the pH range 5 to 9 on montmorillonite in 0.1 M $NaClO_4$ calculated using the surface complexation constants given in Tab. 6.1.

6.3 Metals for which the LFER approach is not applicable

With reference to the list of safety relevant radionuclides (Nagra 2008) sorption parameters for the following metals Ag(I), Be(II), Pd(II), Tc(IV), Po(IV), Zr(IV), Nb(V) cannot be deduced from LFERs.

6.3.1 Ag(I)

Silver is a monovalent transition metal for which no LFER exists.

6.3.2 Be(II)

Beryllium is an alkaline earth metal. The speciation given in Fig. 6.8 shows that it hydrolyses more strongly than the metals included in the LFER given in Fig. 4.7. According to the approach described in section 4.1, $BeOH^+$ would be expected to be the main sorbing species in the pH range 5 to 9 and the corresponding surface complexation constant would be correlated with the hydrolysis constant for $Be(OH)_2^0$. An appropriate LFER is not available.

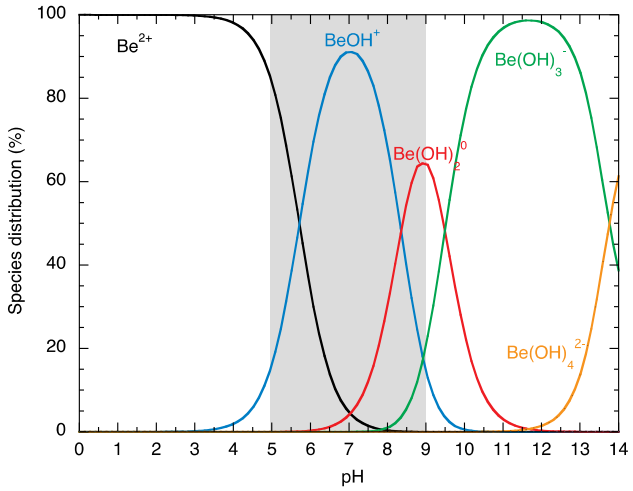

Fig. 6.8: The aqueous speciation of Be(II) in 0.1 M $NaClO_4$ at trace concentration (Be_{TOT} = 10^{-8} M).

6.3.3 Pd(II)

Although palladium is a divalent transition metal, the speciation plot given in Fig. 6.9 shows that it hydrolyses much more strongly that for the metals included in the LFER given in Fig. 4.7. According to the approach described in section 5.1, $Pd(OH)_2^0$ would be expected to be the main sorbing species in the pH range 5 to 9 and the corresponding surface complexation constant would be correlated with the hydrolysis constant for $Pd(OH)_3^-$. Again, an appropriate LFER is not available.

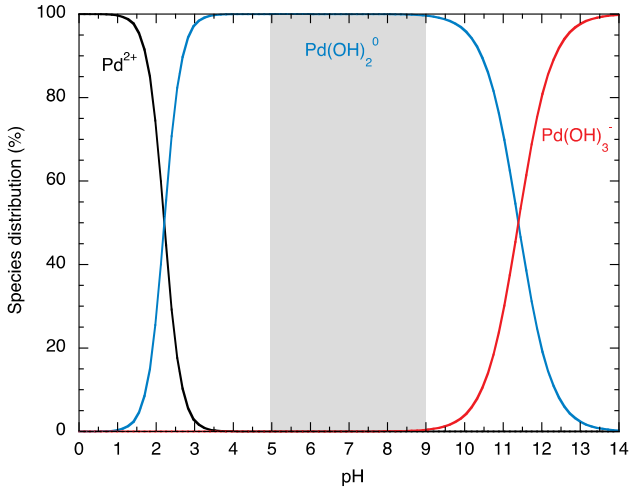

Fig. 6.9: The aqueous speciation of Pd(II) in 0.1 M $NaClO_4$ at trace concentration (Pd_{TOT} = 10^{-8} M).

6.3.4 Tc(IV), Po(IV), Zr(IV)

For Tc(IV), Po(IV) and Zr(IV) the hydrolysis data are somewhat uncertain, or absent (Po(IV)), and, in any case, appropriate LFERs do not exist.

6.3.5 Nb(V)

Nb(V) forms predominantly oxy anions in solution and does not therefore fit into the LFER structure.

7 Comparisons between sorption values measured in complex bentonite/groundwater systems and sorption model predictions

In order to test the capabilities of the model and associated model parameters to quantitatively describe the uptake of radionuclides in complex MX-80 bentonite / porewater systems, blind model predictions were made of sorption isotherms which were then compared with the measured values (see also Bradbury & Baeyens 2011a). The main assumption was that the sorption on MX-80 bentonite is controlled by the montmorillonite content. The MX-80 bentonite/ porewater system is characterised by the data given in Appendix J and the parameters used in the 2SPNE SC/CE sorption model calculations can be found in Appendices A, C, D and E. The hydrolysis constants (Appendix B), the thermodynamic constants (Appendix J) and the PSI/Nagra 12/07 thermodynamic data base (Thoenen et al. 2014) were used in the predictive modelling. Aqueous activity coefficients were calculated using the Davies relation with a value of 0.3 for the C_D constant (Davies 1962). The "correctness" and completeness of the thermodynamic database used in the calculations are critical for the calculations (see below and Appendix K, Fig. K4, for the case of U(VI)). It is important to realise that there were no adjustable parameters in the sorption calculations. The radionuclides included in this exercise were chosen as representatives for divalent transition metals (Ni(II)), lanthanides and trivalent (Eu(III)), tetravalent actinides (Th(IV)) and hexavalent metals (U(VI)).

The sorption isotherms for Ni(II), Eu(III), Th(IV) and U(VI) measured on MX-80 bentonite (Bradbury & Baeyens 2011b) are shown in Fig. 7.1 together with the blind predicted curves which were calculated for montmorillonite and then scaled by the weight fraction of montmorillonite in the bentonite. In most cases the measurements and predictions cover over 4 orders of magnitude of the metal aqueous equilibrium concentration.

In the cases of Eu(III), Th(IV) and U(VI) shown in Fig. 7.1, the agreement between experiment (solid circles) and the blind predictive modelling (black curves) can be seen to be good to very good; the calculated values lie within the experimental error bars given.

In the case of Ni(II), the sorption model over-predicts the measured data at equilibrium concentrations $< 10^{-6}$ M by a factor of ~ 3.

On the basis of the modelling results presented here, the "bottom up" approach, used in conjunction with some simplifying assumptions and the straightforward procedures described, may be regarded as a method for quantitatively calculating radionuclide uptake in complex geochemical systems.

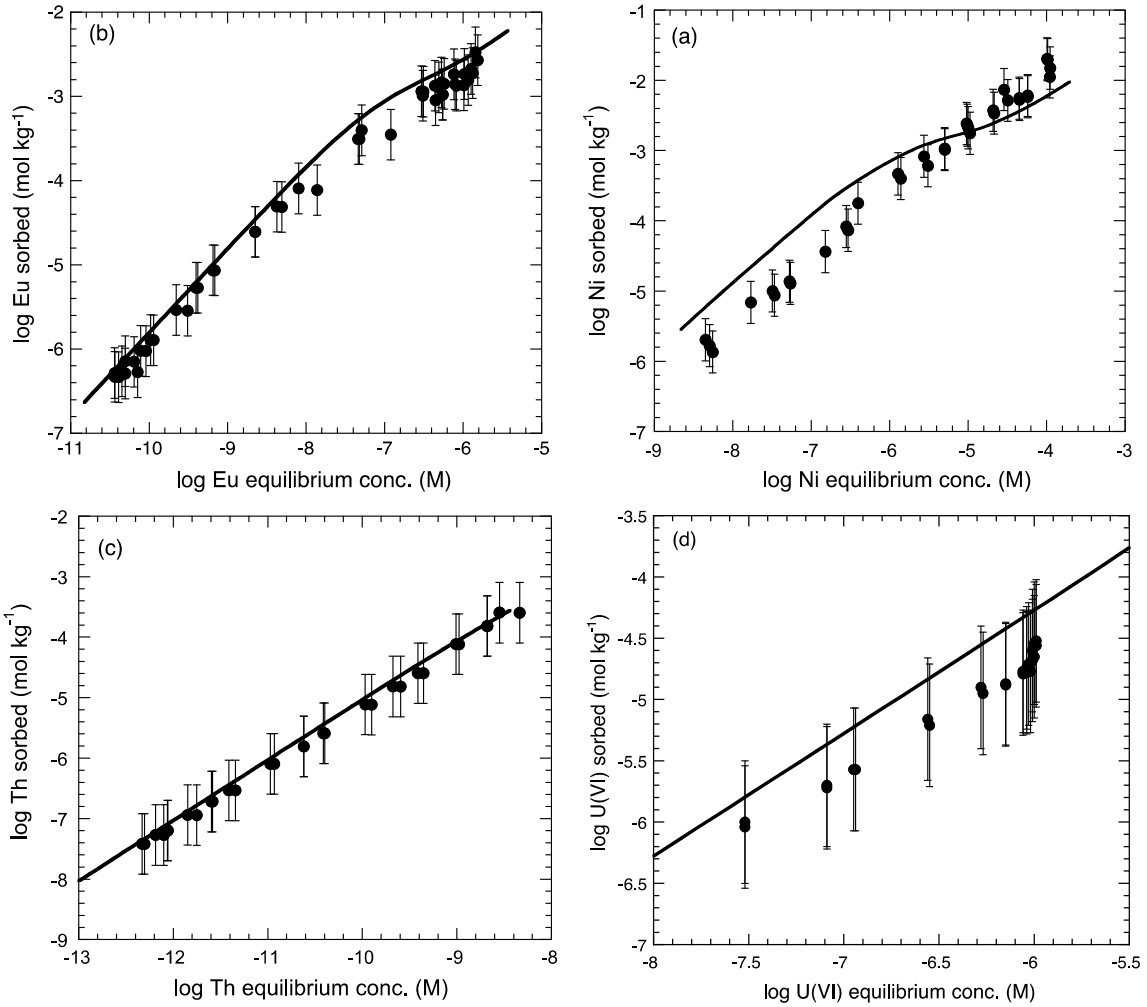

Fig. 7.1: Comparison of isotherms measurements on MX-80 bentonite for (a) Ni(II), (b) Eu(III), (c) Th(IV) and (d) U(VI) and curves calculated with the 2SPNE SC/CE sorption model.

Experimental data (●) and blind model predictions (black curves).

8 Summary

The compiled data sets constitute the core of a Thermodynamic Sorption Data Base (TSDB) for montmorillonite which can be used to calculate sorption values in bentonite systems. Sorption edge/isotherm measurements on montmorillonite for Co(II), Ni(II), Cd(II), Zn(II), Fe(II), Eu(III), Am (III), Sn(IV), Th(IV), Np(V), Pa(V), U(VI), from predominantly "in house" investigations, have been summarised in Chapter 3. These data were modelled using the 2SPNE SC/CE sorption model using the fixed model parameters in Appendix A and the metal hydrolysis constants selected in Appendix B. The surface complexation reactions and derived constants for strong and weak sites are tabulated in Appendices C and D respectively. The cation exchange selectivity coefficients (K_c values) are listed separately in Appendix F.

A number of cases have been described in Chapter 6, for montmorillonite in simple 1:1 electrolytes, and in Chapter 7 for chemically realistic bentonite systems, in which blind predictions of sorption values have been compared with the measured ones. In general, the correspondences have been good to very good which should, within the framework given, provide confidence in using the data in the Thermodynamic Sorption Data Base for the predictive modelling of sorption.

Surface complexation constants are difficult to predict from theoretical considerations; therefore, a means was sought to allow estimates to be made for these constants for metals where the data are either very poor or non-existent and which would then allow sorption values to be calculated. Good systematic linear correlations between the logarithms of the surface site binding constants on the strong and weak sites and the logarithm of the corresponding aqueous hydrolysis constants were found, so called Linear Free Energy Relationships, (LFERs). Separate LFERs have been constructed for bivalent transition metals, lanthanides and trivalent actinides and tetravalent actinides for strong and weak sites valid in the pH range 5 to 9. However, the LFERs should be used judiciously. Sometimes they are based on (very) limited data sets and there are restrictions in their use. These issues are discussed fully in Chapter 4. LFERs are seen as being complimentary to the TSDB.

The suggested general methodology for estimating surface complexation constants from LFERs is to first select the best available aqueous hydrolysis data for the metal in question, and then to calculate the speciation in a simple 1:1 background electrolyte at 0.1 M. The dominant aqueous hydroxyl species occurring in the pH window from 5 to 9 are considered to be the sorbing species. Surface complexation constants can then be deduced from the corresponding hydrolysis constants (for the appropriate LFER) using Eqs. 4.1 to 4.3 given in section 4.1.

Sorption edges/isotherms have been predicted for Mn(II), Cu(II), Pu(III), U(IV), Np(IV) and Pu(IV) in simple 1:1 electrolytes and are illustrated, together with the corresponding aqueous speciations, in Chapter 6 (Figs. 6.2 to 6.7). Clearly, the quality of these predictions, and therefore the validity of the approach, can ultimately only be decided when experimental data are available.

With reference to the list of safety relevant radionuclides (Nagra 2008), sorption data for the following metals Ag(I), Be(II), Pd(II), Tc(IV), Po(IV), Zr(IV), Nb(V) do not exist and the necessary sorption parameters cannot be derived, mainly because the appropriate LFERs do not exist.

Acknowledgements

We would like to express our gratitude to Dr. V. Brendler (Helmholtz-Zentrum Dresden Rossendorf, Germany) and Dr. J. Mibus (Nagra) for reviewing the manuscript. The final layout of the report was carried out by B. Gschwend. Partial financial support was provided by Nagra.

9 References

Baes, C.F. & Mesmer, R.E. (1976): The hydrolysis of cations. Wiley, New York.

Baeyens, B. & Bradbury, M.H. (1995a): A quantitative mechanistic description of Ni, Zn and Ca sorption on Na-montmorillonite. Part I: Physico-chemical characterisation and titration measurements. PSI Bericht Nr. 95-10 and Nagra Tech. Report NTB 95-04.

Baeyens, B. & Bradbury, M.H. (1995b): A quantitative mechanistic description of Ni, Zn and Ca sorption on Na-montmorillonite. Part II: Sorption measurements. PSI Bericht Nr. 95-11 and Nagra Tech. Report NTB 95-05.

Baeyens, B. & Bradbury, M.H. (1997): A mechanistic description of Ni and Zn sorption on Na-montmorillonite. Part I: Titration and sorption measurements. J. Contam. Hydrol. 27, 199-222.

Bradbury, M.H.. & Baeyens, B. (1995): A quantitative mechanistic description of Ni, Zn and Ca sorption on Na-montmorillonite. Part III: Modelling. PSI Bericht Nr. 95-12 and Nagra Tech. Report NTB 95-06.

Bradbury, M.H. & Baeyens, B. (1997): A mechanistic description of Ni and Zn sorption on Na-montmorillonite. Part II: Modelling. J. Contam. Hydrol. 27, 223-248.

Bradbury, M.H. & Baeyens, B. (1999): Modelling the sorption of Zn and Ni on Ca-montmorillonite. Geochim. Cosmochim. Acta 63, 325-336.

Bradbury, M.H. & Baeyens, B. (2002a): Sorption of Eu on Na- and Ca-montmorillonites: Experimental investigations and modelling with cation exchange and surface complexation. Geochim. Cosmochim. Acta 66, 2325-2334.

Bradbury, M.H. & Baeyens, B. (2002b): Porewater chemistry in compacted re-saturated MX-80 bentonite: Physico-chemical characterisation and geochemical modelling. PSI Report 02-10 and Nagra Tech. Report NTB 01-08.

Bradbury, M.H. & Baeyens, B. (2005a): Modelling the sorption of Mn(II), Co(II), Ni(II), Cd(II), Eu(III), Am(III), Sn(IV), Th(IV), Np(V) and U(VI) on montmorillonite: Linear free energy relationships and predictions of surface binding constants for some selected heavy metals and actinides. Geochim. Cosmochim. Acta 69, 875-892.

Bradbury, M.H. & Baeyens, B. (2005b): Erratum to M.H. Bradbury and B. Baeyens (2005a) "Modelling the sorption of Mn(II), Co(II), Ni(II), Zn(II), Cd(II), Eu(III), Am(III), Sn(IV), Th(IV), Np(V) and U(VI) on montmorillonite: Linear free energy relationships and estimates of surface binding constants for some selected heavy metals and actinides". Geochim. Cosmochim. Acta 69, 5391-5392.

Bradbury, M.H. & Baeyens, B. (2005c): Experimental measurements and modelling of sorption competition on montmorillonite. Geochim. Cosmochim. Acta 69, 4187-4197.

Bradbury, M.H. & Baeyens, B. (2006a): A quasi-mechanistic non-electrostatic modelling approach to metal sorption on clay minerals. *In:* Lützenkirchen, J. (ed.): Surface complexation modelling. Elsevier Ltd., 518-538.

Bradbury, M.H. & Baeyens, B. (2006b): Modelling sorption data for the actinides Am(III), Np(V) and Pa(V) on montmorillonite. Radiochim. Acta 94, 619-625.

Bradbury, M.H. & Baeyens, B. (2009a): Sorption modelling on illite. Part I: Titration measurements and the sorption of Ni, Co, Eu and Sn. Geochim. Cosmochim. Acta 73, 990-1003.

Bradbury, M.H. & Baeyens, B. (2009b): Sorption modelling on illite. Part II Actinide sorption and linear free energy relationships. Geochim. Cosmochim. Acta 73, 1004-1013.

Bradbury M.H. & Baeyens, B. (2011a): Predictive sorption modelling of Ni(II), Co(II), Eu(III), Th(IV) and U(VI) on MX-80 bentonite and Opalinus Clay: A "bottom-up" approach. Appl. Clay Sci. 52, 27-33.

Bradbury, M.H. & Baeyens, B. (2011b): Physico-chemical characterisation data and sorption measurements of Cs, Ni, Eu, Th, U, Cl, I and Se on MX-80 bentonite. Nagra Tech. Report NTB 09-08.

Bradbury, M.H.,, Marques Fernandes, M. & Baeyens, B. (2017): Estimates of the influence of radionuclide solubility limits and sorption competition on the sorption values in the SDBs of MX-80 bentonite and Opalinus Clay. Nagra Tech. Report NTB 17-11.

Brown, P.L., Curti, E. & Grambow, B. (2005): Chemical thermodynamics of zirconium. Chemical Thermodynamics, Vol. 8. OECD Nuclear Energy Agency Data Bank, Eds., North Holland Elsevier Science Publishers B.V., Amsterdam, The Netherlands.

Chapman, N.B. & Shorter, J. (1972): Advances in linear free energy relationships. Plenum Press, London.

Cremers, A & Thomas, H.C. (1968): The thermodynamics of sodium-cesium exchange on Camp Berteau montmorillonite: An almost ideal case. Israel J. Chem. 6, 949-957.

Dähn, R., Scheidegger, A.M., Manceau, A., Curti, E., Baeyens, B., Bradbury, M.H. & Chateigner, D. (2002): Th uptake on montmorillonite: A powder and polarized extended X-ray absorption fine structure (EXAFS) study. J. Colloid Interface Sci. 249, 8-21.

Dähn, R., Scheidegger, A.M., Manceau, A., Schlegel, M.L., Baeyens, B., Bradbury, M.H. & Chateigner, D. (2003): Structural evidence for the sorption of Ni(II) atoms on the edges of montmorillonite clay minerals. A polarized X-ray absorption fine structure study. Geochim. Cosmochim. Acta 67/1, 1-15.

Dähn, R., Baeyens, B., & Bradbury, M.H. (2011): Investigation of the different binding edge sites for Zn on montmorillonite using P-EXAFS – the strong/weak site concept in the 2SPNE SC/CE sorption model. Geochim. Cosmochim. Acta 75, 5154-5168.

Davies, C.W. (1962): Ion association. Butterworths, London.

Davis, J.A. & Kent, D.B. (1990): Surface complexation modelling in aqueous geochemistry. *In:* Hochella, M.F. & Waite, A.F. (eds.): Mineral-Water Interface Geochemistry. Rev. Mineral. 23, 177-260. Mineralogical Society of America, Washington, D.C.

Gaines G.I. & Thomas, H.C. (1953): Adsorption studies on clay minerals. II. A formulation of the thermodynamics of exchange adsorption. J. Chem. Phys. 21, 714-718.

Gast, R.G. (1969): Standard free energies of exchange for alkali metal cations on Wyoming bentonite. Soil Sci. Am. Proc. 33, 37-41.

Gorgeon, L. (1994): Contribution à la modélisation physico-chimique de la retention de radio-eléments à vie longue par des materiaux argileux. Unpubl. PhD Thesis. Université Paris 6.

Grenthe, I., Fuger, J., Konings, R.J., Lemire, R.J., Muller, A.B., Nguyen-Trung, C. & Wanner, H. (1992): Chemical thermodynamics of uranium. Chemical Thermodynamics 1. OECD Nuclear Energy Agency Data Bank, Eds., North Holland Elsevier Science Publishers B.V., Amsterdam, The Netherlands.

Guillaumont, R., Fanghänel, T., Fuger, J., Grenthe, I., Neck, V., Palmer, D.A. & Rand, M.H. (2003): Update on the chemical thermodynamics of uranium, neptunium, plutonium, americium and technetium. Chemical Thermodynamics 5. OECD Nuclear Energy Agency Data Bank, Eds., North Holland Elsevier Science Publishers B.V., Amsterdam, The Netherlands.

Hammett, L.P. (1940): Physical Organic Chemistry. McGraw-Hill, New York.

Hummel, W., Berner, U., Curti, E., Pearson, F.J. & Thoenen, T. (2002): Nagra / PSI Chemical Thermodynamic Data Base 01/01. Nagra Tech. Report NTB 02-16 and Universal Publishers/uPublish.com, Parkland, Florida, USA.

Larsson, E. (1934): Die Dissoziationskonstanten von Aminium- und Silberdiaminionen und ein Zusammenhang zwischen ihnen. Z. Phys. Chem. A 169, 207-223.

Lemire, R., Fuger, J., Nitsche, H., Potter, P., Rand, M., Rydberg, J., Spahiu, K., Sullivan, J., Ullman, W. & Vitorge, P. (2001): Chemical thermodynamics of neptunium and plutonium. Chemical Thermodynamics 4. OECD Nuclear Energy Agency Data Bank, Eds., North Holland Elsevier Science Publishers B.V., Amsterdam, The Netherlands.

Lemire, R., Berner, U., Musikas, C., Palmer, D., Taylor, P. & Tochiyama, O. (2013): Chemical thermodynamics of iron. Part 1. Chemical Thermodynamics 13a. OECD Nuclear Energy Agency Data Bank, Eds., OECD Publications, Paris, France.

Maes, A., Peigneur, P. & Cremers, A. (1976): Thermodynamics of transition metal ion exchange in montmorillonite. Proc. Int. Clay Conf. New Mexico, 1975, 319-329.

Maes, A. & Cremers, A. (1986): Europium sorption on a clay sediment: sulphate and ionic strength effects. *In:* Sibley, T.H. & Myttenaere, C. (eds.): Application of distribution coefficients to radiological assessment models. Elsevier, Amsterdam, pp. 103-110.

Marques Fernandes, M., Stumpf, T.R., Bosbach, D. & Fanghänel, T. (2008): Incorporation of trivalent actinides into calcite: A time resolved laser fluorescence spectrocopy (TRLFS) study. Geochim. Cosmochim. Acta 72, 464-474.

Marques Fernandes, M., Baeyens, B. & Bradbury, M.H. (2008): The influence of carbonate complexation on lanthanide/actinide sorption on montmorillonite. Radiochim. Acta 96, 691-697.

Marques Fernandes, M., Baeyens, B., Dähn, R., Scheinost, A.C. & Bradbury, M.H. (2012): U(VI) sorption on montmorillonite in the absence and presence of carbonate: A macroscopic and microscopic study. Geochim. Cosmochim. Acta 93, 267-277.

Marques Fernandes, M., Scheinost, A.C. & Baeyens, B. (2016): Sorption of trivalent lanthanides and actinides onto montmorillonite: Macroscopic, thermodynamic and structural evidence for ternary hydroxo and carbonato surface complexes on multiple sorption sites. Water Research 99, 74-82.

Müller-Vonmoos, M. & Kahr, G. (1983): Mineralogische Untersuchungen von Wyoming Bentonit MX-80 und Montigel. Nagra Tech. Report NTB 83-12.

Nagra (2002): Project Opalinus Clay: Safety Report. Demonstration of disposal feasibility for spent fuel, vitrified high-level waste and long-lived intermediate-level waste (Entsorgungsnachweis). Nagra Tech. Report NTB 02-05.

Nagra (2008): Vorschlag geologischer Standortgebiete für das SMA- und das HAA-Lager: Begründung der Abfallzuteilung, der Barrierensysteme und der Anforderungen an die Geologie (Bericht zur Sicherheit und technischen Machbarkeit). Nagra Tech. Report NTB 08-05.

NEA (2005): NEA Sorption Project Phase II: Interpretation and prediction of radionuclide sorption onto substrates relevant for radioactive waste disposal using thermodynamic sorption models. OECD/NEA, Paris.

Neck, V. & Kim, J.I. (2001): Solubility and hydrolysis of tetravalent actinides. Radiochim. Acta 89, 1.

Pabalan, R.T. & Turner, D.R. (1997): Uranium (6+) sorption on montmorillonite: Experimental and surface complexation modeling study. Aquatic Geochem. 2, 203-226.

Pfingsten, W., Bradbury, M.H. & Baeyens, B. (2011): The influence of Fe(II) competition on the sorption and migration of Ni(II) in MX-80 Bentonite. Appl. Geochem. 26, 1414-1422.

Powell, K.J., Brown, P.L., Byrne, R.H., Gajda, T., Hefter, G., Söberg, S. & Wanner, H. (2007): Chemical speciation of environmentally significant metals with inorganic ligands. Part 2: The Cu^{2+}- OH^{-}, Cl^{-}, CO_3^{2-}, SO_4^{2-} and PO_4^{3-} systems (IUPAC Technical Report). Pure Appl. Chem. 79/5, 895-950.

Soltermann, D., Baeyens, B., Bradbury, M.H. & Marques Fernandes, M. (2014): Fe(II) uptake on natural montmorillonites. Part II Surface complexation modelling. Environ. Sci. Technol. 48, 8698-8705.

Sposito, G. (1984): The surface chemistry of soils. Oxford University Press, New York, NY.

Strawn, D.G. & Sparks, D.L. (1999): The use of XAFS to distinguish between inner- and outer-sphere lead adsorption complexes on montmorillonite. J. Colloid Interface Sci. 216, 257-269.

Taylor, J.R. (1982): An introduction to error analysis. University Science Books, Mill Valey, USA.

Thoenen, T., Hummel, W., Berner, U. & Curti, E. (2014): The PSI/Nagra Chemical Thermodynamic Database 12/07. PSI Bericht Nr. 14-04. Paul Scherrer Insitut, Villigen PSI.

Trubert, D., Le Naour, C., Jaussaud, C. & Mrad, O. (2003): Hydrolysis of protactinium(V): III. Determination of standard thermodynamic data. J. Solution Chem. 32, 505-517.

Turner, D.R., Pabalan, R.T. & Bertetti, F.P. (1998): Neptunium (V) sorption on montmorillonite: An experimental and surface complexation modelling study. Clays and Clay Minerals 46/3, 256-269.

Van Bladel, R. & Menzel, R. (1969): A thermodynamic study of sodium-strontium exchange on Wyoming bentonite. Proc. Int. Clay Conf. Tokyo, 619-634.

Vanselow, A.P. (1932): Equilibria of the base exchange reaction of bentonites, permutites, soil colloids and zeolites. Soil Sci. 33/2, 95-114.

Yun, J.I., Cho, H.R., Neck, V., Altmaier, M., Seibert, A., Marquardt, C.M., Walther, C. & Fanghänel, T. (2007): Investigation of the hydrolysis of plutonium (IV) by a combination of spectroscopy and redox potential measurements: Radiochim. Acta 95, 89-95.

Zachara, J.M., Smith, C.S., McKinley, J.P. & Resch, C.T. (1993): Cadmium sorption on specimen and soil smectites in sodium and calcium electrolytes. Soil Sci. Soc. Am. J. 57, 1491-1501.

Appendix A: Surface complexation site types and capacities and protolysis constants

Summary of site types, site capacities and protolysis constants were determined for Na-montmorillonite (Baeyens & Bradbury 1997, Bradbury & Baeyens 1997) and used as non-adjustable parameters in the model calculations of the sorption edges and isotherms on Na-montmorillonite.

Site types	**Site capacities**
$\equiv S^{S}OH$	2.0×10^{-3} mol kg^{-1}
$\equiv S^{W1}OH$	4.0×10^{-2} mol kg^{-1}
$\equiv S^{W2}OH$	4.0×10^{-2} mol kg^{-1}
Cation exchange capacity [#]	8.7×10^{-1} mol kg^{-1}
Surface protolysis reactions	**log $K_{protolysis}$**
$\equiv S^{S}OH + H^{+} \Leftrightarrow \equiv S^{S}OH_2^{+}$	4.5
$\equiv S^{S}OH \Leftrightarrow \equiv S^{S}O^{-} + H^{+}$	-7.9
$\equiv S^{W1}OH + H^{+} \Leftrightarrow \equiv S^{W1}OH_2^{+}$	4.5
$\equiv S^{W1}OH \Leftrightarrow \equiv S^{W1}O^{-} + H^{+}$	-7.9
$\equiv S^{W2}OH + H^{+} \Leftrightarrow \equiv S^{W2}OH_2^{+}$	6.0
$\equiv S^{W2}OH \Leftrightarrow \equiv S^{W2}O^{-} + H^{+}$	-10.5

[#] Average of 46 measurements determined by the ^{22}Na isotopic dilution method (Baeyens & Bradbury 1995a)

Appendix B: Metal hydrolysis constants used in the modelling of sorption edges and isotherms on montmorillonite

Metal	Hydrolysis reactions	log ^{OH}K	Reference
Mn(II)	$Mn^{2+} + H_2O \Leftrightarrow MnOH^+ + H^+$	-10.59	Baes & Mesmer (1976)
	$Mn^{2+} + 2H_2O \Leftrightarrow Mn(OH)_2^0 + 2H^+$	(-22.2)	
	$Mn^{2+} + 3H_2O \Leftrightarrow Mn(OH)_3^- + 3H^+$	(-34.8)	
Fe(II)	**$Fe^{2+} + H_2O \Leftrightarrow FeOH^+ + H^+$**	**-9.1**	Lemire et al. (2013)
	$Fe^{2+} + 2H_2O \Leftrightarrow Fe(OH)_2^0 + 2H^+$	-20.6	Baes & Mesmer (1976)
	$Fe^{2+} + 3H_2O \Leftrightarrow Fe(OH)_3^- + 3H^+$	-31	
Co(II)	**$Co^{2+} + H_2O \Leftrightarrow CoOH^+ + H^+$**	**-9.65**	Baes & Mesmer (1976)
	$Co^{2+} + 2H_2O \Leftrightarrow Co(OH)_2^0 + 2H^+$	-18.8	
	$Co^{2+} + 3H_2O \Leftrightarrow Co(OH)_3^- + 3H^+$	-31.5	
Ni(II)	**$Ni^{2+} + H_2O \Leftrightarrow NiOH^+ + H^+$**	**-9.86**	Baes & Mesmer (1976)
	$Ni^{2+} + 2H_2O \Leftrightarrow Ni(OH)_2^0 + 2H^+$	-19	
	$Ni^{2+} + 3H_2O \Leftrightarrow Ni(OH)_3^- + 3H^+$	-30	
Cu(II)	$Cu^{2+} + H_2O \Leftrightarrow CuOH^+ + H^+$	-7.95	Powell et al. (2007)
	$Cu^{2+} + 2H_2O \Leftrightarrow Cu(OH)_2^0 + 2H^+$	-16.2	
	$Cu^{2+} + 3H_2O \Leftrightarrow Cu(OH)_3^- + 3H^+$	-26.6	
Zn(II)	**$Zn^{2+} + H_2O \Leftrightarrow ZnOH^+ + H^+$**	**-8.96**	Baes & Mesmer (1976)
	$Zn^{2+} + 2H_2O \Leftrightarrow Zn(OH)_2^0 + 2H^+$	-16.9	
	$Zn^{2+} + 3H_2O \Leftrightarrow Zn(OH)_3^- + 3H^+$	-28.4	
Cd(II)	**$Cd^{2+} + H_2O \Leftrightarrow CdOH^+ + H^+$**	**-10.08**	Baes & Mesmer (1976)
	$Cd^{2+} + 2H_2O \Leftrightarrow Cd(OH)_2^0 + 2H^+$	-20.35	
	$Cd^{2+} + 3H_2O \Leftrightarrow Cd(OH)_3^- + 3H^+$	<-33.3	
Pb(II)	$Pb^{2+} + H_2O \Leftrightarrow PbOH^+ + H^+$	-7.71	Baes & Mesmer (1976)
	$Pb^{2+} + 2H_2O \Leftrightarrow Pb(OH)_2^0 + 2H^+$	-17.12	
	$Pb^{2+} + 3H_2O \Leftrightarrow Pb(OH)_3^- + 3H^+$	-28.06	
Pd(II)	$Pd^{2+} + 2H_2O \Leftrightarrow Pd(OH)_2^0 + 2H^+$	-4.0	Hummel et al. (2002)
	$Pd^{2+} + 3H_2O \Leftrightarrow Pd(OH)_3^- + 3H^+$	-15.5	
Be(II)	$Be^{2+} + H_2O \Leftrightarrow BeOH^+ + H^+$	-5.40	Baes & Mesmer (1976)
	$Be^{2+} + 2H_2O \Leftrightarrow Be(OH)_2^0 + 2H^+$	-13.65	
	$Be^{2+} + 3H_2O \Leftrightarrow Be(OH)_3^- + 3H^+$	-23.25	

Metal	Hydrolysis reactions	log ^{OH}K	Reference
Eu(III)	**$Eu^{3+} + H_2O \Leftrightarrow EuOH^{2+} + H^+$**	**-7.2**	Guillaumont et al. (2003)
	$Eu^{3+} + 2H_2O \Leftrightarrow Eu(OH)_2^+ + 2H^+$	**-15.1**	(Am hydrolysis data)
	$Eu^{3+} + 3H_2O \Leftrightarrow Eu(OH)_3^0 + 3H^+$	**-26.2**	
Am(III)	**$Am^{3+} + H_2O \Leftrightarrow AmOH^{2+} + H^+$**	**-7.2**	Guillaumont et al. (2003)
	$Am^{3+} + 2H_2O \Leftrightarrow Am(OH)_2^+ + 2H^+$	**-15.1**	
	$Am^{3+} + 3H_2O \Leftrightarrow Am(OH)_3^0 + 3H^+$	**-26.2**	
Pu(III)	$Pu^{3+} + H_2O \Leftrightarrow PuOH^{2+} + H^+$	-6.9	Guillaumont et al. (2003)
	$Pu^{3+} + 2H_2O \Leftrightarrow Pu(OH)_2^+ + 2H^+$	-14.8	
	$Pu^{3+} + 3H_2O \Leftrightarrow Pu(OH)_3^0 + 3H^+$	-25.9	
Sn(IV)	$Sn^{4+} + H_2O \Leftrightarrow SnOH^{3+} + H^+$	1.18	Baes & Mesmer (1976)
	$Sn^{4+} + 2H_2O \Leftrightarrow Sn(OH)_2^{2+} + 2H^+$	1.65	log Q values converted
	$Sn^{4+} + 3H_2O \Leftrightarrow Sn(OH)_3^+ + 3H^+$	1.55	to log K (I = 0) using
	$Sn^{4+} + 4H_2O \Leftrightarrow Sn(OH)_4^0 + 4H^+$	**0.33**	Hummel et al. (2002)
	$Sn^{4+} + 5H_2O \Leftrightarrow Sn(OH)_5^- + 5H^+$	**-7.67**	and Davies (1962)
	$Sn^{4+} + 6H_2O \Leftrightarrow Sn(OH)_6^{2-} + 6H^+$	**-18.07**	
Zr(IV)	$Zr^{4+} + H_2O \Leftrightarrow ZrOH^{3+} + H^+$	0.32	Brown et al. (2005)
	$Zr^{4+} + 2H_2O \Leftrightarrow Zr(OH)_2^{2+} + 2H^+$	0.98	
	$Zr^{4+} + 4H_2O \Leftrightarrow Zr(OH)_4^0 + 4H^+$	-2.19	
	$Zr^{4+} + 6H_2O \Leftrightarrow Zr(OH)_6^{2-} + 6H^+$	-29.0	
Th(IV)	$Th^{4+} + H_2O \Leftrightarrow ThOH^{3+} + H^+$	-2.2	Neck & Kim (2001)
	$Th^{4+} + 2H_2O \Leftrightarrow Th(OH)_2^{2+} + 2H^+$	**-6.0**	
	$Th^{4+} + 3H_2O \Leftrightarrow Th(OH)_3^+ + 3H^+$	**-11.0**	
	$Th^{4+} + 4H_2O \Leftrightarrow Th(OH)_4^0 + 4H^+$	**-17.5**	
U(IV)	$U^{4+} + H_2O \Leftrightarrow UOH^{3+} + H^+$	-0.54	Grenthe et al. (1992)
	$U^{4+} + 2H_2O \Leftrightarrow U(OH)_2^{2+} + 2H^+$	-1.1	Thoenen et al. (2014)
	$U^{4+} + 3H_2O \Leftrightarrow U(OH)_3^+ + 3H^+$	-4.7	Thoenen et al. (2014)
	$U^{4+} + 4H_2O \Leftrightarrow U(OH)_4^0 + 4H^+$	-10	Guillaumont et al. (2003)
Np(IV)	$Np^{4+} + H_2O \Leftrightarrow NpOH^{3+} + H^+$	0.55	Guillaumont et al. (2003)
	$Np^{4+} + 2H_2O \Leftrightarrow Np(OH)_2^{2+} + 2H^+$	0.35	"
	$Np^{4+} + 3H_2O \Leftrightarrow Np(OH)_3^+ + 3H^+$	-2.8	Neck & Kim (2001)
	$Np^{4+} + 4H_2O \Leftrightarrow Np(OH)_4^0 + 4H^+$	-8.3	Guillaumont et al. (2003)

Metal	**Hydrolysis reactions**	**log ^{OH}K**	**Reference**
Pu(IV)	$Pu^{4+} + H_2O \Leftrightarrow PuOH^{3+} + H^+$	0.0	Yun et al. (2007)
	$Pu^{4+} + 2H_2O \Leftrightarrow Pu(OH)_2^{2+} + 2H^+$	-1.2	
	$Pu^{4+} + 3H_2O \Leftrightarrow Pu(OH)_3^{+} + 3H^+$	-3.1	
	$Pu^{4+} + 4H_2O \Leftrightarrow Pu(OH)_4^{0} + 4H^+$	-9.3	
Pa(V)	$PaOOH^{2+} + H_2O \Leftrightarrow PaO(OH)_2^{+} + H^+$	-1.24	Trubert et al. (2003)
	$PaOOH^{2+} + 3H_2O \Leftrightarrow Pa(OH)_5^{0} + 2H^+$	-8.27	
Np(V)	$NpO_2^{+} + H_2O \Leftrightarrow NpO_2(OH)^0 + H^+$	-11.3	Lemire et al. (2001)
	$NpO_2^{+} + 2H_2O \Leftrightarrow NpO_2(OH)_2^{-} + 2H^+$	-23.6	
U(VI)	$UO_2^{2+} + H_2O \Leftrightarrow UO_2OH^{+} + H^+$	-5.25	Guillaumont et al. (2003)
	$UO_2^{2+} + 2H_2O \Leftrightarrow UO_2(OH)_2^{0} + 2H^+$	-12.15	"
	$UO_2^{2+} + 3H_2O \Leftrightarrow UO_2(OH)_3^{-} + 3H^+$	-20.25	"
	$UO_2^{2+} + 4H_2O \Leftrightarrow UO_2(OH)_4^{2-} + 4H^+$	-32.4	"
	$2UO_2^{2+} + H_2O \Leftrightarrow (UO_2)_2OH + H^+$	-2.7	Grenthe et al. (1992)
	$2UO_2^{2+} + 2H_2O \Leftrightarrow (UO_2)_2(OH)_2 + 2H^+$	-5.62	"
	$3UO_2^{2+} + 4H_2O \Leftrightarrow (UO_2)_3(OH)_4 + 4H^+$	-11.9	"
	$3UO_2^{2+} + 5H_2O \Leftrightarrow (UO_2)_3(OH)_5 + 5H^+$	-15.55	"
	$3UO_2^{2+} + 7H_2O \Leftrightarrow (UO_2)_3(OH)_7 + 7H^+$	-32.2	Guillaumont et al. (2003)
	$4UO_2^{2+} + 4H_2O \Leftrightarrow (UO_2)_4(OH)_7 + 7H^+$	-21.9	Grenthe et al. (1992)

Note: Hydrolysis reactions and log K values in bold have been used in the LFERs.

Appendix C: Compilation of strong site surface complexation constants

Tab. C1: Surface complexation data of transition metals on strong sites.

Surface complexation formation reaction	log K	Source of experimental data
$\equiv S^SOH + Co^{2+} \Leftrightarrow \equiv S^SOCo^+ + H^+$	**0.0**	*This study*
$\equiv S^SOH + Co^{2+} + H_2O \Leftrightarrow \equiv S^SOCoOH^0 + 2H^+$	-10.5	
$\equiv S^SOH + Co^{2+} + 2H_2O \Leftrightarrow \equiv S^SOCo(OH)_2^- + 3H^+$	-20.0	
$\equiv S^SOH + Ni^{2+} \Leftrightarrow \equiv S^SONi^+ + H^+$	**-0.6**	Bradbury & Baeyens (1997)
$\equiv S^SOH + Ni^{2+} + H_2O \Leftrightarrow \equiv S^SONiOH^0 + 2H^+$	-10.0	
$\equiv S^SOH + Ni^{2+} + 2H_2O \Leftrightarrow \equiv S^SONi(OH)_2^- + 3H^+$	-20.0	
$\equiv S^SOH + Zn^{2+} \Leftrightarrow \equiv S^SOZn^+ + H^+$	**1.6**	Bradbury & Baeyens (1997)
$\equiv S^SOH + Zn^{2+} + H_2O \Leftrightarrow \equiv S^SOZnOH^0 + 2H^+$	-7.4	
$\equiv S^SOH + Zn^{2+} + 2H_2O \Leftrightarrow \equiv S^{Sv}OZn(OH)_2^- + 3H^+$	-17	
$\equiv S^SOH + Cd^{2+} \Leftrightarrow \equiv S^SOCd^+ + H^+$	**-1.0**	Zachara et al. (1993)
$\equiv S^SOH + Fe^{2+} \Leftrightarrow \equiv S^SOFe^+ + H^+$	**1.7**	Soltermann et al. (2014)

Tab. C2: Surface complexation data of trivalent elements on strong sites.

Surface complexation reaction	log K	Source of experimental data
$\equiv S^SOH + Eu^{3+} \Leftrightarrow \equiv S^SOEu^{2+} + H^+$	**1.6**	Bradbury & Baeyens (2002b)
$\equiv S^SOH + Eu^{3+} + H_2O \Leftrightarrow \equiv S^SOEuOH^+ + 2H^+$	**-6.4**	
$\equiv S^SOH + Eu^{3+} + 2H_2O \Leftrightarrow \equiv S^SOEu(OH)_2^0 + 3H^+$	**-14.0**	
$\equiv S^SOH + Eu^{3+} \Leftrightarrow \equiv S^SOEu^{2+} + H^+$	**2.3**	Bradbury & Baeyens (2005a)
$\equiv S^SOH + Eu^{3+} + H_2O \Leftrightarrow \equiv S^SOEuOH^+ + 2H^+$	**-5.9**	
$\equiv S^SOH + Eu^{3+} + 2H_2O \Leftrightarrow \equiv S^SOEu(OH)_2^0 + 3H^+$	**-13.8**	
$\equiv S^SOH + Am^{3+} \Leftrightarrow \equiv S^SOAm^{2+} + H^+$	**2.3**	Bradbury & Baeyens (2005a)
$\equiv S^SOH + Am^{3+} + H_2O \Leftrightarrow \equiv S^SOAmOH^+ + 2H^+$	**-5.9**	
$\equiv S^SOH + Am^{3+} + 2H_2O \Leftrightarrow \equiv S^SOAm(OH)_2^0 + 3H^+$	**-14.2**	
$\equiv S^SOH + Am^{3+} \Leftrightarrow \equiv S^SOAm^{2+} + H^+$	**1.6**	Gorgeon (1994)
$\equiv S^SOH + Am^{3+} + H_2O \Leftrightarrow \equiv S^SOAmOH^+ + 2H^+$	**-6.8**	
$\equiv S^SOH + Am^{3+} + 2H_2O \Leftrightarrow \equiv S^SOAm(OH)_2^0 + 3H^+$	**-14.6**	

Tab. C3: Surface complexation data of tetravalent elements on strong sites.

Surface complexation formation reaction	**log K**	**Source of experimental data**
$\equiv S^SOH + Sn^{4+} + 2H_2O \Leftrightarrow \equiv S^SOSn(OH)_2^+ + 3H^+$	13.3	Bradbury & Baeyens (2005a)
$\equiv S^SOH + Sn^{4+} + 3H_2O \Leftrightarrow \equiv S^SOSn(OH)_3^0 + 4H^+$	**9.15**	
$\equiv S^SOH + Sn^{4+} + 4H_2O \Leftrightarrow \equiv S^SOSn(OH)_4^- + 5H^+$	**1.6**	
$\equiv S^SOH + Sn^{4+} + 5H_2O \Leftrightarrow \equiv S^SOSn(OH)_5^{2-} + 6H^+$	**-7.6**	
$\equiv S^SOH + Th^{4+} \Leftrightarrow \equiv S^SOTh^{3+} + H^+$	7.2	Bradbury & Baeyens (2005a)
$\mathbf{\equiv S^SOH + Th^{4+} + H_2O \Leftrightarrow \equiv S^SOTh(OH)^{2+} + 2H^+}$	**2.7**	
$\mathbf{\equiv S^SOH + Th^{4+} + 2H_2O \Leftrightarrow \equiv S^SOTh(OH)_2^+ + 3H^+}$	**-2.6**	
$\mathbf{\equiv S^SOH + Th^{4+} + 3H_2O \Leftrightarrow \equiv S^SOTh(OH)_3^0 + 4H^+}$	**-9.1**	
$\equiv S^SOH + Th^{4+} + 4H_2O \Leftrightarrow \equiv S^SOTh(OH)_4^- + 5H^+$	-16.9	

Tab. C4: Surface complexation data of Np(V), Pa(V) and U(VI) on strong sites.

Surface complexation formation reaction	**log K**	**Source of experimental data**
$\equiv S^SOH + NpO_2^+ \Leftrightarrow \equiv S^SONpO_2^0 + H^+$	-2.0	Bradbury & Baeyens (2005a)
$\equiv S^SOH + NpO_2^+ + H_2O \Leftrightarrow \equiv S^SONpO_2OH^- + H^+$	-12.0	
$\equiv S^SOH + NpO_2^+ \Leftrightarrow \equiv S^SONpO_2^0 + H^+$	-2.8	*This study*
$\equiv S^SOH + NpO_2^+ + H_2O \Leftrightarrow \equiv S^SONpO_2OH^- + H^+$	-11.6	
$\equiv S^SOH + NpO_2^+ \Leftrightarrow \equiv S^SONpO_2^0 + H^+$	-2.9	Turner et al. (1998)
$\equiv S^SOH + NpO_2^+ + H_2O \Leftrightarrow \equiv S^SONpO_2OH^- + H^+$	-12.7	
$\equiv S^SOH + NpO_2^+ \Leftrightarrow \equiv S^SONpO_2^0 + H^+$	-2.8	Gorgeon (1994)
$\equiv S^SOH + NpO_2^+ + H_2O \Leftrightarrow \equiv S^SONpO_2OH^- + H^+$	-12.8	
$\equiv S^SOH + PaOOH^{2+} \Leftrightarrow \equiv S^SOPaOOH^+ + H^+$	6.7	Bradbury & Baeyens (2006b)
$\equiv S^SOH + PaOOH^{2+} \Leftrightarrow \equiv S^SOPaO_2^0 + 2H^+$	-0.5	
$\equiv S^SOH + PaOOH^{2+} + H_2O \Leftrightarrow \equiv S^SOPaO_2OH^- + 3H^+$	-8.6	
$\equiv S^SOH + UO_2^{2+} \Leftrightarrow \equiv S^SO\ UO_2^+ + H^+$	3.1	Marques Fernandes et al. (2012)
$\equiv S^SOH + UO_2^{2+} + H_2O \Leftrightarrow \equiv S^SOUO_2OH^0 + 2H^+$	-4.6	
$\equiv S^SOH + UO_2^{2+} + 2H_2O \Leftrightarrow \equiv S^SOUO_2(OH)_2^- + 3H^+$	-12.6	
$\equiv S^SOH + UO_2^{2+} + 3H_2O \Leftrightarrow \equiv S^SOUO_2(OH)_3^{2-} + 4H^+$	-20.9	
$\equiv S^SOH + UO_2^{2+} \Leftrightarrow \equiv S^SO\ UO_2^+ + H^+$	2.2	Pabalan & Turner (1997)

Note: Surface complexation reactions and log K values in bold have been used in the LFERs for strong sites.

Appendix D: Compilation of weak site surface complexation constants

Surface complexation formation reaction	log K	Source of experimental data
$\equiv S^{W1}OH + Co^{2+} \Leftrightarrow \equiv S^{W1}OCo^{+} + H^{+}$	**-3.3**	*This study*
$\equiv S^{W1}OH + Ni^{2+} \Leftrightarrow \equiv S^{W1}ONi^{+} + H^{+}$	**-3.3**	Baeyens & Bradbury (1995b)
$\equiv S^{W1}OH + Zn^{2+} \Leftrightarrow \equiv S^{W1}OZn^{+} + H^{+}$	**-2.7**	Baeyens & Bradbury (1995b)
$\equiv S^{W1}OH + Fe^{2+} \Leftrightarrow \equiv S^{W1}Fe^{+} + H^{+}$	**-2.0**	Soltermann et al. (2014)
$\equiv S^{W1}OH + Eu^{3+} \Leftrightarrow \equiv S^{W1}OEu^{2+} + H^{+}$	**-0.5**	Bradbury & Baeyens (2002b)
$\equiv S^{W1}OH + UO_2^{2+} \Leftrightarrow \equiv S^{W1}OUO_2^{+} + H^{+}$ $\equiv S^{W1}OH + UO_2^{2+} + H_2O \Leftrightarrow \equiv S^{W1}OUO_2OH^{0} + 2H^{+}$	**0.5** **-5.7**	Marques Fernandes et al. (2012)

Note: Surface complexation constants in bold have been used in the LFER for weak sites.

Appendix E: Ternary surface complexes (trivalent metals and U)

One of the main assumptions in the sorption modelling is that the sorbing metal aqueous species are cations and positively charged and neutral hydrolysis species. While this assumption has been shown to be sufficient to model a wide range of experimental data, ternary carbonate surface complexes have been used to model the sorption of trivalent metals and U(VI) on clay minerals in the alkali pH range at high carbonate concentrations (Marques Fernandez et al. 2008, and 2012). Such ternary compounds have been confirmed by EXAFS investigations (Marques Fernandez et al. 2012 and 2015). These data are included in Tab. E1. (At the present time, no evidence has been found for the existence of ternary carbonate surface complexes for di-, tetra- and pentavalent metals.)

Tab. E1: Ternary surface reactions and constants for Eu and U.

Surface complexation on strong and weak sites	**log K**	**Source of experimental data**
$\equiv S^{S}OH + Eu^{3+} + CO_3^{2-} \Leftrightarrow \equiv S^{S}OEuCO_3^{0} + H^{+}$	8.3	Marques Fernandes et al. (2008b)
$\equiv S^{S}OH + Eu^{3+} + CO_3^{2-} + H_20 \Leftrightarrow \equiv S^{S}OEuOHCO_3^{0} + 2H^{+}$	-0.25	
$\equiv S^{S}OH + UO_2^{2+} + CO_3^{2-} \Leftrightarrow \equiv S^{S}OUO_2CO_3^{-} + H^{+}$	9.8	Marques Fernandes et al. (2012)
$\equiv S^{S}OH + UO_2^{2+} + 2CO_3^{2-} \Leftrightarrow \equiv S^{S}OUO_2(CO_3)_2^{3-} + H^{+}$	15.5	
$\equiv S^{W1}OH + UO_2^{2+} + CO_3^{2-} \Leftrightarrow \equiv S^{S}OUO_2CO_3^{-} + H^{+}$	9.3	

Appendix F: Cation exchange reactions and selectivity coefficients

Tab. F1: Selectivity coefficients at trace concentrations of K(I), Cs(I), Mg(II), Ca(II), Sr(II), Ni(II), Zn(II), Cd(II), Co(II), Pb(II), Eu(III), Am(III) and Np(V) and U(VI) with respect to Na for Na-montmorillonite.

A-clay + B	Smectite	N_B range	Background electrolyte	K_C	Reference
Na-mont. + K^+	Wyoming B	< 0.01 – 1	0.1 M $NaNO_3$	3	Vanselow (1932)
Na-mont. + Cs^+	C. Berteau	< 0.01 – 1	0.01 M $NaNO_3$	33	Cremers & Thomas (1968)
	Wyoming B	< 0.01 – 1	0.01 M $NaNO_3$	6.2	Gast (1969)
Na-mont. + Mg^{2+}	MX-80	0.05	0.005 M NaCl	2.2	Bradbury & Baeyens (2002b)
Na-mont. + Ca^{2+}	SWy-1	< 0.01	0.01 – 0.267 $NaClO_4$	4.1	Baeyens & Bradbury (1995b)
	MX-80	0.08	0.005 M NaCl	2.6	Bradbury & Baeyens (2002b)
Na-mont. + Sr^{2+}	Wyoming B	< 0.01 – 1	0.025 M NaCl	1.5	Van Bladel & Menzel (1969)
Na-mont. + Ni^{2+}	SWy-1	< 0.01	0.01, 0.03, 0.1 M $NaClO_4$	3.1	Baeyens & Bradbury (1995b)
	C. Berteau	< 0.2	0.01 M $NaNO_3$	3.7	Maes et al. (1976)
Na-mont. + Zn^{2+}	SWy-1	< 0.01	0.1 M $NaClO_4$	3.9	Baeyens & Bradbury (1995b)
	C. Berteau	< 0.2	0.01 M $NaNO_3$	3.7	Maes et al. (1976)
Na-mont. + Cd^{2+}	SWy-1	< 0.1	0.1 M $NaClO_4$	2.8	Zachara et al. (1993)
	"	< 0.1	0.014 M $NaClO_4$	2.0	"
	C. Berteau	< 0.2	0.01 M $NaNO_3$	3.3	Maes et al. (1976)
Na-mont. + Co^{2+}	C. Berteau	< 0.2	0.01 M $NaNO_3$	3.7	Maes et al. (1976)
Na-mont. + Fe^{2+}	STx-1	< 0.01	0.1 M $NaNO_3$	6.3	Soltermann et al. (2014)
Na-mont. + Eu^{3+}	SWy-1	< 0.01	0.1 M $NaClO_4$	30	Bradbury& Baeyens (2002a)
	C. Berteau	< 0.1	0.1 M $NaNO_3$	40	Maes & Cremers (1986)
	"	< 0.1	0.25 M $NaNO_3$	200	"
	"	< 0.1	0.4 M $NaNO_3$	398	"
Na-mont. + Am^{3+}	SWy-1	< 0.1	0.1 M $NaClO_4$	29	Bradbury & Baeyens (2006b)
	Wyoming	< 0.1	0.1 M $NaClO_4$	47	Gorgeon (1994)
		< 0.1	1 M $NaClO_4$	297	"
Na-mont. + NpO_2^+	SWy-1	< 0.1	0.1 M $NaClO_4$	1.1	Bradbury & Baeyens (2006b)
	SAz-1	< 0.1	0.1 M $NaClO_4$	0.8	Turner et al. (1998)
	Wyoming	< 0.1	0.1 M $NaClO_4$	1.0	Gorgeon (1994)
	"	< 0.1	0.025 M $NaNO_3$	0.4	"
Na-mont. + UO_2^{2+}	SWy-1	< 0.01	0.01 M $NaClO_4$	0.7	Bradbury & Baeyens (2005b)
	"	< 0.01	0.1 M $NaClO_4$	1.4	"
	SAz-1	< 0.1	0.1 M NaCl	1.4	Pabalan & Turner (1997)

Appendix G: Eu isotherm: modelling silicate complex sorbing and $Eu(OH)^{2+}$

Dissolved silica is ubiquitous in all clay mineral systems and arises from the clay mineral itself or from the presence of quartz/chalcedony. It is well accepted that trivalent lanthanides and actinides form aqueous silicate complexes (NEA 2005).

In the sorption experiments for Eu on montmorillonite (Chapter 3) there are low concentrations of Si present in the system (between 10^{-5} and ~ 8×10^{-5} M), arising mainly from the equilibration of the clay mineral with the background electrolyte. The aqueous speciation of Eu (10^{-8} M) in the presence of 4×10^{-5} M Si was calculated using the hydrolysis data given in Appendix B, and the Eu-silicate formation reaction and stability constant given in Hummel et al. (2002), i.e.:

$$Eu^{3+} + Si(OH)_{4(aq)} \Leftrightarrow EuSiO(OH)_3^{2+} + H^+ \qquad \log K = -1.71 \qquad (G1)$$

and is shown in Fig. G1.

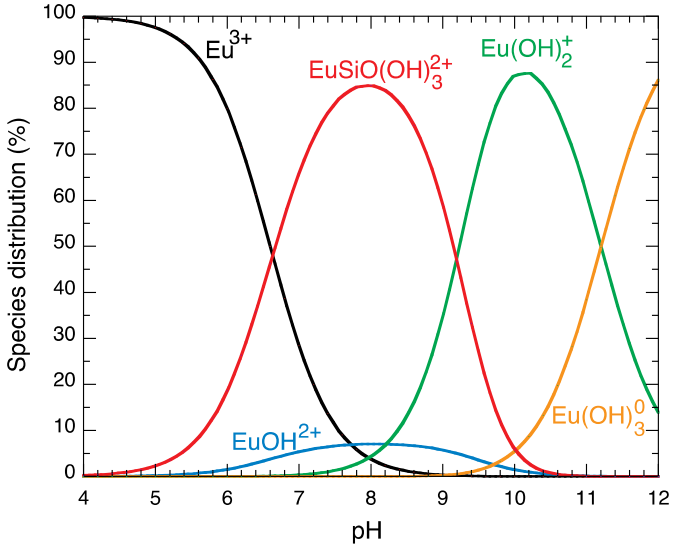

Fig. G1: Aqueous Eu speciation in 0.1 M $NaClO_4$ including complexation with Si (Si_{TOT} = 4×10^{-5} M).

In the pH range from ~ 7 to ~ 9 the aqueous speciation of Eu is dominated by $EuSiO(OH)_3^{2+}$. If this picture of Eu speciation is accepted, then two bounding assumptions can be made regarding the sorbing species in this pH region.

Either:

(i) $EuOH^{2+}$ sorbs and the silicate complex is non sorbing,

or:

(ii) the species $EuSiO(OH)_3^{2+}$ sorbs in preference to $EuOH^{2+}$.

If the data for the Eu sorption edges and isotherms given in Figs. 3.7 and 3.21 respectively are considered, all data sets can be modelled with assumption (i) using the surface complexation constants given in Tab. G1. The modelling results are shown in Fig. G2 (edges) and G3 (isotherms).

Tab. G1: Surface complexation data of trivalent elements on strong and weak sites.

Surface complexation reaction	**log K**	**Source of experimental data**
$\equiv S^{S}OH + Eu^{3+} \Leftrightarrow \equiv S^{S}OEu^{2+} + H^{+}$	1.6	Bradbury & Baeyens (2002b)
$\equiv S^{S}OH + Eu^{3+} + H_2O \Leftrightarrow \equiv S^{S}OEuOH^{+} + 2H^{+}$	-5.1	
$\equiv S^{S}OH + Eu^{3+} + 2H_2O \Leftrightarrow \equiv S^{S}OEu(OH)_2^{0} + 3H^{+}$	-14.0	
$\equiv S^{W1}OH + Eu^{3+} \Leftrightarrow \equiv S^{W1}OEu^{2+} + H^{+}$	-0.5	
$\equiv S^{S}OH + Eu^{3+} \Leftrightarrow \equiv S^{S}OEu^{2+} + H^{+}$	2.3	Bradbury & Baeyens (2006a)
$\equiv S^{S}OH + Eu^{3+} + H_2O \Leftrightarrow \equiv S^{S}OEuOH^{+} + 2H^{+}$	-4.5	
$\equiv S^{S}OH + Eu^{3+} + 2H_2O \Leftrightarrow \equiv S^{S}OEu(OH)_2^{0} + 3H^{+}$	-13.8	
$\equiv S^{S}OH + Am^{3+} \Leftrightarrow \equiv S^{S}OAm^{2+} + H^{+}$	2.3	Bradbury & Baeyens (2006a)
$\equiv S^{S}OH + Am^{3+} + H_2O \Leftrightarrow \equiv S^{S}OAmOH^{+} + 2H^{+}$	-4.8	
$\equiv S^{S}OH + Am^{3+} + 2H_2O \Leftrightarrow \equiv S^{S}OAm(OH)_2^{0} + 3H^{+}$	-14.2	
$\equiv S^{S}OH + Am^{3+} \Leftrightarrow \equiv S^{S}OAm^{2+} + H^{+}$	1.9	Gorgeon (1994)
$\equiv S^{S}OH + Am^{3+} + H_2O \Leftrightarrow \equiv S^{S}OAmOH^{+} + 2H^{+}$	-5.5	
$\equiv S^{S}OH + Am^{3+} + 2H_2O \Leftrightarrow \equiv S^{S}OAm(OH)_2^{0} + 3H^{+}$	-14.9	

Note: The log K values are modelled including Eu/Am silicate complexes. Total Si concentration is taken to be 4×10^{-5} M.

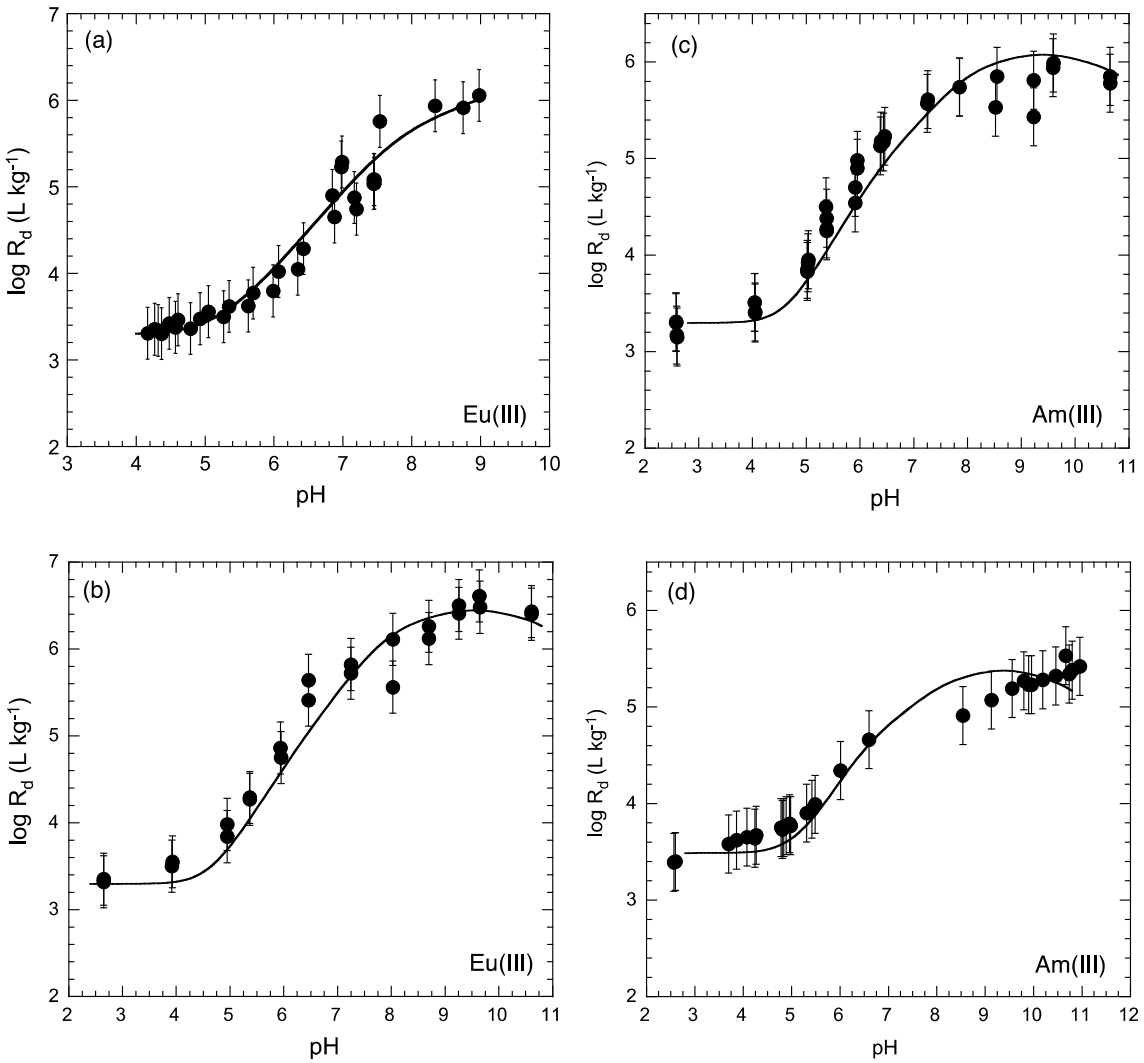

Fig. G2: Sorption edge for Eu(III) on Na-SWy-1 in 0.1 M $NaClO_4$ from (a) Bradbury & Baeyens (2002a) and (b) Bradbury & Baeyens (2006a) and sorption edges for Am(III) in 0.1 M $NaClO_4$ (c) on Na-SWy-1 from Bradbury & Baeyens (2005a) and (d) on Na-smectite from Gorgeon (1994).

Experimental data (●). Modelled curves (—) (*this study*). The modelling is done with the parameters given in Tab. G1 in the presence of 4×10^{-5} M Si.

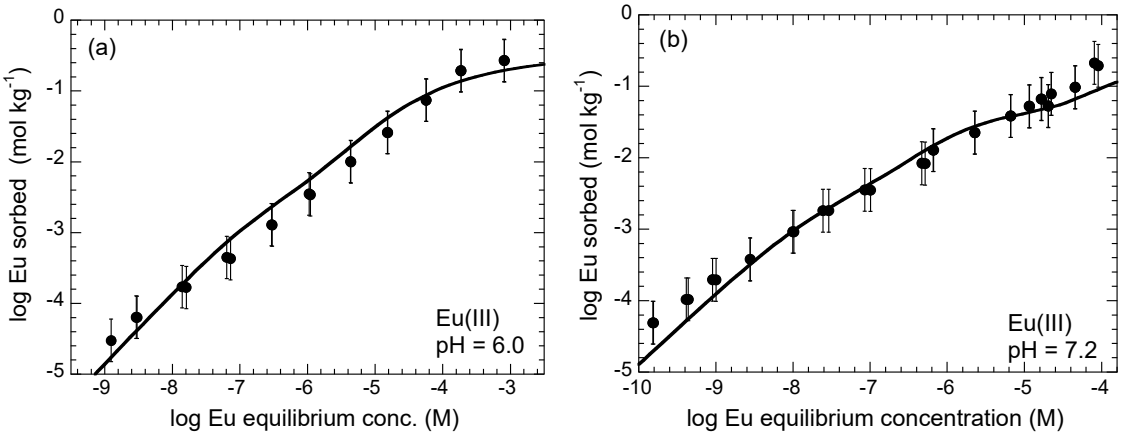

Fig. G3: Sorption isotherms for Eu(III) on Na-SWy-1 in 0.1 M $NaClO_4$.

Experimental data (●) from (a) Baeyens & Bradbury (2002a). The modelling is done with the parameters given in Tab. G1 in the presence of 4×10^{-5} M Si.

Alternatively, the data can be equally well modelled if assumption (ii) is considered and the following ternary surface complexation reactions on the strong and weak sites are considered.

$$\equiv S^{S/W1}OH + Eu^{3+} + H_4SiO_4 \Leftrightarrow \equiv S^{S/W1}OEuSi(OH)_3^{+} + 2H^{+} \quad (G2)$$

The modelling results using the data given in Tab. G2 are shown in Fig. G4.

Tab. G2: Surface complexation constants for the Eu sorption modelling on Na-SWy-1 including a ternary Eu-silicate surface complex.

Surface complexes		**log $^{S/W1}K$**	**Site type**
$\equiv S^{S}OH + Eu^{3+}$	$\Leftrightarrow \equiv S^{S}OEu^{2+} + H^{+}$	1.6	strong sites
$\equiv S^{S}OH + Eu^{3+} + H_4SiO_4$	**$\Leftrightarrow \equiv S^{S}OEuSi(OH)_3^{+} + 2H^{+}$**	**-0.6**	
$\equiv S^{S}OH + Eu^{3+} + 2H_2O$	$\Leftrightarrow \equiv S^{S}OEu(OH)_2^{0} + 3H^{+}$	-14.0	
$\equiv S^{W1}OH + Eu^{3+}$	$\Leftrightarrow \equiv S^{W1}OEu^{2+} + H^{+}$	-0.5	weak sites
$\equiv S^{W1}OH + Eu^{3+} + H_4SiO_4$	**$\Leftrightarrow \equiv S^{W1}OEuSi(OH)_3^{+} + 2H^{+}$**	**-2.6**	
Cation exchange		**K_c**	
3Na-mont + Eu	$\Leftrightarrow$ Eu^{3+}-mont + 3 Na^{+}	29	planar sites

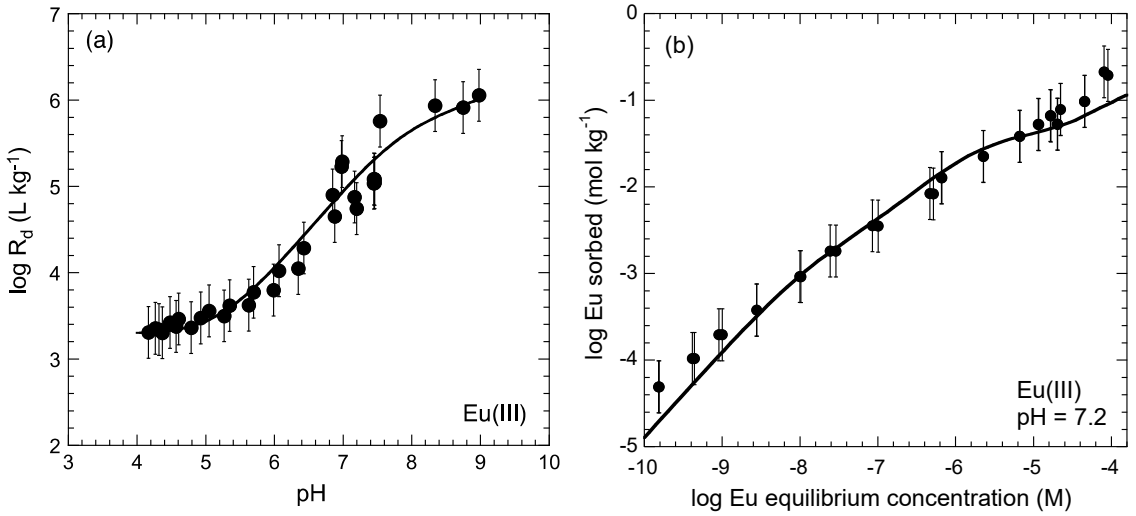

Fig. G4: (a) Sorption edge and (b) sorption isotherm of Eu on 0.1 M Na-SWy in 0.1 M $NaClO_4$.

The modelling is done with the parameters given in Tab. F2 in the presence of 4×10^{-5} M Si.

Just on this basis, neither of these possibilities can be excluded. However, there are additional measurements on the uptake of Eu on an MX-80 bentonite/porewater system (Appendix H) as a function of concentration (see Fig. 7.1). In Chapter 7 the bottom up modelling shown was carried out according to assumption (i). If the same system is modelled according to assumption (ii), then the modelled curve is as shown below.

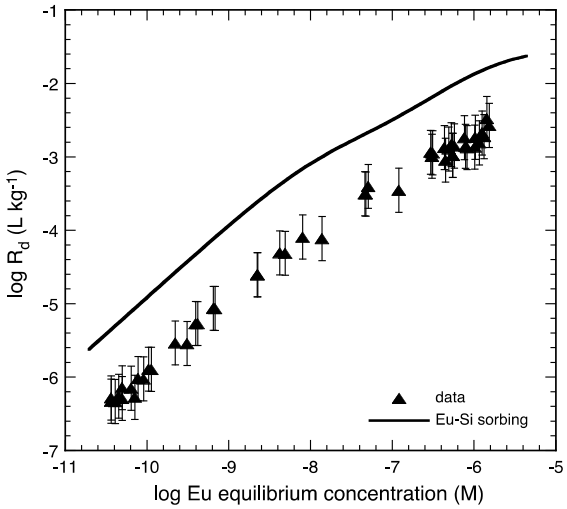

Fig. G5: Isotherm data for Eu on MX-80 bentonite, corresponding to Fig. 7.1.

The continuous black line is modelled assuming that the species $EuSiO(OH)_3^{2+}$ sorbs in preference to $EuOH^{2+}$ and clearly overestimates the measured data.

As can be clearly seen, assuming that the species $EuSiO(OH)_3^{2+}$ sorbs in preference to $EuOH^{2+}$, leads to a significant over prediction of the sorption measurements. This additional information/ modelling indicates that assumption (i), i.e. $EuOH^{2+}$, sorbs and the silicate complex is non sorbing, is the more plausible interpretation.

One final comment; the interpretations given above are strongly dependent on the "correctness" of the Eu-silicate stability constant given in Eq. G1 (Hummel et al. 2002).

Appendix H: Bentonite mineralogy and water chemistry

Tab. H1: Mineralogical composition of MX-80 bentonite (Müller-Vonmoos & Kahr 1983).

Mineral	[wt.-%]
Clay minerals	
Montmorillonite	75
Illite	-
Illite/Smectite mixed layers	-
Kaolinite	< 1
Mica	<1
Chlorite	-
Quartz	15.2
K-Feldspar/albite	6.5 ± 1.5
Calcite	0.7
Dolomite/Ankerite	-
Siderite	0.7
Pyrite	0.3

Tab. H2: Synthetic porewater compositions of MX-80 bentonite used in the sorption isotherm experiments (Bradbury & Baeyens 2011b).

Dissolved constituents	**Concentration** [M]
Na	5.7×10^{-1}
K	2.8×10^{-3}
Mg	2.3×10^{-2}
Ca	3.0×10^{-2}
Sr	2.7×10^{-4}
Al	4.2×10^{-8}
Mn	1.3×10^{-6}
F	7.4×10^{-5}
Cl	6.2×10^{-1}
SO_4	2.9×10^{-2}
$C_{inorg.}$	4.2×10^{-4}
Si	1.8×10^{-4}

Appendix J: Thermodynamic data used in the modelling of natural bentonite/groundwater systems

Tab. J1: Summary of the aqueous complexation constants (log K values) for Ni(II), Eu(III), Th(IV) and U(VI) with chloro, sulphato and carbonato species used in the calculations (Thoenen et al. 2014).

Metal complex	**Ni**	**Eu**	**Th**	**UO_2**
MeCl	0.08	1.1	1.70	0.17
$MeCl_2$	-	1.5	-	-1.1
$MeSO_4$	2.35	3.95	6.17	3.15
$Me(SO_4)_2$	-	5.7	9.69	4.14
$Me(SO_4)_3$	-	-	10.75	3.02
$MeCO_3$	4.2	8.1	-	9.94
$Me(CO_3)_2$	6.2	12.1	-	16.61
$Me(CO_3)_3$	-	-	-	21.84
$MeHCO_3$	11.72	-	-	-
$Me(CO_3)_4$	-	-	-	-
$Me(CO_3)_5$	-	-	31.0	-
$Me(OH)_3CO_3$	-	-	-3.1*	-
$Me(OH)_2(CO_3)_2$	-	-	8.80	-
$Me(OH)(CO_3)_4$	-	-	21.6	-
$Me(OH)_4CO_3$	-	-	-15.6	-
$MeMg(CO_3)_3$	-	-	-	26.11
$MeCa(CO_3)_3$	-	-	-	27.18
$MeCa_2(CO_3)_3$	-	-	-	29.22
$Me_2(OH)_3CO_3$	-	-	-	-0.86

* Hummel et al. (2002).